SCORE - View Sequence Detail(s) for Application 10671316

Enter SEQ ID No:

Submit

Enter Application ID No:

Submit

First Sequence

Next Sequence

Previous Sequence

Last Sequence

Convert To Search Format

Go back to Table of Contents Page

Download All Sequences

Here is the list of the requested sequences:

<110> APPLICANT: Trimeris, Inc.
<120> TITLE OF INVENTION: Method for production of antivirals by use of HIV-derived HR1 peptides, and trimers formed therefrom
<130> FILE REFERENCE: TRM-002
<140> CURRENT APPLICATION NUMBER: US/10/671,316
<141> CURRENT FILING DATE: 2003-09-24
<150> PRIOR APPLICATION NUMBER: 60/414,515
<151> PRIOR FILING DATE: 2002-09-27
<160> NUMBER OF SEQ ID NOS: 48
<170> SOFTWARE: PatentIn version 3.2

<210> SEQ ID NO 1
<211> LENGTH: 59
<212> TYPE: PRT
<213> ORGANISM: Human immunodeficiency virus
<400> SEQUENCE: 1

```
Thr Leu Thr Val Gln Ala Arg Gln Leu Leu Ser Gly Ile Val Gln Gln
1               5                  10                  15
Gln Asn Asn Leu Leu Arg Ala Ile Glu Ala Gln Gln His Leu Leu Gln
            20                  25                  30
Leu Thr Val Trp Gly Ile Lys Gln Leu Gln Ala Arg Ile Leu Ala Val
        35                  40                  45
Glu Arg Tyr Leu Lys Asp Gln Leu Leu Gly Ile
    50                  55
```

Table 1: Biophysical and antiviral Parameters

Parameter	SEQ ID NO:23	SEQ ID NO:24	SEQ ID NO:32	SEQ ID NO:34
Oligomerization	Aggregates	Best modeled As a tetramer	Best modeled as a trimeric species*	Best modeled as a trimeric species*
Helicity (at 10μM, 25°C)	83%	74%	87%	100%
Stability(at 10μM)	T_m 83°C	T_m 82°C	T_m 69°C	T_m 71°C
HR2 peptide binding K on / K off/ Kd	Yes	yes; 1.2×10^6 / 1.2×10^{-3} / 1.1 nM	Yes; 6.1×10^5 / 1.9×10^{-3} / 3.1 nM	Yes
Antiviral activity Against HIV IIIB (μg/ml) IC50 IC90	4.69 23.24	3.73 12.301	0.59 1.90	0.19 0.62

SEQ ID NO:47	SEQ ID NO:48
Best modeled as a trimeric species*	Best modeled as a trimeric species*
68%	72%
T_m 77°C	T_m 68°C
Yes	Yes
0.61	0.89

* with only a small fraction (e.g., between about 1 to about 10%) of higher order oligomer (e.g., hexamer) and therefore is considered to self assemble into trimers.

It was an unexpected result that by replacing the leucine at the aforementioned "c" position of the hydrophobic domain (e.g., as exemplified by synthetic peptides having the amino acid sequence of SEQ ID NOs:47 & 48) , or replacing the leucine or methionine at the aforementioned "g" position of the hydrophobic domain and the leucine at the aforementioned "c" position of the hydrophobic domain (e.g., as exemplified by synthetic peptides having the amino acid sequence of SEQ ID NOs:32 & 34) with a less bulky amino acid (an amino acid having a less bulky side chain or R group than leucine or methionine), altered in the synthetic peptide derived from the HR1

Several assays were used to assess the ability of the synthetic peptides/trimers employed with the present invention to retain the ability to complex with peptides derived from the HR2 region of HIV-1 gp41. These include a protein chip assay (using Biacore analysis) in which surface plasmon resonance is used to detect the binding, and kinetics thereof, between a synthetic peptide and an HR2 peptide; and a fluorescence polarization assay. In the fluorescence polarization assay, a detectable moiety comprising a fluorescent dye (e.g., rhodamine and/or fluorescein) was used to label HR2 peptide, and the assay was then allowed to proceed under sufficient conditions and for a sufficient period of time for labeled peptide to bind to HR1 peptide, or synthetic peptide (or trimer formed therefrom). Fluorescence intensity of polarized light was then measured with a detection system comprising a spectrophotometer, and the amount of polarized light was calculated (units = mP). As illustrated in FIG. 4, and exemplified by synthetic peptide having the amino acid sequence of SEQ ID NO:32, the synthetic peptides supplied in the present invention (trimers formed therefrom) retain the ability to complex with peptides derived from the HR2 region of HIV-1 gp41. In some instances throughout the Examples illustrated herein, such ability to complex with HR2 peptides as demonstrated by this binding assay is denoted as "yes" with reference to such binding activity.

Comparison of synthetic peptides (illustrated as SEQ ID NO:32 and SEQ ID NO:34) with HR1 peptides of native sequence (illustrated as SEQ ID NO:23 and SEQ ID NO:24,respectively) is illustrated in Table 1. As shown in Table 1, as compared to a respective peptide having the native sequence of HR1 (e.g., SEQ ID NOs: 23 & 24), a synthetic peptide provided with the present invention (e.g., as exemplified by SEQ ID NOs:32, 34, 47, and 48) resulted in an alteration in the oligomerization state. Additionally, as shown in Table 1 (and subsequent Tables herein), a synthetic peptide (trimers formed therefrom) provided with the present invention can demonstrate relatively good binding to HR2 peptide, and a significant increase in antiviral activity (e.g., 3 fold or greater increase in potency, as observed by a 1/3 or greater decrease in either or both of IC50 and IC90) as compared to an HR1 peptide of native sequence.

region can be (a) the oligomerization state of such synthetic peptide, in that it can self-assemble in solution to predominately trimers rather than tetramers (e.g., the latter being the predominant oligomeric state in solution of respective native sequence having the amino acid sequences of SEQ ID NOs:23 & 24); and (b) antiviral activity to a significant improvement (increase) in antiviral activity against HIV isolates (e.g., compare the statistically significant difference in the antiviral activity of a trimer of a synthetic peptide having the amino acid sequence of any one of SEQ ID NOs:32, 34, 47 or 48 versus a tetramer of an HR1 peptide of native sequence shown in SEQ ID NO:24). Amino acid residues which are less bulky than leucine and methionine are known to those skilled in the art to include, but are not limited to, alanine, glycine, valine, serine, threonine, and the like. Also, one skilled in the art would appreciate from the data presented in Table 1, that the synthetic peptides provided with the present invention have utility in a method for identifying or producing a compound or drug. More particularly, the synthetic peptide can self-assemble into trimers, thereby presenting a structure like that of the native trimeric core of the HR1 region of HIV gp41 to which can bind molecules (compounds and/or drugs) having binding specificity for such structure. Since the trimers employed in the method according to the present invention retain the ability to complex with HR2 peptide, provided is the means to evaluate the ability of a molecule to inhibit the binding interaction between the HR1 and HR2 regions of HIV gp41 (e.g., by contacting trimer provided with the present invention, in the presence of HR2 peptide, with the molecule). More particularly, the synthetic peptides self assemble into trimers, and the trimers, when used in a method according to the present invention, provide a structure *in vitro* which mimics the trimers formed by the HR1 region of gp41 *in vivo*. Thus, a method of the present invention utilizing such trimers *in vitro* provide a means by which compounds can be identified or drugs produced which can inhibit/prevent six helix bundle formation between the trimers formed by the interaction of HR1 region of gp41 and trimer formed form the HR2 region of gp41 in forming a six-helix bundle *in vivo*.

Further, as illustrated in FIG. 4, in a fluorescence polarization assay to detect binding, the synthetic peptides (or trimers formed therefrom) provided with the present invention may exhibit a cooperative transition at a narrow concentration range, beyond which no significant change is observed. As exemplified using trimers formed from synthetic peptide having the sequence of SEQ ID NO:32, the sharpness of the transition enables more sensitive and accurate detection of a molecule (compound and/or drug) that can inhibit the binding between HR1 and HR2 regions of HIV gp41, as compared to

<!--StartFragment-->RESULT 7
ABO10357
ID   ABO10357 standard; peptide; 63 AA.
XX
AC   ABO10357;
XX
DT   23-OCT-2003 (revised)
DT   19-AUG-2003 (first entry)
XX
DE   HIV-1 BRU gp41 DP107-like region.
XX
KW   HIV; DP107; DP178; glycoprotein 41; antiviral; virucide; EBV;
KW   Epstein-Barr virus infection; heptad repeat motif.
XX
OS   Human immunodeficiency virus; isolate BRU.
XX
PN   US6518013-B1.
XX
PD   11-FEB-2003.
XX
PF   07-JUN-1995;   95US-00485546.
XX
PR   07-JUN-1993;   93US-00073028.
PR   07-JUN-1994;   94US-00255208.
PR   20-DEC-1994;   94US-00360107.
XX
PA   (TRIM-) TRIMERIS INC.
XX
PI   Barney SO, Lambert DM, Petteway SR;
XX
DR   WPI; 2003-465599/44.
XX
PT   Inhibiting transmission of Epstein-Barr virus to a cell, by contacting
PT   the cell with a peptide consisting of a region of Epstein-Barr virus
PT   protein.
XX
PS   Example; Fig 50A-B; 716pp; English.
XX
CC   The invention relates to inhibiting (M) transmission of an Epstein-Barr
CC   virus to a cell, comprising contacting the cell with an effective
CC   concentration of a peptide consisting of a region of 16-39 consecutive
CC   amino acids of an Epstein-Barr virus protein for an effective period of
CC   time, where the region is recognised by one or more of ALLMOTI5,
CC   107x178x4 or PLZIP sequence search motifs, the peptide further comprises
CC   an amino terminal X, and a carboxy terminal Z in which X comprises an
CC   amino group, acetyl group, 9-fluorenylmethoxy-carbonyl group, hydrophobic
CC   group or macromolecular carrier group, and Z comprises a carboxyl group,
CC   amido group, hydrophobic group, or macromolecular carrier group, and
CC   fusion of the virus to the cell is inhibited. The peptides were
CC   identified by analysing the structure/motifs present in the HIV-1
CC   glycoprotein 41 anti-HIV peptides DP107 and DP178. These heptad repeat
CC   motif containing peptides were used to design the motifs cited above,
CC   which in turn were used to analyse proteins from other pathogenic
CC   organisms and HIV isolates, looking for DP107/178 structural analogues.
CC   The method is useful for inhibiting transmission of Epstein-Barr virus to
CC   a cell and Epstein-Barr virus infection. The present sequence is a region
CC   of a protein from a pathogenic organism analogous to DP107 or DP178.
CC   (Updated on 23-OCT-2003 to standardise OS field)
XX
SQ   Sequence 63 AA;

  Query Match   96.3%; Score 273.5; DB 6; Length 63;
  Best Local Similarity   98.3%; Pred. No. 4.1e-22;
  Matches   59; Conservative   0; Mismatches   0; Indels   1; Gaps   1;

Qy   1 TLTVQARQLLSGIVQQQNNLLRAIEAQQHLLQLTVWGIKQLQARILAVERYLKD-QLLGI 59
              ||||||||||||||||||||||||||||||||||||||||||||||||||||| |||||

Db 2 TLTVQARQLLSGIVQQQNNLLRAIEAQQHLLQLTVWGIKQLQARILAVERYLKDQQLLGI 61

<!--EndFragment-->

<!--StartFragment-->RESULT 7
ABO10357
ID   ABO10357 standard; peptide; 63 AA.
XX
AC   ABO10357;
XX
DT   23-OCT-2003 (revised)
DT   19-AUG-2003 (first entry)
XX
DE   HIV-1 BRU gp41 DP107-like region.
XX
KW   HIV; DP107; DP178; glycoprotein 41; antiviral; virucide; EBV;
KW   Epstein-Barr virus infection; heptad repeat motif.
XX
OS   Human immunodeficiency virus; isolate BRU.
XX
PN   US6518013-B1.
XX
PD   11-FEB-2003.
XX
PF   07-JUN-1995;   95US-00485546.
XX
PR   07-JUN-1993;   93US-00073028.
PR   07-JUN-1994;   94US-00255208.
PR   20-DEC-1994;   94US-00360107.
XX
PA   (TRIM-) TRIMERIS INC.
XX
PI   Barney SO, Lambert DM, Petteway SR;
XX
DR   WPI; 2003-465599/44.
XX
PT   Inhibiting transmission of Epstein-Barr virus to a cell, by contacting
PT   the cell with a peptide consisting of a region of Epstein-Barr virus
PT   protein.
XX
PS   Example; Fig 50A-B; 716pp; English.
XX
CC   The invention relates to inhibiting (M) transmission of an Epstein-Barr
CC   virus to a cell, comprising contacting the cell with an effective
CC   concentration of a peptide consisting of a region of 16-39 consecutive
CC   amino acids of an Epstein-Barr virus protein for an effective period of
CC   time, where the region is recognised by one or more of ALLMOTI5,
CC   107x178x4 or PLZIP sequence search motifs, the peptide further comprises
CC   an amino terminal X, and a carboxy terminal Z in which X comprises an
CC   amino group, acetyl group, 9-fluorenylmethoxy-carbonyl group, hydrophobic
CC   group or macromolecular carrier group, and Z comprises a carboxyl group,
CC   amido group, hydrophobic group, or macromolecular carrier group, and
CC   fusion of the virus to the cell is inhibited. The peptides were
CC   identified by analysing the structure/motifs present in the HIV-1
CC   glycoprotein 41 anti-HIV peptides DP107 and DP178. These heptad repeat
CC   motif containing peptides were used to design the motifs cited above,
CC   which in turn were used to analyse proteins from other pathogenic
CC   organisms and HIV isolates, looking for DP107/178 structural analogues.
CC   The method is useful for inhibiting transmission of Epstein-Barr virus to
CC   a cell and Epstein-Barr virus infection. The present sequence is a region
CC   of a protein from a pathogenic organism analogous to DP107 or DP178.
CC   (Updated on 23-OCT-2003 to standardise OS field)
XX
SQ   Sequence 63 AA;

  Query Match   96.3%; Score 273.5; DB 6; Length 63;
  Best Local Similarity   98.3%; Pred. No. 4.1e-22;
  Matches   59; Conservative   0; Mismatches   0; Indels   1; Gaps   1;

Qy   1 TLTVQARQLLSGIVQQQNNLLRAIEAQQHLLQLTVWGIKQLQARILAVERYLKD-QLLGI 59
              ||||||||||||||||||||||||||||||||||||||||||||||||||||| |||||

Db 2 TLTVQARQLLSGIVQQQNNLLRAIEAQQHLLQLTVWGIKQLQARILAVERYLKDQQLLGI 61

<!--EndFragment-->

<!--StartFragment-->RESULT 3
US-08-919-597-201
; Sequence 201, Application US/08919597
; Patent No. 6054265
; GENERAL INFORMATION:
; APPLICANT: Bolognesi, Dani P.
; APPLICANT: Matthews, Thomas J.
; APPLICANT: Wild, Carl T.
; APPLICANT: Barney, Shawn O.
; APPLICANT: Lambert, Dennis M.
; APPLICANT: Petteway, Stephen R.
; APPLICANT: Langlois, Alphonse J.
; TITLE OF INVENTION: METHODS AND COMPOSITIONS FOR INHIBITION
; TITLE OF INVENTION: OF MEMBRANE FUSION-ASSOCIATED EVENTS, INCLUDING HIV
; TITLE OF INVENTION: TRANSMISSION
; NUMBER OF SEQUENCES: 273
; CORRESPONDENCE ADDRESS:
; ADDRESSEE: Pennie & Edmonds
; STREET: 1155 Avenue of the Americas
; CITY: New York
; STATE: New York
; COUNTRY: USA
; ZIP: 10036-2711
; COMPUTER READABLE FORM:
; MEDIUM TYPE: Floppy disk
; COMPUTER: IBM PC compatible
; OPERATING SYSTEM: PC-DOS/MS-DOS
; SOFTWARE: PatentIn Release #1.0, Version #1.30
; CURRENT APPLICATION DATA:
; APPLICATION NUMBER: US/08/919,597
; FILING DATE:
; CLASSIFICATION:
; PRIOR APPLICATION DATA:
; APPLICATION NUMBER: US 08/470,896
; FILING DATE: 06-JUN-1995
; ATTORNEY/AGENT INFORMATION:
; NAME: Coruzzi, Laura A.
; REGISTRATION NUMBER: 30,742
; REFERENCE/DOCKET NUMBER: 7872-020
; TELECOMMUNICATION INFORMATION:
; TELEPHONE: (212) 790-9090
; TELEFAX: (212) 869-9741/8864
; TELEX: 66141 PENNIE
; INFORMATION FOR SEQ ID NO: 201:
; SEQUENCE CHARACTERISTICS:
; LENGTH: 63 amino acids
; TYPE: amino acid
; STRANDEDNESS:
; TOPOLOGY: unknown
; MOLECULE TYPE: peptide
US-08-919-597-201

Query Match 96.3%; Score 273.5; DB 2; Length 63;
Best Local Similarity 98.3%; Pred. No. 9.7e-28;
Matches 59; Conservative 0; Mismatches 0; Indels 1; Gaps 1;

```
Qy          1 TLTVQARQLLSGIVQQQNNLLRAIEAQQHLLQLTVWGIKQLQARILAVERYLKD-QLLGI 59
              ||||||||||||||||||||||||||||||||||||||||||||||||||| |||||
Db          2 TLTVQARQLLSGIVQQQNNLLRAIEAQQHLLQLTVWGIKQLQARILAVERYLKDQQLLGI 61
```

<!--EndFragment-->

JOURNAL OF VIROLOGY, Nov. 2001, p. 11146–11156 Vol. 75, No. 22
0022-538X/01/$04.00+0 DOI: 10.1128/JVI.75.22.11146–11156.2001

Structural and Functional Analysis of Interhelical Interactions in the Human Immunodeficiency Virus Type 1 gp41 Envelope Glycoprotein by Alanine-Scanning Mutagenesis

MIN LU,[1]* MARISA O. STOLLER,[2] SHILONG WANG,[1] JIE LIU,[1] MELINDA B. FAGAN,[2]† AND JACK H. NUNBERG[2]*

Department of Biochemistry, Weill Medical College of Cornell University, New York, New York 10021,[1] and Montana Biotechnology Center, The University of Montana, Missoula, Montana 59812[2]

Received 23 May 2001/Accepted 8 August 2001

Membrane fusion by human immunodeficiency virus type 1 (HIV-1) is promoted by the refolding of the viral envelope glycoprotein into a fusion-active conformation. The structure of the gp41 ectodomain core in its fusion-active state is a trimer of hairpins in which three antiparallel carboxyl-terminal helices pack into hydrophobic grooves on the surface of an amino-terminal trimeric coiled coil. In an effort to identify amino acid residues in these grooves that are critical for gp41 activation, we have used alanine-scanning mutagenesis to investigate the importance of individual side chains in determining the biophysical properties of the gp41 core and the membrane fusion activity of the gp120-gp41 complex. Alanine substitutions at Leu-556, Leu-565, Val-570, Gly-572, and Arg-579 positions severely impaired membrane fusion activity in envelope glycoproteins that were for the most part normally expressed. Whereas alanine mutations at Leu-565 and Val-570 destabilized the trimer-of-hairpins structure, mutations at Gly-572 and Arg-579 led to the formation of a stable gp41 core. Our results suggest that the Leu-565 and Val-570 residues are important determinants of conserved packing interactions between the amino- and carboxyl-terminal helices of gp41. We propose that the high degree of sequence conservation at Gly-572 and Arg-579 may result from selective pressures imposed by prefusogenic conformations of the HIV-1 envelope glycoprotein. Further analysis of the gp41 activation process may elucidate targets for antiviral intervention.

Infection by human immunodeficiency virus type 1 (HIV-1) is initiated by fusion of the viral and cellular membranes to allow virus entry into the cell. This process is mediated by the viral envelope glycoprotein through interaction with cellular receptors. The HIV-1 envelope glycoprotein is synthesized as a precursor polyprotein, gp160, that is proteolytically processed to generate two subunits, the surface glycoprotein gp120 and the transmembrane glycoprotein gp41 (53). These subunits remain noncovalently associated to form the oligomeric envelope glycoprotein spike on the viral membrane. gp120 is responsible for the sequential binding of the envelope glycoprotein spike to CD4 and a chemokine receptor (typically CCR5 or CXCR4) on the surface of target cells (reviewed in references 2 and 75). These events trigger gp41 to undergo conformational changes that are crucial for activation of HIV-1 membrane fusion. By analogy with the pH-induced structural changes in the hemagglutinin (HA) protein of influenza virus, the HIV-1 fusion activation process likely involves substantial conformational changes from a metastable prefusogenic state to an energetically more stable fusogenic conformation (reviewed in references 14 and 64). The control of these structural rearrangements is thought to be central to HIV-1 entry and to strategies for intervention.

The structure and mechanism of the gp41 molecule have been extensively studied. Protein dissection studies demonstrated that the N- and C-terminal heptad repeat regions of the gp41 ectodomain associate to form an α-helical trimer of antiparallel dimers (50). X-ray crystallographic analysis confirmed that this gp41 core is a trimer of hairpins (13, 68, 69). Three N-terminal helices form a trimeric coiled coil, and three C-terminal helices pack in the reverse direction into three hydrophobic grooves on the surface of the coiled coil. Recent evidence indicates that this helical-hairpin structure corresponds to the fusion-active conformation of gp41 (13, 36, 50, 68, 69). Because the membrane anchor and the fusion peptide of the gp41 ectodomain are embedded in the viral and target cell membranes, respectively, the formation of the fusogenic hairpin structure results in the colocalization of the two membranes and thus overcomes the energy barrier for membrane fusion (27, 32, 69).

Peptides corresponding to the C-terminal heptad repeat region, referred to as C peptides, can specifically inhibit viral entry into target cells at nanomolar concentrations (37, 73). One such peptide (T-20) is in clinical study and has shown antiviral activity in humans (42). T-20 binds to gp41 only after interaction of the envelope glycoprotein complex with the cellular receptors (27, 39, 56) and is thought to act in a dominant-negative manner by binding to the N-terminal coiled coil of gp41 during its conformational change to the fusogenic state (15, 50, 72). Considerations of the efficiency of C peptide competition with its cognate sequence suggest a relatively long-

* Corresponding author. Mailing address for Jack H. Nunberg: Montana Biotechnology Center, The University of Montana, Missoula, MT 59812. Phone: (406) 243-6421. Fax: (406) 243-6425. E-mail: nunberg@selway.umt.edu. Mailing address for Min Lu: Department of Biochemistry, Weill Medical College of Cornell University, New York, NY 10021. Phone: (212) 746-6562. Fax: (212) 746-8875. E-mail: mlu@med.cornell.edu.

† Present address: Department of Philosophy, University of Texas, Austin, TX 78712.

lived prehairpin intermediate (14, 27, 39, 56). Intermediate states of the gp41 molecule may serve as a target for the development of small-molecule HIV-1 inhibitors (22, 25).

Considerable evidence now implies that packing interactions between the central coiled-coil trimer and the C-terminal helix are important determinants of HIV-1 entry and its inhibition (35, 54, 60, 63). For example, the replacement of a conserved glutamine (Gln-652), buried in this helical interface, by the hydrophobic residue leucine increases HIV-1 infectivity and underlies an enhancement in the antiviral activity of C peptides (8, 63). Biophysical and structural characterization directly demonstrates that this substitution strengthens the interhelix interaction in the fusogenic hairpin structure by providing additional hydrophobic packing forces (63). Taken together, these results have been interpreted to indicate that the receptor-triggered conformational changes of the HIV-1 envelope glycoprotein are thermodynamically controlled and that the process of membrane apposition and lipid bilayer fusion is driven by the currency of energy released from the formation of the fusogenic gp41 core (33, 49, 51, 63, 69).

Therefore, it is of fundamental importance to understand the structural and mechanistic basis for the helical interactions in this core. We show here, using alanine-scanning mutagenesis, that amino acids Leu-556, Leu-565, Val-570, Gly-572, and Arg-579 at e and g positions of the N34 coiled coil are essential for envelope glycoprotein function. Whereas Leu-565 and Val-570 contribute to the conserved packing interactions between the N- and C-terminal helices of gp41, Gly-572 and Arg-579 appear to be critical for prefusogenic conformations of the HIV-1 envelope glycoprotein complex.

MATERIALS AND METHODS

Plasmid construction and mutagenesis. High-fidelity XL PCR (rTth and Vent DNA polymerases; PE Applied Biosystems) and oligonucleotide primers envA and envN (29) were used to adapt the HIV-1 HXB2 *rev* and *env* genes from the plasmid pIIIenv 3-1 (65). Expression of the HXB2 envelope glycoprotein was within the context of the eukaryotic expression vector pCR-Uni 3.1 (Invitrogen) (45). Alanine mutations were introduced into the HXB2 envelope glycoprotein and the N34(L6)C28 peptide (51) using QuikChange mutagenesis (Stratagene, La Jolla, Calif.) and single-stranded mutagenesis (44), respectively. Mutations were verified by DNA sequencing.

Envelope glycoprotein expression. Simian COS-7 cells were used for transient expression of the envelope glycoprotein (75). Typically, 3 μg of the HIV-1 *env* expression plasmid and 9 μl of FuGENE-6 reagent (Roche Molecular Biochemicals) were used, according to the manufacturer's instructions, to transfect 4×10^5 to 8×10^5 cells in a 6-cm culture dish. Cultures were washed 18 h later with physiological buffered saline (PBS) and refed with Dulbecco's modified Eagle's medium with 10% fetal bovine serum. Transfection efficiencies were determined in microcultures from the transfected cell cultures. These microcultures were fixed with −20°C methanol-acetone (1:1) and stained using biotinylated anti-HIV immunoglobulin (HIVIG) from infected persons, NeutrAvidin-horseradish peroxidase (HRP) (Pierce Chemical Corp., Rockford, Ill.), and diaminobenzidine.

Western blot analysis. Two days after transfection, cell culture supernatants were harvested and filtered. gp120 shed from expressing cells was immunoprecipitated using HIVIG and protein A-Sepharose (Sigma). Cell monolayers were surface biotinylated using EZ-Link NHS-LC-biotin (Pierce Chemical) as previously described (48, 76). Cells were then lysed on ice in 50 mM Tris-HCl (pH 7.5)–150 mM NaCl–1% Triton X-100 containing 1 μg ml^{-1} each of aprotinin, leupeptin, and pepstatin. Biotinylated surface proteins were isolated by using NeutrAvidin-agarose (Pierce Chemical). Envelope glycoprotein was detected by Western blot analysis using the gp120-specific monoclonal antibody (MAb) Chessie B13 (kindly provided by George Lewis [1]). Western blots were visualized by chemifluorescence using ECL-Plus (Amersham Pharmacia Biotech) and quantitated by fluorescence imaging using a Fuji FLA3000G instrument.

Deglycosylation of cell surface Env. Biotinylated envelope glycoprotein was isolated from the cell surface using NeutrAvidin-agarose and was deglycosylated using protein *N*-glycanase F (New England Biolabs, Beverly, Mass.). The resulting polypeptides were analyzed by Western blot using MAb Chessie 12 (kindly provided by George Lewis [1]). gp160 from a cleavage-defective envelope glycoprotein mutant (26) and soluble gp120 from a truncated envelope glycoprotein construct were deglycosylated and used as size markers.

Pulse-chase analysis. COS-7 cells expressing envelope glycoprotein were pulse-labeled for 30 min in replicate six-well cluster dishes using 100 μCi each of [^{35}S]cysteine and [^{35}S]methionine in 1 ml of cysteine- and methionine-free medium. Cultures were then washed and grown in cysteine- and methionine-containing medium for the indicated times. gp120 was isolated from cell culture supernatants by immunoprecipitation. Proteins were separated by sodium dodecyl sulfate-polyacrylamide gel electrophoresis and visualized by phosphorimaging.

Cell-cell fusion assay. The ability of the wild-type and mutant envelope glycoproteins to mediate cell-cell fusion was determined by coculturing envelope glycoprotein-expressing COS-7 cells with U87 cells expressing CD4 and CXCR4 coreceptor (31, 45, 49). Transfected COS-7 cells were resuspended using PBS with 0.5 mM EDTA, and 5×10^3 cells were added to 96-well microcultures containing 5×10^3 U87-CD4-CXCR4 cells. In order to assess the rate and extent of syncytium formation, cocultures were fixed and immunochemically stained after 6 and 24 h. The number of envelope glycoprotein-expressing cells involved in syncytium formation and the number of nuclei contained within each syncytium were determined microscopically.

Peptide production. Mutant N34(L6)C28 peptides were expressed in *Escherichia coli* BL21(DE3)/pLysS using the T7 expression system (67). Cells, freshly transformed with an appropriate plasmid, were grown to late log phase. Protein expression was induced by addition of 0.5 mM isopropylthio-β-D-galactoside. After another 3 h of growth at 37°C, the bacteria were harvested by centrifugation, and the cells were lysed by glacial acetic acid as described previously (52). Proteins were purified from the soluble fraction to homogeneity by reverse-phase high-pressure liquid chromatography (Waters) with a Vydac C_{18} preparative column using a water-acetonitrile gradient in the presence of 0.1% (vol/vol) trifluoroacetic acid.

CD spectroscopy. Circular dichroism (CD) spectra were acquired on an AVIV 62DS CD spectrometer with a thermoelectric sample temperature controller. Samples for wavelength spectra were 10 μM peptide in 50 mM sodium phosphate (pH 7.0) and 150 mM NaCl. The cuvette was 0.1 cm in path length. The wavelength dependence of molar ellipticity, [θ], was monitored at 4°C as the average of five scans, using a 5-s integration time at 1.0-nm wavelength increments. Spectra were baseline corrected against the value for the cuvette with buffer alone. Fractional helix content was calculated from the CD signal by dividing the mean residue ellipticity at 222 nm by the value expected for 100% helix formation by helices of comparable size (−33,000° cm^2 $dmol^{-1}$) (17). Thermal stability was determined in the same buffer by measuring $[\theta]_{222}$ as a function of temperature. A 1.0-cm path length cell was used with continuous stirring. Thermal melts were monitored in 2°C intervals with a 2-min equilibration at the desired temperature and an integration time of 30 s. The midpoint of the thermal unfolding transition (T_m) was determined from the maximum of the first derivative, with respect to the reciprocal of the temperature, of the $[\theta]_{222}$ values (7). The error in estimation of T_m is ±1°C. Protein concentrations were determined by measuring absorbance at 280 nm in 6 M guanidinium chloride (23).

Sedimentation equilibrium. Sedimentation equilibrium measurements were performed on a Beckman XL-A Optima analytical ultracentrifuge, using an An-Ti rotor and six-sectored equilibrium centrifugation centerpieces. Protein samples were dialyzed overnight against 50 mM sodium phosphate (pH 7.0)–150 mM NaCl, loaded at initial concentrations of 10, 30, and 100 μM, and analyzed at rotor speeds of 20 and 23 krpm at 20°C. Data were acquired at two wavelengths per rotor speed and processed simultaneously with a nonlinear least-squares fitting routine (38). Solvent density and protein partial specific volume were calculated according to solvent and protein composition, respectively (47). Molecular weights were all within 10% of those calculated for an ideal trimer, with no systematic deviation of the residuals.

Crystallization, data collection, and structure determination. The G572A and R579A peptides were crystallized by hanging-drop vapor diffusion at room temperature. Initial crystallization conditions were screened by using sparse matrix crystallization kits (Crystal Screen I and II; Hampton Research, Riverside, Calif.) and then optimized. Rhombohedral crystals of G572A were grown from 10 mg ml^{-1} of peptide, 0.1 M sodium acetate (pH 5.2), 0.2 M ammonium sulfate, and 10% polyethylene glycol 4000. Rhombohedral crystals of R579A peptide were obtained from 20 mg ml^{-1} of peptide, 0.1 M sodium acetate (pH 4.5), 0.2 M ammonium sulfate, and 29% polyethylene glycol methyl ether 2000. Crystals were transferred to a cryoprotectant solution containing 15% (vol/vol) glycerol in

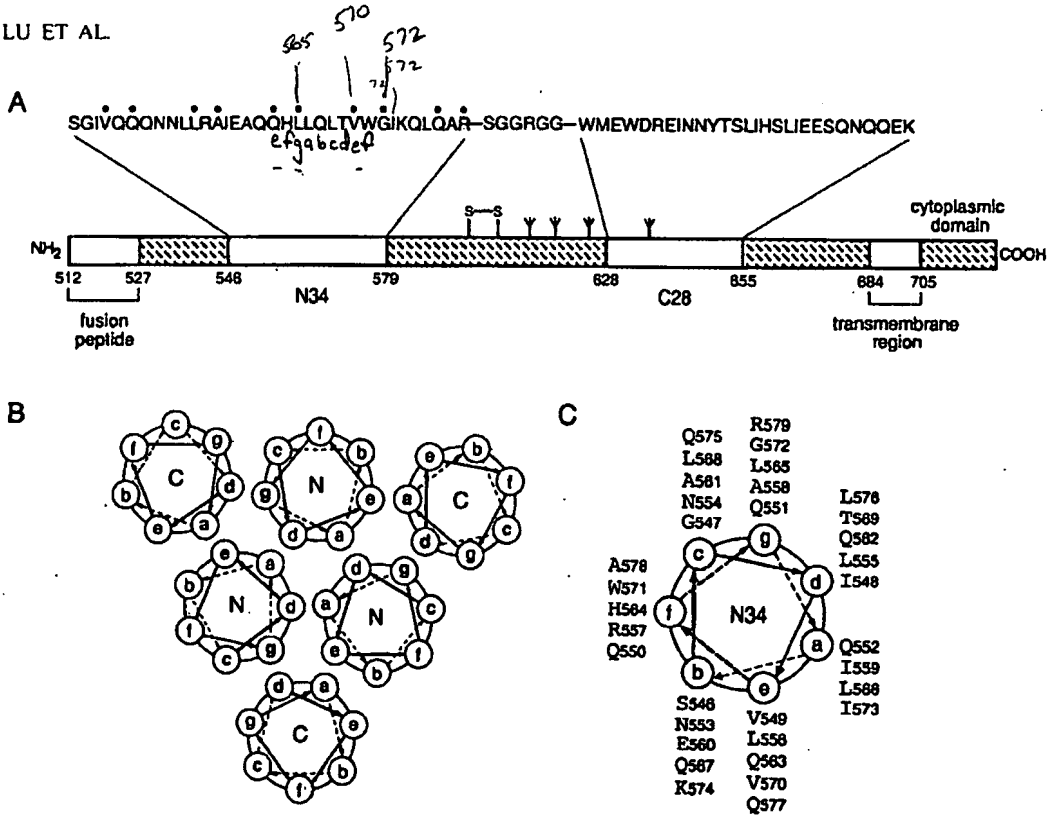

FIG. 1. Core structure of the HIV-1 gp41 envelope glycoprotein. (A) Schematic representation of gp41. The important functional features of the gp41 ectodomain and the amino acid sequences of the N34 and C28 segments are shown. Amino acids mutated to alanine in this study are indicated by dots above the sequence. The naturally occurring alanine at position 558 was not altered. The disulfide bond and four potential N-glycosylation sites are depicted. The residues are numbered according to their position in gp160. The recombinant N34(L6)C28 peptide model consists of N34 and C28 plus a linker of six hydrophilic residues. (B) Cross-section of helix packing in the gp41 core. Residues at the a and d positions of the N helices form the hydrophobic interface of the trimeric coiled coil, and residues at the a and d positions of the C helices pack in an antiparallel orientation against residues at the e and g positions of adjacent N helices. (C) Helical wheel projection of the heptad repeat sequence of the N34 peptide. The view is from the NH_2 terminus.

the corresponding mother liquor and frozen in liquid nitrogen for data collection. Diffraction data on the G572A peptide trimer were collected at 95 K using an R-axis IV image plate detector mounted on a Rigaku RU200 rotating anode X-ray generator at the X-ray Crystallography Facility at the Weill Medical College of Cornell University. Data on the R579A peptide trimer were collected at 95 K using a Quantum-4 charge-coupled device-based detector at the X12B beamline of the National Synchrotron Light Source. Diffraction intensities were integrated by using Denzo and Scalepack software (59) and reduced to structural factors with the program Truncate from the CCP4 program suite (10).

The structures of the G572A and R579A peptides were determined by molecular replacement with the program AMoRe (57) using the N34(L6)C28 trimer (Protein Data Bank [PDB] file name 1SZT) as a search model. The initial models were built by using conventional $(2F_o - F_c)F_{calc}$ and $(F_o - F_c)F_{calc}$ maps at 3.0 Å. Overall anisotropic B-factor and bulk solvent corrections were applied. Many cycles of torsional angle simulated annealing and grouped B-factor refinement (4) were followed by extensive rebuilding. The models were rebuilt to reflect the sequences of the G572A and R579A peptides by using the $(2F_o - F_c)F_{calc}$ and $(F_o - F_c)F_{calc}$ maps with the program O (40). The structures were refined by using positional and B-factor refinements (4). Crystallographic refinement of the structures was done with the program CNS 1.0 (5). Model geometry was analyzed by Procheck (46), with all residues occupying most-preferred regions of the Ramanchandran space. Ser-546, Gly-547, Asn-651, Gln-652, Gln-653, Glu-654, and Lys-655 of the G572A and R579A peptides were left out of the model because of the absence of interpretable electron density for these atoms. Atomic coordinates for G572A peptide (PDB file name 1I5Y) and R579A peptide (PDB file name 1I5X) have been deposited in the PDB.

RESULTS

In the trimer-of-hairpins structure, residues at positions a and d of the C28 helix pack against residues at the e and g positions of the N34 coiled-coil trimer in an antiparallel orientation (Fig. 1). Sequence comparisons among HIV-1 isolates and between HIV-1 and simian immunodeficiency virus (SIV) show that the residues at these contact positions are highly conserved (43). This high degree of sequence conservation may result from selective pressure to maintain interhelical packing interactions and, hence, the structural integrity of the trimer of hairpins. To directly test this hypothesis, we changed the individual e and g residues of N34 to alanine in both the recombinant N34(L6)C28 peptide model and the intact envelope glycoprotein (Fig. 1C). Alanine-scanning mutagenesis was chosen because alanine, albeit a good helix-inducing residue, has a relatively low hydrophobicity and contributes little to protein-protein interactions (19). We reasoned that alanine replacements were likely to alter the stability of the trimer-of-hairpins structure but not to disrupt its folding per se. In this analysis, the biophysical properties of mutant N34(L6)C28 peptides were compared with the biological phenotypes of mutant envelope glycoproteins.

Expression of mutant envelope glycoproteins. Alanine mutant envelope glycoproteins were expressed by transient transfection in COS-7 cells. As determined by Western blot analysis of cell surface-biotinylated proteins, all mutant envelope glycoproteins were expressed and transported to the cell surface with efficiencies comparable to that of the wild-type glycopro-

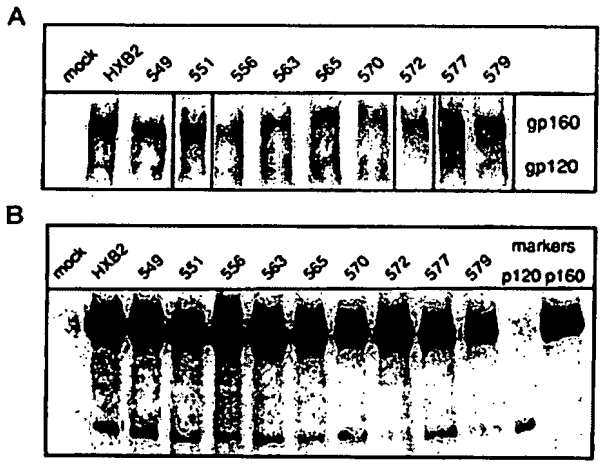

FIG. 2. Cell surface expression of mutant envelope glycoproteins. Mutant and wild-type envelope glycoproteins were transiently expressed in COS-7 cells, and cell surface proteins were biotinylated using NHS-LC-biotin. Mutant envelope glycoprotein names are abbreviated by the position number. (A) Envelope glycoprotein was immunoprecipitated using HIVIG and detected by Western blot analysis using NeutrAvidin-HRP and ECL-Plus imaging. Representative images obtained from the analysis of comparably transfected cell cultures (40 to 60% transfection efficiency) are shown. (B) Biotinylated envelope glycoproteins were deglycosylated and detected by Western blot analysis using the gp120-specific MAb Chessie 12 (1) and ECL-Plus imaging. HXB2 gp160 and gp120 were similarly deglycosylated to provide size markers (p160, 94 kDa; and p120, 55 kDa). Using this method of analysis, we noted a consistent diminution in the ratio of gp120 to gp160. Although the basis for this apparent skewing is not known, the relative amounts of gp120 among the mutants are retained relative to the analysis of the unmodified glycoproteins. A dark image is used to emphasize deglycosylated gp120s.

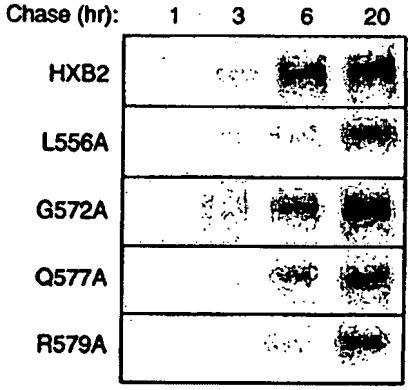

FIG. 3. Pulse-chase analysis of gp120 shedding by mutant envelope glycoproteins. Cells expressing mutant (L556A, G572A, Q577A, or R579A) and wild-type envelope glycoproteins were pulse-labeled for 30 min using [^{35}S]cysteine and [^{35}S]methionine. Comparable amounts of radioactivity were incorporated in envelope glycoproteins by all cultures (1.2×10^4 to 2.2×10^4 phosphostimulated luminescence units in gp160). Culture supernatants were harvested at 1, 3, 6, and 20 h, and gp120 was immunoprecipitated using HIVIG. Proteins were resolved by SDS-polyacrylamide gel electrophoresis, and radioactivity was visualized by phosphorimaging.

tein (Fig. 2A). The predominant species of envelope glycoprotein on the cell surface was gp160. The incomplete cleavage of the gp160 precursor is likely due to saturation of the cellular furin-like proteases that are responsible for envelope glycoprotein processing (3). gp120 represented ~10 to 20% of the envelope glycoprotein on the cell surface. This was observed in the wild-type and in all alanine mutant proteins except G572A.

In order to quantitate the relative amounts of cell surface gp120 among the mutants, we deglycosylated the cell surface glycoproteins to generate discrete polypeptides (Fig. 2B). Steady-state levels of gp120 in the alanine mutants V549A, Q551A, Q563A, L565A, V570A, and Q577A were similar to that in the wild-type glycoprotein. We conclude that alanine substitutions at Val-549, Gln-551, Gln-563, Leu-565, Val-570, and Gln-577 did not affect envelope glycoprotein transport to the cell surface, gp160 cleavage, or gp120-gp41 association. By contrast, the G572A mutant glycoprotein exhibited a 10-fold reduction in the relative amount of cell surface gp120. Lesser reductions were also noted in the L556A and R579A mutants (two- and fourfold, respectively).

To examine whether the marked decrease in the steady-state level of gp120 in the G572A mutant was due to a reduction in the efficiency of gp160 cleavage, we analyzed the rate of appearance of gp120 in the cell culture medium. Given the high rate of spontaneous gp120 shedding from the envelope glycoprotein complex (55), we reasoned that this assay would provide a sensitive measure for gp160 cleavage efficiency. If proteolytic cleavage were reduced by the mutation, the amount of shed gp120 would likewise be reduced. Figure 3 shows the time course from a pulse-chase labeling experiment. The rate and/or extent of gp120 shedding in G572A was not decreased relative to that of the wild-type glycoprotein. We conclude that the reduction in gp120 accumulation in G572A is not due to a defect in proteolytic cleavage. By extension, the reduction in the steady-state level of gp120 in the G572A mutant may be caused by an increase in gp120 shedding; the Gly-572-to-Ala mutation may affect the stability of the gp120-gp41 association.

In the pulse-chase labeling experiments (Fig. 3), the L556A and R579A mutants exhibited a slight reduction in the rate and/or extent of gp120 shedding relative to the wild-type glycoprotein. The significance of this finding is unclear, as a similar decrease was observed in Q577A, a mutant in which the gp120 accumulation on the cell surface was unaltered. The mechanism for the two- to fourfold reduction in the steady-state levels of gp120 in L556A and R579A remains undefined.

Taken together, our results indicate that the biosynthesis and expression of the V549A, Q551A, Q563A, L565A, V570A, and Q577A envelope glycoproteins were unaffected by alanine substitutions (Table 1). On the other hand, G572A, L556A, and R579A displayed reduced steady-state levels of gp120 on the cell surface.

Fusogenic potential of mutant envelope glycoproteins. The ability of the alanine mutant envelope glycoproteins to mediate cell-cell fusion was assessed by coculturing transfected COS-7 cells with a fusion partner, U87 cells expressing CD4 and CXCR4. In this assay, syncytium formation proceeds rapidly, and the maximum number of syncytia is typically attained by 6 h of coculture. Thereafter, neighboring syncytia begin to fuse, resulting in a decreased number of syncytia and an increased number of nuclei per syncytium. By these criteria, V549A, Q551A, Q563A, and Q577A were indistinguishable

TABLE 1. Expression and fusion activity of mutant envelope glycoproteins

Glycoprotein	Cell surface expression[a]	Cell surface gp120/gp160[b] ratio	gp120 shedding[c]	Fusion activity[d]
Wild type	+++	+++	+++	+++
V549A	+++	+++	+++	+++
Q551A	+++	+++	+++	+++
L556A	+++	++	++	±
Q563A	+++	+++	+++	+++
L565A	+++	+++	+++	±
V570A	+++	+++	+++	±
G572A	+++	+	+++	−
Q577A	+++	+++	++	+++
R579A	+++	++	++	±

[a] +++, comparable to wild-type envelope glycoprotein.
[b] +++, comparable to wild-type envelope glycoprotein; ++, 2- to 4-fold reduction; +, 10-fold reduction.
[c] +++, comparable to wild-type envelope glycoprotein, as assessed by Western blot analysis and/or by pulse-chase measurements; ++, slight reduction in gp120 shedding.
[d] +++, comparable to wild-type envelope glycoprotein; ±, severe (≥100-fold) reduction in fusion ability; −, complete absence of fusion. Intermediate levels of impairment were not represented in these mutations.

from the wild-type envelope glycoprotein in fusogenic potential (Fig. 4). In contrast, V570A, G572A, and R579A failed to produce syncytia within 6 h of coculture, and L556A and L565A yielded 100-fold fewer syncytia than the wild-type glycoprotein. By 20 h of coculture, R579A, L556A, and L565A were able to generate similar numbers of syncytia as the wild-type envelope glycoprotein, but these syncytia were small and similar to those seen at 6 h with the wild-type glycoprotein. The V570A mutant produced only a few binucleated cells after 20 h of coculture, and G572A was entirely defective.

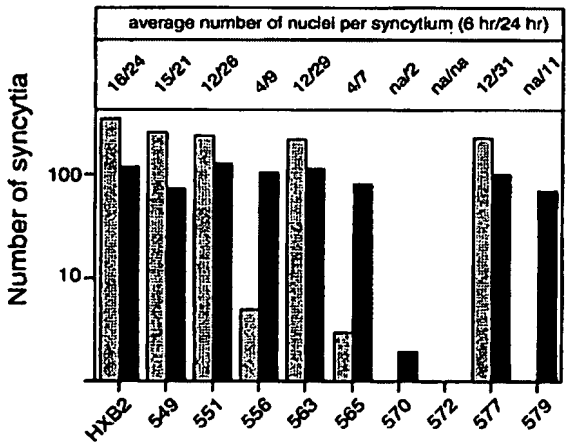

FIG. 4. Cell-cell fusion activity of mutant envelope glycoproteins. Cells expressing mutant and wild-type envelope glycoproteins were cocultured with U87-CD4-CXCR4 cells for either 6 or 24 h. Cultures were fixed with −20°C methanol-acetone (1:1), and envelope glycoprotein-expressing cells were visualized by immunochemical staining. The number of envelope glycoprotein-expressing cells involved in syncytium formation and the average number of nuclei contained within each syncytium were determined. Mutant envelope glycoprotein labels are abbreviated by the position number. The graph indicates the number of syncytia at 6 and 24 h (gray and black bars, respectively). The average size of the syncytia (number of nuclei per syncytium at 6 and 24 h) is indicated at the top. na, not applicable. Results depicted are from one experiment and are representative of relative differences among mutants. Note that the number of syncytia is biphasic with time and typically decreases at longer times as syncytia merge.

In summary, V570A, G572A, R579A, L556A, and L565A were severely debilitated in their ability to mediate membrane fusion (Table 1). Because the alanine substitutions in these mutants did not grossly affect envelope glycoprotein biosynthesis, our results raise the possibility that the alanine mutations may perturb the interhelical packing interactions in the gp41 core structure, thereby modulating the membrane fusion activity of the envelope glycoprotein complex.

Biophysical analysis of mutant N34(L6)C29 peptides. Variants of the recombinant N34(L6)C28 peptide with single alanine substitutions at the e and g positions of the N34 coiled coil were produced by bacterial expression and purified by reverse-phase high-performance liquid chromatography. Sedimentation equilibrium measurements indicated that each peptide sedimented as a discrete trimer over a total peptide concentration of 10 to 100 μM at neutral pH (Fig. 5A; Table 2). The helical content and stability of mutant N34(L6)C28 complexes were quantitated by CD. Each peptide was >90% helical at 4°C at 10 μM peptide (Table 2), and each exhibited a cooperative thermal unfolding transition (Fig. 5B; Table 2). Under these conditions, the midpoints of the thermal transition (T_m) for N34(L6)C28 (wild type), V549A, Q551A, L556A, Q563A, L565A, V570A, G572A, Q577A and R579A were 70, 73, 74, 64, 68, 50, 56, 82, 76, and 72°C, respectively (Fig. 5B; Table 2). Therefore, alanine mutations at the e and g residues of the N34 helix caused only changes in thermal stability, without significantly influencing the overall topology. In general, introduction of alanine for bulky hydrophobic residues markedly destabilized the trimer-of-hairpins structure; the decrease in thermal stability, ΔT_m, between the wild-type and mutant peptides was 6, 20, and 14°C for Leu-556, Leu-565, and Val-570, respectively. On the other hand, the Gly-572-to-Ala substitution led to appreciable stabilization of the trimer of hairpins, reinforcing the observation that glycine in α-helices is generally destabilizing (reviewed in reference 41).

These results indicate that the destabilization of the gp41 ectodomain core by alanine mutations at Leu-565 and Val-570 may underlie the fusion-defective phenotype of the mutant envelope glycoproteins (Tables 1 and 2). In contrast, alanine mutations at Gly-572 and Arg-579 stabilized the gp41 core structure but severely impaired membrane fusion activity. This effect on fusogenicity may reflect the reduced level of mature gp120 in these mutants. The L556A mutant had an intermediate phenotype, where both the thermal stability of the gp41 core and the level of cell surface gp120 in the envelope glycoprotein complex were slightly reduced. Interestingly, the Gly-572 residue is involved in the formation of hydrophobic cavities on the surface of the N34 trimer that are crucial for interhelical packing interactions (13, 35, 60). The Arg-579 side chain, on the other hand, does not directly participate in the helical interactions (13, 68, 69).

Crystal structures of G572A and R579A peptides. The unexpected observation that alanine mutations at Gly-572 and Arg-579 disrupt envelope glycoprotein function while maintaining the thermal stability of the gp41 ectodomain core led us to examine the atomic detail of the respective trimer-of-dimer

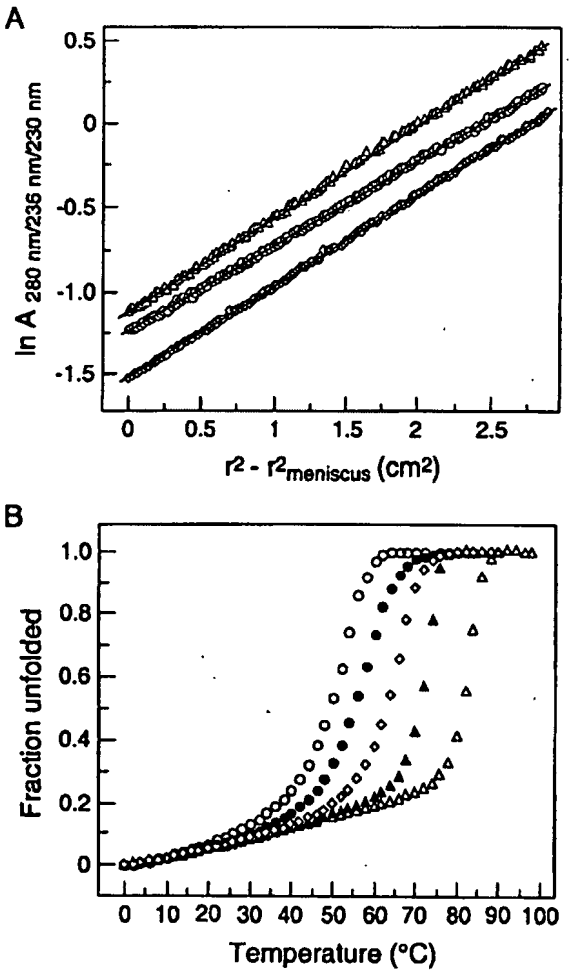

FIG. 5. Biophysical characterization of mutant N34(L6)C28 peptides. (A) The L556A (open rhombs), L565A (open circles), and G572A (open triangles) peptides form three-stranded bundles. Sedimentation equilibrium data (20 krpm) were collected at 20°C at pH 7.0 for L556A (30 μM), L565A (100 μM), and G572A (10 μM). The natural logarithm of the absorbance at 280, 236, and 230 nm is plotted against the square of the radial position. For an ideal single-species system, this plot is linear, with the slope proportional to the molecular weight of the molecule. (B) Thermal melts monitored by CD at 222 nm for L556A (open rhombs), L565A (open circles), V570A (solid circles), G572A (open triangles), and R579A (solid triangles) peptides at 10 μM at pH 7.0.

structures. The G572A and R579A peptides were crystallized, and their X-ray structures were determined to 2.1 and 1.8 Å, respectively, using molecular replacement methods. The crystals of both G572A and R579A belong to the space group *R*3 and contain the trimer formed around the crystallographic threefold axis. The electron density maps of G572A and R579A reveal the positions of all of the amino acid residues except a few disordered side chains at the helix termini (see Materials and Methods). Simulated-annealing omit maps were calculated to confirm the assignment of the side chains. The structure of the the G572A peptide was refined to a conventional *R*-factor of 20.6%, with a free *R*-factor of 23.4% over a

TABLE 2. Alanine mutants of the HIV-1 gp41 ectodomain core form trimer-of-hairpins structures

Mutant	$-[\theta]_{222}$ (degrees cm^2 dmol^{-1})	T_m (°C)	Molecular mass (kDa)
N34(L6)C28	31,300	70	24.4
V549A	31,100	73	23.9
Q551A	30,800	74	23.7
L556A	30,500	64	23.2
Q563A	31,200	68	24.2
L565A	31,500	50	22.9
V570A	29,900	56	23.3
G572A	31,400	82	23.5
Q577A	31,000	76	23.6
R579A	31,900	72	24.1

resolution range of 50.0 to 2.1 Å, and the final model consists of 61 amino acid residues and incorporates 38 water molecules and a sulfate ion. The structure of the R579A peptide was refined against 50.0 to 1.8 Å resolution data to yield a conventional *R*-factor of 17.9%, with a free *R*-factor of 19.8%, and the final model includes 61 residues, 83 water molecules, and a sulfate ion. Table 3 summarizes the data collection and refinement statistics for these two structures.

As expected, the overall folds of G572A and R579A are very similar to those of the wild-type molecule. In all cases, the interior N34 coiled coil of three parallel helices, wrapped in a gradual left-handed superhelix, is surrounded by a sheath of antiparallel C28 helices (Fig. 6). At the center of the trimer of hairpins, the N34 three-stranded coiled coil displays typical

TABLE 3. X-ray data collection and refinement statistics

Statistic	G572A	R579A
Unit cell dimensions		
a, b, c (Å)	52.06, 52.06, 59.74	51.25, 51.25, 59.87
α, β, γ (degrees)	90, 90, 120	90, 90, 120
Space group	*R*3	*R*3
Data processing		
Resolution (Å)	50–2.1	50–1.8
Measured reflections	23,645	40,929
Unique reflections	3,509	5,440
Completeness (%)	99.5	99.6
R_{merge} (%)[a]	2.9	3.5
Refinement		
Resolution (Å)	50–2.1	50–1.8
Reflections in working set	3,153	4,860
Reflections in test set	356	580
Protein nonhydrogen atoms	486	490
Water molecules	38	83
Sulfate ion	1	1
R_{free} (%)[b]	23.4	22.2
R_{cryst} (%)[b]	20.6	17.9
Average B-factor (Å)	37.8	19.8
Rms deviations from ideality		
Bond lengths (Å)	0.004	0.008
Bond angles (degrees)	0.7	1.0
Torsion angles (degrees)	15.0	14.8

[a] $R_{merge} = \Sigma|I - \langle I\rangle|/\Sigma I$, where I is the intensity of an individual measurement and $\langle I\rangle$ is the average intensity from multiply recorded reflections.

[b] $R_{cryst} = \Sigma||F_{obs}| - |F_{calc}||/\Sigma|F_{obs}|$, where F_{obs} and F_{calc} are observed and calculated structural factors, respectively. No σ-cutoff was applied. R_{free} is calculated for a set of reflections that were excluded from refinement.

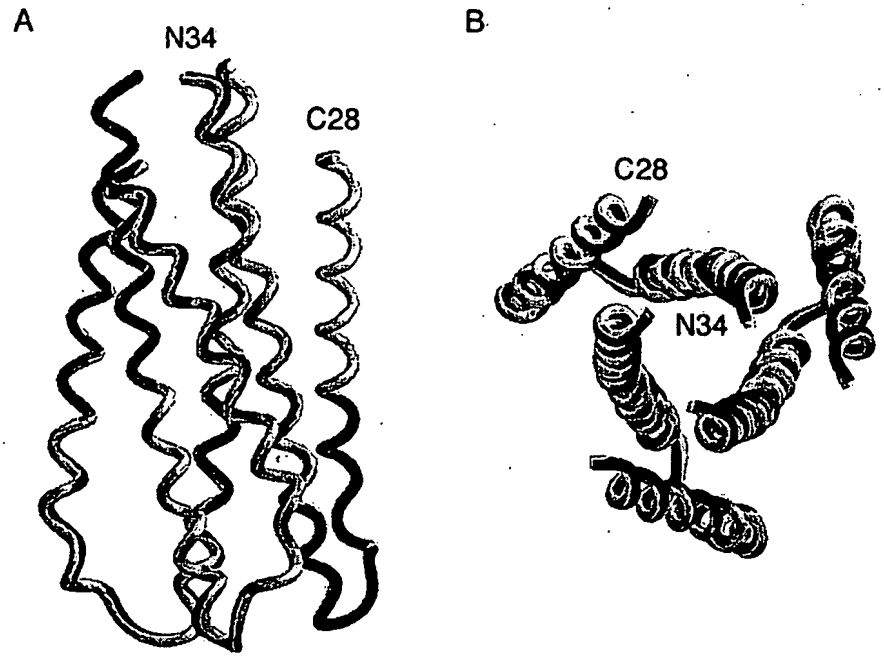

FIG. 6. Overall views of the mutant G572A and R579A peptide six-helix bundles. (A) Side view. The amino termini of N34 and the carboxyl termini of C28 are at the top of the figure. Helices of G572A (yellow) and R579A (pink) peptides were used for the superposition. (B) View from the top, looking down the threefold axis of the trimer of hairpins. Figures were generated with the program Setor (24).

acute knobs-into-holes packing, where the a and d side chains (knobs) fit into the spaces (holes) between four residues on the neighboring helices (Fig. 7A and B) (18, 30). Residues at the e and g positions of the N34 helices lie on the outside of the trimeric coiled coil and form three hydrophobic grooves on the surface of this coiled coil. The Gly-572 and Arg-579 residues replaced in G572A and R579A, respectively, are both in g positions of N34. The root-mean-square (rms) deviations between all Cα atoms of the central N34 coiled coil in the wild-type and mutant molecules are 0.27 Å for G572A and 0.30 Å for R579A. The C28 helices in G572A and R579A can also be superimposed upon the wild-type counterpart with rms deviations of 0.40 and 0.35 Å, respectively. Thus, the fusion-defective Gly-572-to-Ala and Arg-579-to-Ala mutations do not significantly alter the trimer-of-hairpins structure.

On the surface of the N34 trimeric coiled coil, there are three prominent, symmetry-related cavities (~400 Å^3) that each accommodate three hydrophobic residues from the abutting C28 helix: Trp-628, Trp-631, and Ile-635 (13, 68, 69). These conserved coiled-coil cavities have been shown to be critical for HIV-1 entry and its inhibition and provide a potential antiviral drug target (12, 13, 22, 25, 35, 66). The Gly-572 residue, which is involved in forming this cavity, is invariant in all 251 fully sequenced M group HIV-1 isolates (43). The substituted Ala-572 side chains point into the triangular interhelical space between two N34 helices and a buttressing C28 helix (Fig. 7C). The favorable van der Waals interactions between the Ala-572 and Trp-631 side chains can strengthen interhelical packing and stabilize the trimer-of-hairpins structure, as suggested by the large increase in T_m of G572A relative to that of N34(L6)C28. In addition, the Gly-572-to-Ala substitution also leads to local structural rearrangements: the side chains of Trp-628 and Ile-635 deviated substantially. Overall, the methyl groups of the Ala-572 residues in G572A pack efficiently into the hydrophobic cavity of N34 and make a good C28 interaction (Fig. 7C).

The conserved grooves along the N34 coiled-coil surface are lined with predominantly hydrophobic residues (Fig. 1C). Interestingly, the Arg-579 residue at a g position is completely conserved in 245 of the 251 sequenced HIV-1 strains. Of the remaining six isolates with different residues at this position, three possess a conservative lysine substitution (43). In gp41 core crystal structures (13, 68, 69), the Arg-579 side chain is poorly ordered, as suggested by very high individual atomic B factors. While electron density for Ala-579 in the R579A peptide is unambiguous, this substituted residue contributes little to the interhelical packing interactions. It would therefore appear that the slight stabilization of the trimer-of-hairpins structure associated with the alanine substitution at Arg-579 reflects the favorable helix propensity of alanine relative to arginine in the wild-type molecule.

DISCUSSION

The HIV-1 envelope glycoprotein complex controls the key process of viral entry. The current model of HIV-1 membrane fusion implies that, as the trimer of hairpins is assembled, a ready source of energy can be made available for overcoming the activation energy needed for lipid bilayer fusion. Because the native and prehairpin intermediate conformations of gp41 are not known, the basic property of gp41 activation during HIV-1 membrane fusion is not well understood. Nevertheless,

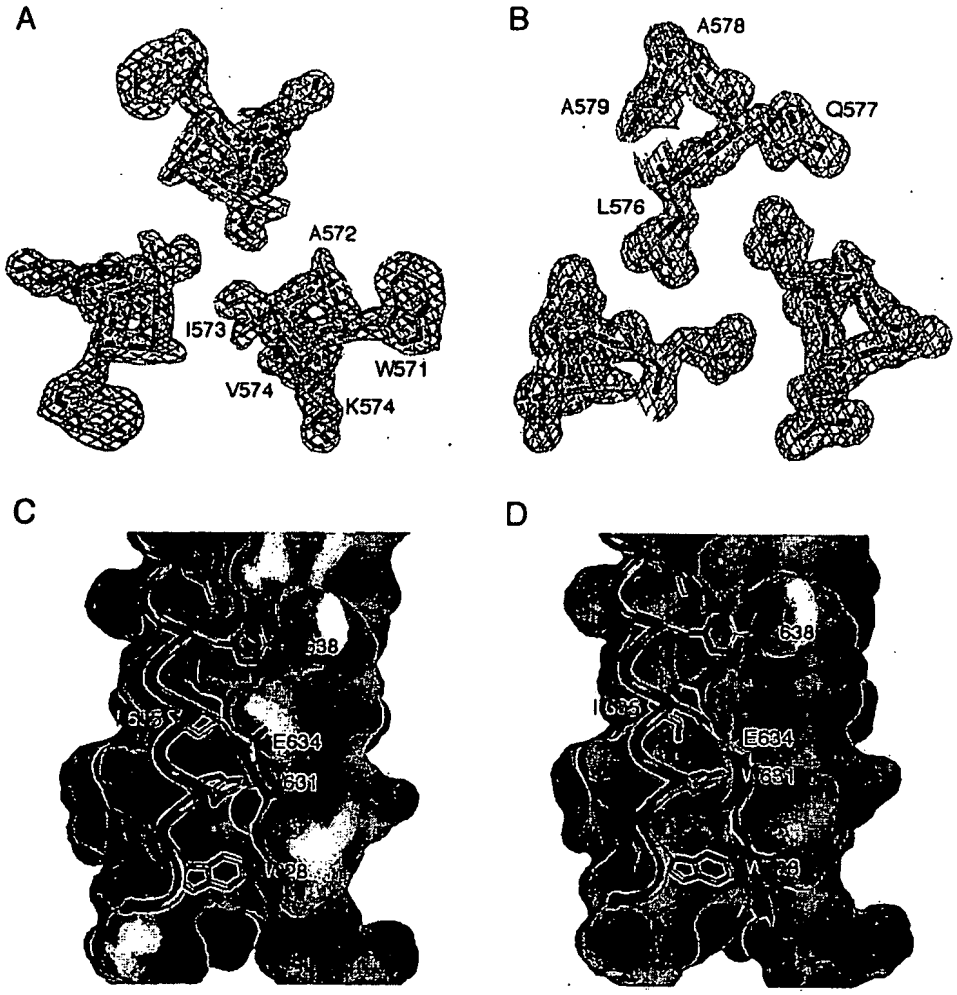

FIG. 7. Conserved interhelical interactions in the crystal structures of the G572A and R579A trimers. The final $2F_o - F_c$ electron density maps of the G572A and R579A peptides are shown with the refined model superimposed (panels A and B, respectively). Oxygen, nitrogen, and carbon atoms are colored red, blue, and yellow, respectively. The maps are contoured at 1.0 standard deviation above the average density. Interactions of the C28 helix with a deep cavity on the surface of the N34 coiled coil of the G572A and R579A peptides are shown (panels C and D, respectively). The C28 helices, represented as ribbons, are drawn against a surface representation of the N34 coiled coil. The side chains of the mutated residues are colored green. Figures were generated with the programs Setor (24) and Grasp (58).

as has been established for the case of influenza virus HA protein (6, 9, 74), it is widely believed that the native gp41 structure is substantially different from the fusogenic trimer-of-hairpins structure. In the simplest model, the N-terminal heptad repeat region of gp41 exists in an non-coiled-coil conformation in the native state but forms a coiled-coil trimer in the prehairpin intermediate and fusogenic hairpin conformations (16, 21, 34, 51, 70, 73). The N-terminal heptad repeat sequence is one of the most highly conserved regions within the primate immunodeficiency virus envelope glycoproteins (11, 20, 28). Residues at the a and d positions form a hydrophobic interface at the interior of the N-terminal trimeric coiled coil (62). There is only one nonconservative substitution at an a position between HIV-1 and SIV (Ile-573 in HIV-1 and Thr in the corresponding position of SIV). Mutations at this position affect the folding and stability of the gp41 ectodomain core and, coordinately, the ability of the mutant envelope glycoproteins to mediate membrane fusion (21, 49, 51). Formation of the N-terminal three-stranded coiled coil appears to occur as an early event in the gp41 refolding process.

The N-terminal coiled-coil surface contains three hydrophobic grooves that are the sites for the C-terminal helix interactions (13, 68, 69). The e and g residues lining these grooves pack against residues at the a and d positions of the C-terminal helices. The high sequence conservation at these contact positions has led to the proposal that interactions between the N- and C-terminal helices are important for the resolution of the prehairpin intermediate into the hairpin structure during membrane fusion (13, 68, 69). Indeed, mutagenesis studies demonstrate that mutations at these interhelical interface positions often abolish infectivity and membrane fusion (70, 71). This proposal is also consistent with a large body of data on the inhibition of HIV-1 infection and syncytium formation by derivatives of the peptides that make up the gp41 core (12, 35, 49,

61). In the present study, we have investigated the role of individual side chains at the nine e and g positions of the N34 coiled coil in conferring structural specificity and conformational stability to the gp41 core and in determining the fusion potential of the envelope glycoprotein complex.

Our alanine-scanning mutagenesis results show that the Leu-556, Leu-565, Val-570, Gly-572, and Arg-579 residues play a critical role in envelope glycoprotein function, while the Val-549, Gln-551, Gln-563, and Gln-577 side chains per se are not essential for this membrane fusion activity. These findings with regard to L556A, Q563A, V570A, G572A, and Q577A agree with those reported previously by Weiss and colleagues (70, 71). Our biophysical analysis reveals that alanine mutations in the fusion-defective L565A and V570A envelope glycoproteins destabilize the trimer of hairpins by a T_m shift of ~14 to 20°C. In contrast, the T_ms of the four mutant gp41 cores carrying the fusion-competent alanine substitutions are comparable to or even higher than that of the wild-type molecule. In general, the stability of the trimer-of-hairpins structure modulates the membrane fusion properties of the gp120-gp41 complex. Interestingly, the fusion-defective Gly-572-to-Ala and Arg-579-to-Ala mutations lead instead to enhanced stabilization of the gp41 core structure.

The conformational stability of the gp41 core structure is thought to play a critical role in the refolding of the envelope glycoprotein into a fusion-active conformation (33, 34, 49, 51). Although melting temperature has been useful as a qualitative guide to thermodynamic stability, it appears that the dependence of HIV-1 fusion potential on the stability of the trimer of hairpins can vary. In contrast to our previous observation that the Ile-573-to-Thr substitution decreases the thermal stability of the gp41 core by 25°C relative to the wild-type molecule and has only moderate effects on membrane fusion activity (49), we show here that a destabilization of the trimer of hairpins by a T_m shift of 14 to 20°C can markedly reduce the fusion potential of the envelope glycoprotein. It is possible that the a position Ile-573-to-Thr mutation affects formation of the N-terminal coiled coil of gp41 after interaction of the envelope glycoprotein complex with cellular receptors, while the alanine mutations at the e and g positions studied here act on the association of the C-terminal helices with the N-terminal coiled coil during the transition from the prehairpin intermediate to the trimer-of-hairpins structure.

The crystal structures of the wild-type gp41 core and the G572A and R579A mutants can be superimposed, with rms deviations of 0.39 and 0.40 Å, respectively. From the structures we can see that each substituted alanine side chain is readily accommodated in the trimer-of-hairpins structure by using different sets of atoms. Our data suggest that local structural perturbations in the gp41 core are unlikely to be a major cause of the fusion-defective phenotype of the G572A and R579A glycoproteins. Instead, both mutant proteins exhibit a reduction in the steady-state level of gp120 on the cell surface. In contrast to an earlier interpretation of the G572A phenotype (70), our results suggest that this reduction is not due to a deficiency in gp160 cleavage but may reflect an increase in gp120 shedding from the envelope glycoprotein complex. We propose that alanine mutations at Gly-572 and Arg-579 affect the association between the gp120 and gp41 subunits in the native envelope glycoprotein. This proposal is consistent with previous disulfide cross-linking studies that demonstrated the physical proximity of the Thr-605 residue of the gp41 ectodomain and the C-terminal region of gp120 (3). Therefore, we suggest that Gly-572 and Arg-579 are required for maintaining the structural integrity of the native gp120-gp41 complex. The defect in membrane fusion may reflect this instability and the resultant reduction in gp120 on the cell surface. Further studies of the G572A and R579A mutant glycoproteins may open new perspectives in the search for effective approaches to stabilizing the native envelope glycoprotein complex for vaccine development.

Several approaches towards antiviral intervention have recently converged to highlight the critical importance of transiently exposed conformations of the HIV-1 envelope glycoprotein. Synthetic peptides targeting the prehairpin intermediate of gp41 are now in clinical study (42). Small-molecule inhibitors of the formation of the trimer-of-hairpins structure have also been developed (22, 25, 66). Mutations in the envelope glycoprotein that specifically arrest the fusion process at critical steps may allow the accumulation of intermediates for vaccine development. Further analysis of protein structure and conformation will also provide insights into the complex biology of HIV-1 entry.

ACKNOWLEDGMENTS

This work was supported by National Institutes of Health grants AI48385 (M.L.) and AI44669 (J.H.N.). J.H.N. is grateful to the J. B. Pendleton Charitable Trustfor enabling the purchase of key instrumentation.

We thank Meg Trahey, Scott Larson, and Amanda Wilhelm for technical help in this project and George Lewis (Institute of Human Virology, University of Maryland) for providing Chessie B13 and 12 monoclonal antibodies.

REFERENCES

1. Abacioglu, Y. H., T. R. Fouts, J. D. Laman, E. Claassen, S. H. Pincus, J. P. Moore, C. A. Roby, R. Kamin-Lewis, and G. K. Lewis. 1994. Epitope mapping and topology of baculovirus-expressed HIV-1 gp160 determined with a panel of murine monoclonal antibodies. AIDS Res. Hum. Retrovir. 10:371–381.
2. Berger, E. A., P. M. Murphy, and J. M. Farber. 1999. Chemokine receptors as HIV-1 coreceptors: roles in viral entry, tropism, and disease. Annu. Rev. Immunol. 17:657–700.
3. Binley, J. M., R. W. Sanders, B. Clas, N. Schuelke, A. Master, Y. Guo, F. Kajumo, P. J. Maddon, W. C. Olson, and J. P. Moore. 2000. A recombinant human immunodeficiency virus type 1 envelope glycoprotein complex stabilized by an intermolecular disulfide bond between gp120 and gp41 subunits is an antigenic mimic of the trimeric virion-associated structure. J. Virol. 74:627–643.
4. Brünger, A. T. 1992. XPLOR version 3.1: a system for X-ray crystallography and NMR. Yale University Press, New Haven, Conn.
5. Brünger, A. T., P. D. Adams, G. M. Clore, W. L. DeLano, P. Gros, R. W. Grosse-Kunstleve, J.-S. Jiang, J. Kuszewski, M. Nilges, N. S. Pannu, R. J. Read, L. M. Rice, T. Simonson, and G. L. Warren. 1998. Crystallography & NMR system: a new software suite for macromolecular structure determination. Acta Crystallogr. D54:905–921.
6. Bullough, P. A., F. M. Hughson, J. J. Skehel, and D. C. Wiley. 1994. Structure of influenza haemagglutinin at the pH of membrane fusion. Nature 371:37–43.
7. Cantor, C., and P. Schimmel. 1980. Biophysical chemistry, part III. W. H. Freeman and Company, New York, N.Y.
8. Cao, J., L. Bergeron, E. Helseth, M. Thali, H. Repke, and J. Sodroski. 1993. Effects of amino acid changes in the extracellular domain of the human immunodeficiency virus type 1 gp41 envelope glycoprotein. J. Virol. 67:2747–2755.
9. Carr, C. M., and P. S. Kim. 1993. A spring-loaded mechanism for the conformational change of influenza hemagglutinin. Cell 73:823–832.
10. CCP4. 1994. Collaborative computational project number 4. Acta Crystallogr. D50:760–763.
11. Chambers, P., C. R. Pringle, and A. J. Easton. 1990. Heptad repeat sequences are located adjacent to hydrophobic regions in several types of virus

fusion glycoproteins. J. Gen. Virol. 71:3075–3080.
12. Chan, D. C., C. T. Chutkowski, and P. S. Kim. 1998. Evidence that a prominent cavity in the coiled coil of HIV type 1 gp41 is an attractive drug target. Proc. Natl. Acad. Sci. USA 95:15613–15617.
13. Chan, D. C., D. Fass, J. M. Berger, and P. S. Kim. 1997. Core structure of gp41 from the HIV envelope glycoprotein. Cell 89:263–273.
14. Chan, D. C., and P. S. Kim. 1998. HIV entry and its inhibition. Cell 93:681–684.
15. Chen, C. H., T. J. Matthews, C. B. McDonal, D. P. Bolognesi, and M. L. Greenberg. 1995. A molecular clasp in the human immunodeficiency virus (HIV) type 1 TM protein determines the anti-HIV activity of gp41 derivatives: implication for viral fusion. J. Virol. 69:3771–3777.
16. Chen, S. S.-L., C.-N. Lee, W.-R. Lee, K. McIntosh, and T.-H. Lee. 1993. Mutational analysis of the leucine zipper-like motif of the human immunodeficiency virus type 1 envelope transmembrane protein. J. Virol. 67:3615–3619.
17. Chen, Y.-H., J. T. Yang, and K. H. Chau. 1974. Determination of the helix and β form of proteins in aqueous solution by circular dichroism. Biochemistry 13:3350–3359.
18. Crick, F. H. C. 1953. The packing of α-helices: simple coiled coils. Acta Crystallogr. 6:689–697.
19. Cunningham, B. C., and J. A. Wells. 1989. High-resolution epitope mapping of hGH-receptor interactions by alanine-scanning mutagenesis. Science 244: 1081–1085.
20. Delwart, E. J., G. Mosialos, and T. Gilmore. 1990. Retroviral envelope glycoproteins contain a "leucine zipper"-like repeat. AIDS Res. Hum. Retrovir. 6:703–706.
21. Dubay, J. W., S. J. Roberts, B. Brody, and E. Hunter. 1992. Mutations in the leucine zipper of the human immunodeficiency virus type 1 transmembrane glycoprotein affect fusion and infectivity. J. Virol. 66:4748–4756.
22. Eckert, D. M., V. N. Malashkevich, L. H. Hong, P. A. Carr, and P. S. Kim. 1999. Inhibiting HIV-1 entry: discovery of D-peptide inhibitors that target the gp41 coiled-coil pocket. Cell 99:103–115.
23. Edelhoch, H. 1967. Spectroscopic determination of tryptophan and tyrosine in proteins. Biochemistry 6:1948–1954.
24. Evans, S. V. 1993. SETOR: hardware-lighted three-dimensional solid model representations of macromolecules. J. Mol. Graph. 11:134–138.
25. Ferrer, M., T. M. Kapoor, T. Strassmaier, W. Weissenhorn, J. J. Skehel, D. Oprian, S. L. Schreiber, D. C. Wiley, and S. C. Harrison. 1999. Selection of gp41-mediated HIV-1 cell entry inhibitors from biased combinatorial libraries of nonnatural binding elements. Nat. Struct. Biol. 6:953–960.
26. Freed, E. O., D. J. Myers, and R. Risser. 1989. Mutational analysis of the cleavage sequence of the human immunodeficiency virus type 1 envelope glycoprotein precursor gp160. J. Virol. 63:4670–4675.
27. Furuta, R. A., C. T. Wild, Y. Weng, and C. D. Weiss. 1998. Capture of an early fusion-active conformation of HIV-1 gp41. Nat. Struct. Biol. 5:276–279.
28. Gallaher, W. R., J. M. Ball, R. F. Garry, M. C. Griffin, and R. C. Montelaro. 1989. A general model for the transmembrane proteins of HIV and other retroviruses. AIDS Res. Hum. Retrovir. 5:431–440.
29. Gao, F., S. G. Morrison, D. L. Robertson, C. L. Thornton, S. Craig, G. Karlsson, J. Sodroski, M. Morgado, B. Galvao-Castro, H. von Briesen, S. Beddows, J. Weber, P. M. Sharp, G. M. Shaw, B. H. Hahn, and WHO and NIAID Networks for HIV Isolation and Characterization. 1996. Molecular cloning and analysis of functional envelope genes from human immunodeficiency virus type 1 sequence subtypes A through G. J. Virol. 70:1651–1667.
30. Harbury, P. B., P. S. Kim, and T. Alber. 1994. Crystal structure of an isoleucine-zipper trimer. Nature 371:80–83.
31. Hill, C. M., H. Deng, D. Unutmaz, V. N. Kewalramani, L. Bastiani, M. K. Gorny, S. Zolla-Pazner, and D. R. Littman. 1997. Envelope glycoproteins from human immunodeficiency virus types 1 and 2 and simian immunodeficiency virus can use human CCR5 as a coreceptor for viral entry and make direct CD4-dependent interactions with this chemokine receptor. J. Virol. 71:6296–6304.
32. Hughson, F. M. 1997. Enveloped viruses: a common mode of membrane fusion? Curr. Biol. 7:R565–R569.
33. Jelesarov, I., and M. Lu. 2001. Thermodynamics of trimer-of-hairpins formation by the SIV gp41 envelope protein. J. Mol. Biol. 307:637–656.
34. Ji, H., C. Bracken, and M. Lu. 2000. Buried polar interactions and conformational stability in the simian immunodeficiency virus (SIV) gp41 core. Biochemistry 39:676–685.
35. Ji, H., W. Shu, F. T. Burling, S. Jiang, and M. Lu. 1999. Inhibition of human immunodeficiency virus type 1 infectivity by the gp41 core: role of a conserved hydrophobic cavity in membrane fusion. J. Virol. 73:8578–8586.
36. Jiang, S., K. Lin, and M. Lu. 1998. A conformation-specific monoclonal antibody reacting with fusion-active gp41 from the human immunodeficiency virus type 1 envelope glycoprotein. J. Virol. 72:10213–10217.
37. Jiang, S., K. Lin, N. Strick, and A. R. Neurath. 1993. HIV-1 inhibition by a peptide. Nature 365:113.
38. Johnson, M. L., J. J. Correia, D. A. Yphantis, and H. R. Halvorson. 1981. Analysis of data from the analytical ultracentrifuge by nonlinear least-squares techniques. Biophys. J. 36:575–588.
39. Jones, P. L., T. Korte, and R. Blumenthal. 1998. Conformational changes in cell surface HIV-1 envelope glycoproteins are triggered by cooperation between cell surface CD4 and coreceptors. J. Biol. Chem. 273:404–409.
40. Jones, T. A., J. W. Zou, S. W. Cowan, and M. Kjelgaard. 1991. Improved methods for building protein models in electron density maps and the location of errors in these models. Acta Crystallogr. D47:110–119.
41. Kallenbach, N. R., P. Lyu, and H. Zhou. 1996. CD spectroscopy and the helix-coil transition in peptides and polypeptides, p. 201–259. *In* G. D. Fasman (ed.), Circular dichroism and the conformational analysis of biomolecules. Plenum Press, New York, N.Y.
42. Kilby, J. M., S. Hopkins, T. M. Venetta, B. DiMassimo, G. A. Cloud, J. Y. Lee, L. Alldredge, E. Hunter, D. Lambert, D. Bolognesi, T. Matthews, M. R. Johnson, M. A. Nowak, G. M. Shaw, and M. S. Saag. 1998. Potent suppression of HIV-1 replication in humans by T-20, a peptide inhibitor of gp41-mediated virus entry. Nat. Med. 4:1302–1307.
43. Kuiken, C., B. Foley, B. Hahn, P. Marx, F. McCutchan, J. W. Mellors, J. Mullins, S. Wolinsky, and B. Korber. 2000. Human retroviruses and AIDS: a compilation and analysis of nucleic acid and amino acid sequences. Theoretical Biology and Biophysics Group, Los Alamos National Laboratory, Los Alamos, N.Mex.
44. Kunkel, T. A., J. D. Roberts, and R. A. Zakour. 1987. Rapid and efficient site-specific mutagenesis without phenotypic selection. Methods Enzymol. 154:367–382.
45. LaCasse, R. A., K. E. Follis, T. Moudgil, M. Trahey, J. M. Binley, V. Planelles, S. Zolla-Pazner, and J. H. Nunberg. 1998. Coreceptor utilization by human immunodeficiency virus type 1 is not a primary determinant of neutralization sensitivity. J. Virol. 72:2491–2495.
46. Laskowski, R. A., M. V. MacArthur, D. D. Moss, and J. M. Thornton. 1993. PROCHECK: a program to check the stereochemical quality of protein structures. J. Appl. Crystallogr. 26:283–291.
47. Laue, T. M., B. D. Shah, T. M. Ridgeway, and S. L. Pelletier. 1992. Computer-aided interpretation of analytical sedimentation data for proteins, p. 90–125. *In* S. E. Harding, A. J. Rowe, and J. C. Horton (ed.), Analytical ultracentrifugation in biochemistry and polymer science. Royal Society of Chemistry, Cambridge, England.
48. Lisanti, M. P., M. Sargiacomo, L. Graeve, A. R. Saltiel, and E. Rodriguez-Boulan. 1988. Polarized apical distribution of glycosyl-phosphatidylinositol-anchored proteins in a renal epithelial cell line. Proc. Natl. Acad. Sci. USA 85:9557–9561.
49. Liu, J., W. Shu, M. B. Fagan, J. H. Nunberg, and M. Lu. 2001. Structural and functional analysis of the HIV-1 gp41 core containing an Ile573 to Thr substitution: implications for membrane fusion. Biochemistry 40:2797–2807.
50. Lu, M., S. C. Blacklow, and P. S. Kim. 1995. A trimeric structural domain of the HIV-1 transmembrane glycoprotein. Nat. Struct. Biol. 2:1075–1082.
51. Lu, M., H. Ji, and S. Shen. 1999. Subdomain folding and biological activity of the core structure from human immunodeficiency virus type 1 gp41: implications for viral membrane fusion. J. Virol. 73:4433–4438.
52. Lu, M., and P. S. Kim. 1997. A trimeric structural subdomain of the HIV-1 transmembrane glycoprotein. J. Biomol. Struct. Dyn. 15:465–471.
53. Luciw, P. A. 1996. Human immunodeficiency viruses and their replication, p. 1881–1952. *In* B. N. Fields, D. M. Knipe, P. M. Howley, R. M. Chanock, J. L. Melinick, T. P. Monath, B. Roizman, and S. E. Straus (ed.), Fields virology. Lippincott-Raven, Philadelphia, Pa.
54. Malashkevich, V. N., D. C. Chan, C. T. Chutkowski, and P. S. Kim. 1998. Crystal structure of the simian immunodeficiency virus (SIV) gp41 core: conserved helical interactions underlie the broad inhibitory activity of gp41 peptides. Proc. Natl. Acad. Sci. USA 95:9134–9139.
55. McKeating, J. A., A. McKnight, and J. P. Moore. 1991. Differential loss of envelope glycoprotein gp120 from virions of human immunodeficiency virus type 1 isolates: effects on infectivity and neutralization. J. Virol. 65:852–860.
56. Munoz-Barroso, I., S. Durell, K. Sakaguchi, E. Appella, and R. Blumenthal. 1998. Dilation of the human immunodeficiency virus-1 envelope glycoprotein fusion pore revealed by the inhibitory action of a synthetic peptide from gp41. J. Cell Biol. 140:315–323.
57. Navaza, J. 1994. AMoRe: an automated package for molecular replacement. Acta Crystallogr. A50:157–163.
58. Nichols, A., K. Sharp, and B. Honig. 1991. Protein folding and association: insights from the interfacial and thermodynamic properties of hydrocarbons. Proteins Struct. Funct. Genet. 11:281–296.
59. Otwinowski, Z., and W. Minor. 1996. Processing X-ray diffraction data collected in oscillation mode. Methods Enzymol. 276:307–326.
60. Rimsky, L. T., D. C. Shugars, and T. J. Matthews. 1998. Determinants of human immunodeficiency virus type 1 resistance to gp41-derived inhibitory peptides. J. Virol. 72:986–993.
61. Root, M. J., M. S. Kay, and P. S. Kim. 2001. Protein design of an HIV-1 entry inhibitor. Science 291:884–888.
62. Shu, W., H. Ji, and M. Lu. 1999. Trimerization specificity in HIV-1 gp41: analysis with a GCN4 leucine zipper model. Biochemistry 38:5378–5385.
63. Shu, W., J. Liu, H. Ji, L. Radigen, S. Jiang, and M. Lu. 2000. Helical interactions in the HIV-1 gp41 core reveal structural basis for the inhibitory activity of gp41 peptides. Biochemistry 39:1634–1642.
64. Skehel, J. J., and D. C. Wiley. 1998. Coiled coils in both intracellular vesicle and viral membrane fusion. Cell 95:871–874.

65. Sodroski, J., W. C. Goh, C. Rosen, and W. A. Haseltine. 1986. Role of the HTLVIII/LAV envelope in syncytium formation and cytopathicity. Nature 322:470–474.
66. Sodroski, J. G. 1999. HIV-1 entry inhibitors in the side pocket. Cell 99:243–246.
67. Studier, F. W., A. H. Rosenberg, J. J. Dunn, and J. W. Dubendorff. 1990. Use of T7 RNA polymerase to direct expression of cloned genes. Methods Enzymol. 185:60–89.
68. Tan, K., J. Liu, J. Wang, D. Shen, and M. Lu. 1997. Atomic structure of a thermostable subdomain of HIV-1 gp41. Proc. Natl. Acad. Sci. USA 94: 12303–12308.
69. Weissenhorn, W., A. Dessen, S. C. Harrison, J. J. Skehel, and D. C. Wiley. 1997. Atomic structure of the ectodomain from HIV gp41. Nature 387:426–430.
70. Weng, Y., and C. D. Weiss. 1998. Mutational analysis of residues in the coiled-coil domain of human immunodeficiency virus type 1 transmembrane protein gp41. J. Virol. 72:9676–9682.
71. Weng, Y., Z. Yang, and C. D. Weiss. 2000. Structure-function studies of the self-assembly domain of the human immunodeficiency virus type 1 transmembrane protein gp41. J. Virol. 74:5368–5372.
72. Wild, C., T. Greenwell, D. Shugars, L. Rimsky-Clarke, and T. Matthews. 1995. The inhibitory activity of an HIV type 1 peptide correlates with its ability to interact with a leucine zipper structure. AIDS Res. Hum. Retrovir. 11:323–325.
73. Wild, C. T., D. C. Shugars, T. K. Greenwell, C. B. McDanal, and T. J. Matthews. 1994. Peptides corresponding to a predictive a-helical domain of human immunodeficiency virus type 1 gp41 are potent inhibitors of virus infection. Proc. Natl. Acad. Sci. USA 91:9770–9774.
74. Wilson, I. A., J. J. Skehel, and D. C. Wilson. 1981. Structure of the haemagglutinin membrane glycoprotein of influenza virus at 3 Å resolution. Nature 289:366–375.
75. Wyatt, R., and J. Sodroski. 1998. The HIV-1 envelope glycoproteins: fusogens, antigens, and immunogens. Science 280:1884–1888.
76. York, J., K. E. Follis, M. Trahey, P. N. Nyambi, S. Zolla-Pazner, and J. H. Nunberg. 2001. Antibody binding and neutralization of primary and T-cell line-adapted isolates of human immunodeficiency virus type 1. J. Virol. 75:2741–2752.

Cell, Vol. 89, 263–273, April 18, 1997, Copyright ©1997 by Cell Press

Core Structure of gp41 from the HIV Envelope Glycoprotein

David C. Chan,*† Deborah Fass,*† James M. Berger,* and Peter S. Kim*†
*Whitehead Institute for Biomedical Research
Cambridge, Massachusetts 02142
†Howard Hughes Medical Institute
Department of Biology
Massachusetts Institute of Technology
Cambridge, Massachusetts 02142

Summary

The envelope glycoprotein of human immunodeficiency virus type 1 (HIV-1) consists of a complex of gp120 and gp41. gp120 determines viral tropism by binding to target-cell receptors, while gp41 mediates fusion between viral and cellular membranes. Previous studies identified an α-helical domain within gp41 composed of a trimer of two interacting peptides. The crystal structure of this complex, composed of the peptides N36 and C34, is a six-helical bundle. Three N36 helices form an interior, parallel coiled-coil trimer, while three C34 helices pack in an oblique, antiparallel manner into highly conserved, hydrophobic grooves on the surface of this trimer. This structure shows striking similarity to the low-pH-induced conformation of influenza hemagglutinin and likely represents the core of fusion-active gp41. Avenues for the design/discovery of small-molecule inhibitors of HIV infection are directly suggested by this structure.

Introduction

The surface glycoproteins of enveloped viruses play critical roles in the initial events of viral infection, mediating virion attachment to cells and fusion of the viral and cellular membranes. Envelope glycoproteins are also major targets for the anti-viral immune response in infected hosts. The human immunodeficiency virus type 1 (HIV-1) envelope glycoprotein consists of two noncovalently associated subunits, gp120 and gp41, that are generated by proteolytic cleavage of a precursor polypeptide, gp160 (review, Luciw, 1996; Freed and Martin, 1995). gp120 directs target-cell recognition and viral tropism through interaction with the cell-surface receptor CD4 and one of several coreceptors that are members of the chemokine receptor family (Broder and Dimitrov, 1996; D'Souza and Harden, 1996; Wilkinson, 1996). The membrane-spanning gp41 subunit then promotes fusion of the viral and cellular membranes, a process that results in the release of viral contents into the host cell.

The HIV envelope glycoprotein complex shares several features with other viral membrane-fusion proteins, including the hemagglutinin (HA) protein of influenza virus, for which the mechanism of membrane fusion has been studied in greater detail (Wiley and Skehel, 1987; Stegmann and Helenius, 1993). For example, HA is proteolytically processed, as is the HIV envelope precursor, to generate a receptor-binding subunit (HA_1) and a membrane-spanning subunit (HA_2) which contains the "fusion" peptide. The hydrophobic fusion-peptide region of HA is known to insert into target membranes as an early event in the membrane fusion process (Stegmann et al., 1991; Tsurudome et al., 1992). In both gp41 and HA_2, the fusion-peptide region begins immediately at the new amino terminus that results from proteolytic processing reviews, (Wiley and Skehel, 1987; Hunter and Swanstrom, 1990; White, 1992). In several viral membrane-fusion proteins, including gp41 and HA_2, the region following the fusion peptide has a high α-helical propensity and a 4-3 heptad repeat of hydrophobic residues, a sequence feature characteristic of coiled coils (Chambers et al., 1990; Delwart et al., 1990; Gallaher et al., 1989). X-ray crystallographic studies of fragments of HA_2 and the transmembrane (TM) subunit of Moloney murine leukemia virus (Mo-MLV) demonstrate that these heptad-repeat regions do form coiled coils, in both cases as homotrimers (Bullough et al., 1994; Fass et al., 1996).

Numerous studies have led to the proposal that there are native (nonfusogenic) and fusion-active (fusogenic) states of viral membrane fusion proteins. In the native HA_1/HA_2 influenza complex, for example, part of the heptad-repeat region of HA_2 folds as a nonhelical loop (Wilson et al., 1981) but converts to a coiled coil when exposed to low pH (Bullough et al., 1994). Since low pH also activates influenza membrane fusion, this conformation of HA is generally regarded to be fusogenic, and we will refer to it as such. The loop to coiled-coil transition is the basis of the "spring-loaded" mechanism for activation of membrane fusion (Carr and Kim, 1993).

Extensive conformational changes in the HIV envelope complex are also thought to be involved in the transition from the native to the fusogenic state. Binding of CD4 to gp120 exposes the V3 loop of gp120, which likely interacts with the coreceptors (Choe et al., 1996; Trkola et al., 1996; Wu et al., 1996). For some laboratory-adapted isolates of HIV-1, the conformational changes in gp120 upon CD4 binding are sufficient to cause gp120 to physically dissociate or "shed" from the viral surface, leaving the membrane-anchored gp41 subunit behind (Moore et al., 1990; Hart et al., 1991). Primary isolates of the virus generally do not shed gp120 readily in the presence of CD4 alone, although CD4 binding still induces conformational changes in gp120 (Sattentau and Moore, 1993; Sattentau et al., 1993; Sullivan et al., 1995; Stamatatos and Cheng-Mayer, 1995). CD4 binding also induces conformational changes in gp41, as inferred from changes in antibody binding and sensitivity to limited proteolysis (Sattentau and Moore, 1991, 1993). Moreover, addition of low levels of soluble CD4 enhances the infectivity of some viral isolates, suggesting that the gp120/gp41 conformational changes induced by CD4 play a role in membrane fusion (Allan et al., 1990; Sullivan et al., 1995). These conformational changes are thought to expose the hydrophobic, glycine-rich fusion-peptide region of gp41 that is essential for membrane-fusion activity.

N-36 TREIMER

It has not yet been possible to obtain a detailed structure for gp41, either alone or in complex with gp120. We have therefore applied a protein-dissection approach, in which key substructures of a protein are identified and studied (e.g., Oas and Kim, 1988). Protein dissection has been used successfully to study other viral membrane fusion proteins (Carr and Kim, 1993; Bullough et al., 1994; Fass and Kim, 1995; Fass et al., 1996). Limited proteolysis of a fragment corresponding to the ectodomain of gp41 generated a stable, soluble complex composed of two peptide fragments denoted N51 and C43 (Figure 1) that are derived from the N- and C-terminal regions of the ectodomain, respectively (Lu et al., 1995). The N51 peptide corresponds to the 4-3 hydrophobic repeat region adjacent to the fusion peptide, while the C43 peptide is derived from the region prior to the transmembrane segment (Figure 1).

Interestingly, isolated peptides that overlap, or are derived from, the N51 and C43 regions of gp41 can have potent anti-viral activity (Wild et al., 1992, 1994b; Jiang et al., 1993). Peptides from the C-terminal region of the ectodomain have the highest activity. Consistent with these studies, both N51 and C43 are capable of inhibiting HIV envelope–mediated cell fusion; the C43 peptide exhibits 10-fold greater activity than N51 (Lu et al., 1995). The inhibitory activity of the C43 peptide, however, is markedly reduced when stoichiometric amounts of N51 are present, suggesting that the C43 peptide inhibits membrane fusion in a dominant-negative manner, by associating with an N51 region within intact gp41 (Lu et al., 1995). Thus, in addition to providing insights into the mechanism of membrane fusion, determining the structural basis for interaction between the N51 and C43 regions could assist anti-viral drug-development efforts.

Biophysical studies showed that the N51 and C43 peptides associate to form a highly thermostable, helical, trimeric complex of heterodimers, in which the N51 and C43 helices are oriented in an antiparallel manner (Lu et al., 1995). Analogous experiments with the gp41 ectodomain from simian immunodeficiency virus (SIV) gave almost identical results, indicating that the gp41 core identified in these protein-dissection studies is conserved among lentiviruses (Blacklow et al., 1995). On the basis of these results and other considerations, we proposed that the gp41 core consists of an interior coiled-coil trimer formed by the N51 region, against which three C43 helices pack (Blacklow et al., 1995; Lu et al., 1995).

The thermal denaturation of the N51/C43 complexes from HIV-1 or SIV gp41 are irreversible, probably as a result of aggregation of the unfolded peptides at high temperature (Lu et al., 1995; Blacklow et al., 1995). With a view toward crystallographic studies, further protein dissection experiments were used to define a slightly smaller subdomain with more favorable thermodynamic properties. These studies (M. Lu and P. S. K., unpublished data) led to the identification of the peptides N36 and C34 (Figure 1). Like the longer peptides, N36 and C34 form a stable, trimeric complex of heterodimers with 100% helix content. Unlike the larger complex, however, the N36/C34 complex has a reversible thermal unfolding transition (M. Lu and P. S. K., unpublished data). Here we present the crystal structure of this complex solved to 2.0 Å resolution and discuss the implications of this structure for HIV viral membrane fusion and its inhibition.

Results

Crystals of N36/C34 were grown by sitting-drop vapor diffusion (see Experimental Procedures). An initial model of the complex was built into an electron density map generated by multiwavelength anomalous dispersion (MAD) analysis (review, Hendrickson, 1991) of an osmium-derivatized crystal. Details of data collection and MAD phasing statistics are listed in Table 1. A representative portion of the solvent-flattened electron density map used for building the initial model is shown in Figure 2. The structure was refined against data to 2.0 Å from a native crystal to yield an R_{free} of 0.266 and an R_{cryst} of 0.238 (Table 1).

Structure of the N36/C34 Complex

The N36/C34 complex is a six-stranded helical bundle (Figure 3). The center of this bundle consists of a parallel, trimeric coiled coil of three N36 helices wrapped in a gradual left-handed superhelix. Three C34 helices wrap antiparallel to the N36 helices in a left-handed direction around the outside of the central coiled-coil trimer. This arrangement of helices was anticipated on the basis of sequence analysis and biophysical studies (Lu et al., 1995; Blacklow et al., 1995). The overall dimensions of this complex comprise a cylinder measuring ~35 Å in diameter and ~55 Å in height.

As in other naturally occurring coiled coils (Cohen and Parry, 1990), the interior residues at the a and d positions of the N36 heptad repeat are predominantly hydrophobic, although occasional buried polar interactions are also present in the central three-stranded coiled coil (Figure 4). A sequence comparison of HIV-1 (HXB2 strain) and SIV (Mac239 strain) gp41 shows that the residues at these two heptad-repeat positions are highly

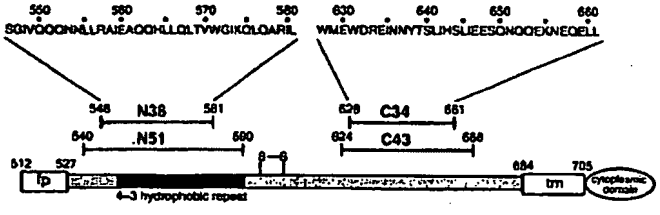

Figure 1. Interacting Peptides Identified in HIV gp41

A schematic view of gp41 showing important functional regions, including the 4-3 hydrophobic repeat, the fusion peptide (fp), a disulfide linkage (S-S), and the transmembrane region (tm). The ectodomain is drawn approximately to scale. The peptides identified by protein dissection are shown above, along with the sequences of N36 and C34. The residues are numbered according to their position in gp160.

Table 1. Crystallographic and Refinement Statistics

Data Collection

Crystal	λ (Å)	Complete (%)	R_{sym}[a] (%)	Resol. (Å)
Native	1.5418	96.5	5.5	2.0
OsO_4 λ1	1.1398	96.4	4.3	2.7
OsO_4 λ2	1.1396	96.4	4.3	2.7
OsO_4 λ3	1.1344	96.8	4.5	2.7
OsO_4 λ4	1.1406	93.4	4.5	2.7

Phasing Statistics[a] (12–2.7 Å)

Derivative	R_{iso}[b] (%)	R_{cr}[c] (%) (weighted)	R_{cullis}[d] Acentric	R_{cullis}[d] Centric	R_{cullis}[d] Anom.	Ph. power[e] Acentric	Ph. power[e] Centric	Occ.[f]	Anom. Occ.[f]
OsO_4 λ1 vs. λ4	4.4	6.7	0.46	0.53	0.21	2.46	1.53	0.075	2.165
OsO_4 λ2 vs. λ4	6.6	9.3	0.37	0.37	0.22	3.34	2.36	0.132	1.784
OsO_4 λ3 vs. λ4	5.4	7.4	0.42	0.44	0.35	2.94	2.12	0.105	1.005

Refinement Statistics (12–2.0 Å)

Nonhydrogen Protein Atoms	Waters	Number of Reflections: Working	Number of Reflections: Free	R_{cryst}[g]	R_{free}[g]	rms Deviations: Bonds (Å)	rms Deviations: Angles (°)
596	43	5212	371 (7.12%)	0.238	0.266	0.014	2.742

[a] $R_{sym} = \Sigma_j|I_j - \langle I\rangle| / \Sigma|\langle I\rangle|$, where I_j is the recorded intensity of the reflection j and $\langle I\rangle$ is the mean recorded intensity over multiple recordings.

[b] $R_{iso} = \Sigma||F_{h\lambda i}| \pm |F_{p\lambda i}| - |F_{p\lambda 4}|| / \Sigma|F_{p\lambda 4}|$, where $F_{h\lambda i}$ is the structure factor at wavelength λi and $F_{p\lambda 4}$ is the structure factor at the reference wavelength λ4.

[c] $R_{cr} = [\Sigma|(|F^+_{h\lambda i}| - \Phi_{meas}) / \varphi F^+_{h\lambda i}| + |(|F^-_{h\lambda i}| - \Phi_{meas}) / \varphi F^-_{h\lambda i}|) / [\Sigma|(|F^+_{h\lambda i}| / \varphi F^+_{h\lambda i}) + (|F^-_{h\lambda i}| / \varphi F^-_{h\lambda i})|]$, where $\Phi_{meas} = [(|F^+_{h\lambda i}| / \varphi F^+_{h\lambda i}) + (|F^-_{h\lambda i}| / \varphi F^-_{h\lambda i})] / [(1/\varphi F^+_{h\lambda i}) + (1/\varphi F^-_{h\lambda i})]$ and $\varphi F^2_{h\lambda i} = [\text{Variance } (F^2_{h\lambda i})]4F^2_{h\lambda i}$.

[d] $R_{cullis} = \Sigma||F_{h\lambda i}| \pm |F_{p\lambda i}| - |F_{h\lambda i,calc}||/\Sigma|F_{h\lambda i} \pm F_{p\lambda i}|$, where $F_{h\lambda i,calc}$ is the calculated heavy atom structure factor.

[e] Phase power = $\langle F_{h\lambda i}\rangle$ / E, where $\langle F_{h\lambda i}\rangle$ is the root-mean-square heavy atom structure factor and E is the residual lack of closure error.

[f] Occupancies are values output from MLPHARE.

[g] $R_{cryst, free} = \Sigma||F_{obs}| - |F_{calc}|| / |F_{obs}|$, where the crystallographic and free R factors are calculated using the working and free reflection sets, respectively.

[h] Overall figure of merit (before solvent flattening): 0.89.

conserved (Figure 4). The characteristic "knobs-into-holes" packing of coiled coils is utilized, whereby the residues (knobs) at the a and d layers pack into cavities (holes) between four residues of an adjacent helix (Crick, 1953; O'Shea et al., 1991). Of the three types of knobs-into-holes packing geometry observed in coiled-coil structures (Harbury et al., 1993, 1994), the N36 trimer demonstrates exclusively "acute" packing geometry (data not shown), similar to that found in the crystal structure of an isoleucine-zipper trimer (Harbury et al., 1994). This type of packing arrangement in the interior of the coiled coil is characteristic of trimers because it allows β-branched residues (e.g., isoleucine) to pack favorably at both the a and d positions (Harbury et al., 1994). Trimeric coiled coils, like the N36 trimer (Figure 4), tend to have β-branched residues at both the a and d positions.

Although complexes of the N and C peptides are clearly trimeric (Lu et al., 1995; Blacklow et al., 1995) isolated N peptides corresponding to the 4-3 hydrophobic repeat from gp41 have been reported to form tetramers, leading to conflicting conclusions regarding the oligomeric state of gp41 (Rabenstein and Shin, 1995, 1996; Lawless et al., 1996; Shugars et al., 1996). An electrostatic potential map of the N36 coiled-coil trimer shows that its surface is largely uncharged (Figure 5). The grooves that are the sites for C34 interaction are lined with predominantly hydrophobic residues (see below) that would be expected to lead to aggregation upon exposure to solvent. Indeed, previous studies have shown that the isolated N-peptides tend to aggregate (Blacklow et al., 1995; Lu et al., 1995). Thus, conclusions regarding the oligomerization state of gp41 based on studies of isolated N-peptides are probably misleading. The N36/C34 complex shows a much more highly charged surface due to acidic residues on the outside of the C34 helices (Figure 5), explaining the greater solubility of the heterodimeric complex.

Interactions between the N and C Peptide Helices

Three C34 helices pack obliquely against the outside of the N36 coiled-coil trimer in an antiparallel orientation. These C34 helices interact with N36 mainly through hydrophobic residues in three grooves on the surface of the central coiled-coil trimer. Sequence comparisons between HIV and SIV gp41 show that the residues lining these grooves are highly conserved (Figure 6). In contrast, the N36 residues flanking the C34 helices are divergent between HIV and SIV (Figure 6).

This pattern of sequence conservation is also apparent on a helical wheel representation of three N36 helices and one C34 helix (Figure 4). In this diagram, the residue positions in C34 are depicted as ellipses to indicate the oblique tilt of the C34 helix relative to the N36 superhelix and to emphasize that C34 is not part of a coiled coil. Residues at the e and g positions of the N36 helices lie on the outside of the central coiled coil and point into the triangular interhelical space between two N36 helices and a buttressing C34 helix. In general, residues at positions a and d of C34 pack against residues at the

Figure 2. Experimental Electron Density Map

A representative portion of the initial electron density map calculated using experimental structure-factor amplitudes and solvent-flattened MAD phases is shown with the refined molecular model. The map is contoured at 1.5 standard deviations above the mean density. The figure was generated with the program O (Jones and Kjeldgaard, 1992).

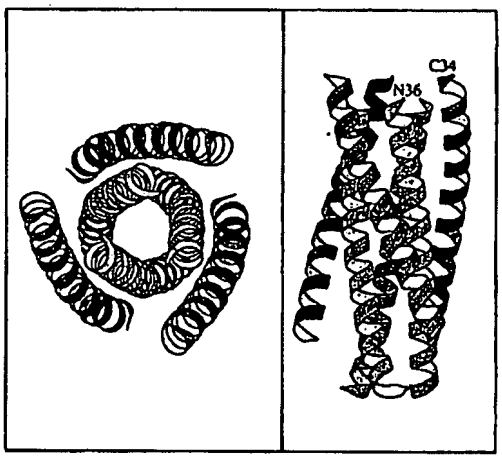

Figure 3. Overall Views of the N36/C34 Complex

The left panel shows an end-on view of the N36/C34 complex looking down the three-fold axis of the trimer. The right panel shows a side view with one N36 and one C34 helix labeled. The amino termini of the N36 helices (blue) point toward the top of the page, while those of the C34 helices (purple) point toward the bottom. Diagrams were prepared using the program MOLSCRIPT (Kraulis, 1991).

e and g positions of the N36 helices (Figure 4), although contacts at other positions are often observed. Comparing HIV and SIV gp41, no nonconservative changes exist at the e and g positions of the N36 helix, and only two such changes occur at the a and d positions of C34. In contrast, 8 of the 9 nonconservative changes in the N36 helix occur at the outside f, b, and c positions, while 13 of the 15 nonconservative changes in the C34 helix occur at positions other than a and d. The sequence of the N-peptide region of gp41 is among the most highly conserved within the HIV envelope glycoprotein. Our results show that the high sequence conservation in this region results from selective pressure on the e and g positions to retain C34 peptide interactions, as well as pressure on the a and d positions to maintain trimeric coiled-coil interactions.

Each of the grooves on the surface of the N36 trimer has a particularly deep cavity (Figure 7, left panel). This cavity is large (~16 Å long, ~7 Å wide, and 5–6 Å deep) and accommodates three hydrophobic residues from the abutting C34 helix: Ile-635, Trp-631, and Trp-628. As depicted in Figure 7 (right panel), the top of the cavity is lined by Leu-566 of the left N36 helix and Leu-565 of the right N36 helix. Side chains from the left N36 helix form the left side of the cavity, including residues (top to bottom) Val-570, Lys-574 (aliphatic portion), and Gln-577. The right wall is formed by residues Leu-568, Trp-571, and Gly-572 of the right N36 helix. The floor of the cavity is composed of Thr-569, Ile-573, and Leu-576. With the exception of Ile-573 (which is replaced by Thr), all the residues forming the cavity are identical between HIV-1 and SIV. In addition to these predominately hydrophobic interactions within the cavity, Asp-632 of C34 forms a conserved salt bridge with Lys-574 of N36 immediately to the left of the cavity.

Similarity to the Low-pH-Induced Conformation of HA

The N36/C34 complex shows striking structural similarity to the low-pH-induced conformation of the influenza HA_2 subunit ($TBHA_2$) (Bullough et al., 1994) and to the TM subunit of Mo-MLV (Fass et al., 1996), each of which has been proposed to be a fusogenic conformation. Remarkably, the core of each of the three structures contains a three-stranded coiled coil that would be adjacent to the amino-terminal fusion peptide (Figure 8). The trimeric coiled coil of gp41 is very similar to that of the Mo-MLV TM, both having a similar superhelical pitch (~175 Å) and a regular 4-3 periodicity. In contrast, the $TBHA_2$ coiled coil is atypical because it contains two regions with skips in the 4-3 periodicity, resulting in an underwound superhelix (pitch of 300–400 Å). As in the gp41 core structure, $TBHA_2$ contains three antiparallel helices that are packed, with a left-handed tilt, against the central trimeric coiled coil.

Discussion

Evidence That the N36/C34 Structure Corresponds to the Core of the Fusion-Active Conformation

The structure obtained in these studies could, in principle, correspond to the core of gp41 in either the fusogenic or the native state of the envelope glycoprotein, or both. Several considerations provide good evidence

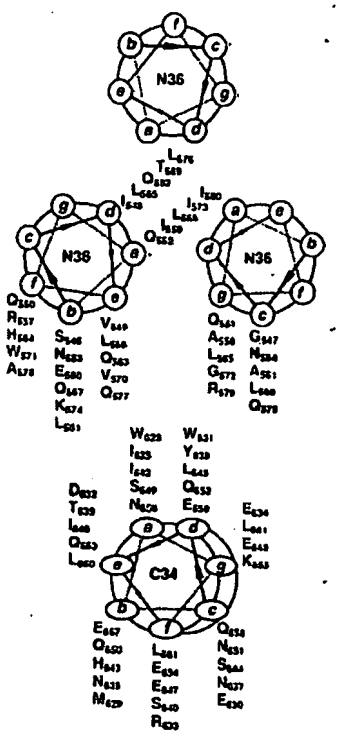

Figure 4. Helical Wheel Representation of N36 and C34

Three N36 helices and one C34 helix are represented as helical wheel projections. The view is from the top of the complex, as in the left panel of Figure 3. The residues at each position are colored according to their conservation between HIV-1 (HXB2) and SIV (Mac239): red, identity; black, conservative change; green, nonconservative change. The N36 helices interact through "knobs-into-holes" packing interactions at the a and d positions (colored orange). Positions of the N36 and C34 helices that occupy the interhelical space between two N36 helices and a C34 helix are shown in yellow. The helical wheel positions in C34 are indicated by ellipses to represent the oblique orientation of this helix relative to N36. At the top of the complex, C34 is slightly tilted toward the left N36 helix, while at the bottom of the complex (indicated by darker shading), it is slightly tilted toward the right N36 helix.

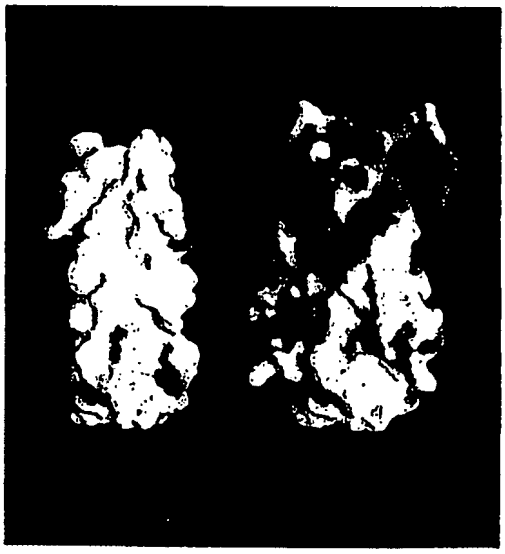

Figure 5. Electrostatic Potential Maps of the Trimer and N36/C34 Complex

An electrostatic potential map (±7 k_BT/e, where k_B = Boltzmann's constant and T = absolute temperature) of the N36 trimer (left) and N36/C34 complex (right). Regions of basic potential are colored blue, while acidic regions are red. Figure was created with the program GRASP (Nicholls et al., 1991).

that this conformation of gp41 is found in the fusion-active state of HIV envelope.

First, the N36/C34 complex folds in the absence of gp120. The fusogenic state of gp41 is expected to be stable in the absence of gp120, since dissociation of gp120 from the envelope glycoprotein is thought to accompany the conversion from a native to a fusogenic state (Cohen, 1996; Wilkinson, 1996). Similarly, the conversion of influenza HA_2 to the fusogenic state is accompanied by loss of most of its contacts with HA_1. Proteolysis of the low-pH-converted form of HA prior to crystallization removes most of the receptor-binding HA_1 subunit (Bullough et al., 1994). Moreover, the structural features of the fusogenic state are preserved in fragments of HA_2 that fold cooperatively in the complete absence of the HA_1 subunit (Carr and Kim, 1993; Chen et al., 1995b).

Second, the isolated gp41 core is exceedingly stable to thermal denaturation. The N51/C43 complex has an apparent melting temperature of approximately 90°C (Lu et al., 1995). In contrast, the native state of the HIV envelope glycoprotein is not particularly stable, as evidenced by the ease with which gp120 is shed in preparations of virus particles (Kalyanaraman et al., 1990; Helseth et al., 1991).

Third, mutations in gp41 that abolish infectivity and membrane fusion often map to residues that are expected to stabilize the gp41 core structure determined here. Numerous studies show that mutations in the 4-3 hydrophobic repeat region abolish membrane fusion, although these mutants tend to have additional defects (Dubay et al., 1992; Chen et al., 1993; Chen, 1994; Wild et al., 1994a; Poumbourios et al., 1997). The Leu-568→Ala, Trp-571→Arg, and Asn-656→Leu mutations are particularly noteworthy because cells expressing mutant envelope glycoproteins with one of these point mutations are completely defective in membrane fusion, as judged by an inability to form syncytia with CD4-positive human lymphocyte lines, even though the mutant proteins exhibit substantial cell-surface expression, CD4 binding, gp120/gp41 association, gp160 precursor processing, and soluble CD4-induced shedding (Cao et al., 1993). Leu-568 and Trp-571 are N36 residues that line the right wall of the cavity shown in Figure 7 (right panel). Asn-656 is in an a position of the C34 peptide and packs against the central N36 coiled-coil trimer. The locations of these key mutations suggest that interactions between the N36 and C34 helices are critical for membrane fusion.

Fourth, our proposal that the N36/34 structure corresponds to the core of the fusogenic state of gp41 is

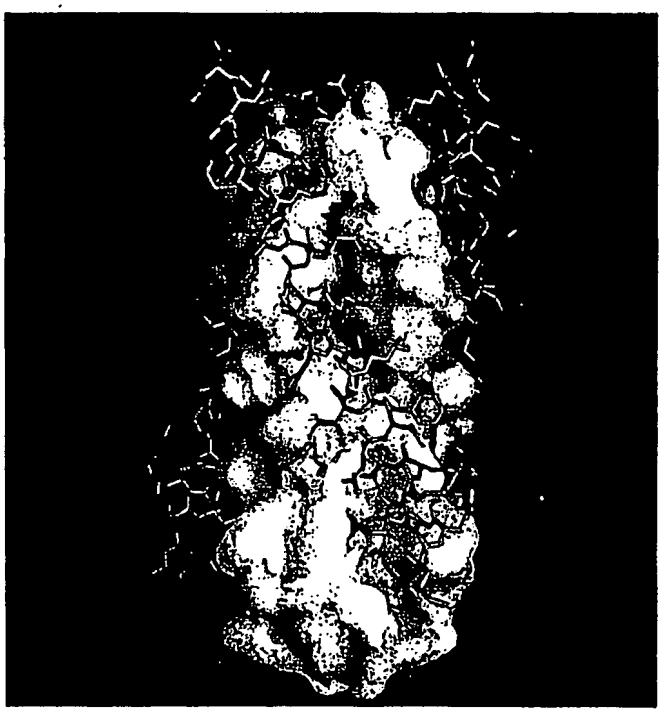

Figure 6. Conserved Grooves on the Surface of the N36 Trimer

The C34 peptides, represented by blue rods, are shown against a surface representation of the N36 trimer. Residues on the surface of the N36 trimer that are identical between HIV and SIV are colored white, and nonidentical residues are green. Note that the C34 helix packs into a conserved (white) groove on the surface of the trimer, while nonconserved (green) regions of N36 are mostly surface-exposed.

consistent with a large body of data on the inhibition of HIV-1 infection and syncytia formation by derivatives of the peptides that make up this core. This issue is discussed in more detail below.

Finally, the structural similarity of the N36/C34 complex to the low-pH-induced conformation of influenza HA_2 (Bullough et al., 1994) and to the structure of Mo-MLV TM (Fass et al., 1996), each of which has been proposed to represent fusion-active conformations, suggests that N36/C34 is the core of the fusogenic conformation of gp41. For all three structures, the hydrophobic fusion peptide would be immediately amino terminal to a central, three-stranded coiled coil. In influenza HA_2 and HIV-1 gp41, the central three-stranded coiled coils are each stabilized by three helices that pack obliquely against the coiled-coil trimer in an antiparallel manner. In the TM subunit of Mo-MLV, these obliquely packed helices are replaced by a short helix and an extended region that serve a similar structural role.

Inhibitors of HIV-1 Infection

Synthetic peptides containing approximately 40 residues from gp41 that overlap, or include all of, the residues in N36 or C34 can be effective inhibitors, at micromolar to nanomolar concentrations, of HIV infection and syncytia formation (Wild et al., 1992, 1994b; Jiang et al., 1993; Lu et al., 1995). Our earlier investigation into the inhibitory properties of the N51 and C43 peptides implied that these peptides work in a dominant-negative manner (Herskowitz, 1987) by binding to viral gp41 (Lu et al., 1995), a conclusion that was also reached through studies of a gp41 ectodomain chimeric protein (Chen et al., 1995a). Further evidence in support of a dominant-negative mechanism is provided by the finding that mutations in C-peptide derivatives that disrupt their interactions with N peptide correlate with decreased potency as inhibitors (Wild et al., 1995).

The gp41 core crystal structure is fully consistent with this dominant-negative mechanism of inhibition (Figures 3 and 6). The C-peptide derivatives could act as dominant-negative inhibitors by binding to the endogenous N-peptide coiled-coil trimer within viral gp41. The N peptides might inhibit fusion by interfering with formation of the central, coiled-coil trimer within viral gp41 and/or by binding to endogenous viral C-peptide regions.

Both the N- and C-peptide classes of inhibitors are effective against a wide range of HIV strains, including laboratory-adapted strains and primary isolates (Wild et al., 1992; Jiang et al., 1993; Wild et al., 1994b). In contrast, soluble CD4 and many neutralizing antibodies are typically effective only on a limited subset of HIV strains (e.g., Nara et al., 1988; Palker et al., 1988; Daar et al., 1990; Moore et al., 1995). There is a striking conservation of residues involved in interactions between the N peptide and C peptide, comparing gp41 from HIV-1 and SIV (Figure 6). We conclude that the broad neutralizing effects of the N and C peptides derive from the strong sequence conservation of these residues.

The highly conserved, deep cavities on the N-peptide coiled-coil trimer that accommodate conserved C-peptide residues are attractive targets for the development of new peptidomimetic or small-molecule inhibitors of HIV infection. The two indole rings and neighboring side chains that occupy the prominent cavity depicted in

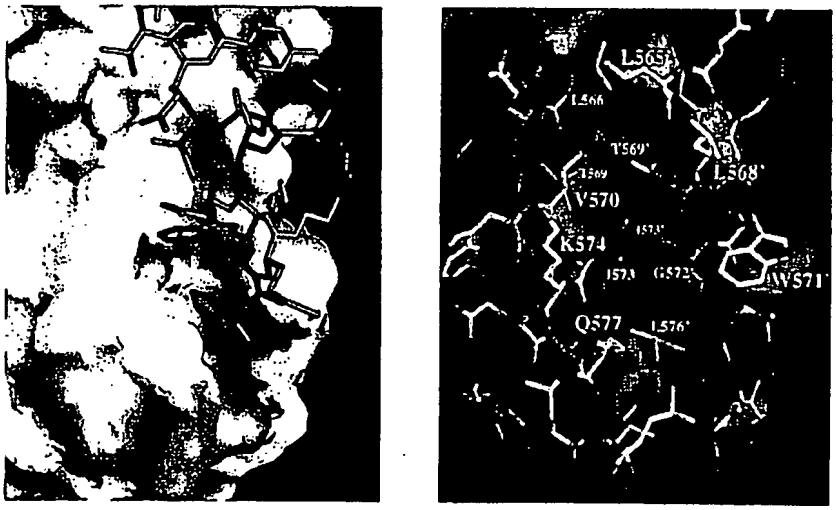

Figure 7. Interaction of C34 Residues with a Large Cavity on the N36 Trimer Surface

(Left panel) A surface representation of the cavity in the carboxy-terminal portion of the N36 trimer, colored as in Figure 6. Residues in C34 that dock into this pocket are colored purple (Ile-635, Asp-632, Trp-631, and Trp-628). (Right panel) Residues that form the cavity in the N36 coiled-coil surface are labeled. A prime (') is used to distinguish residues of one N36 helix from those of an adjacent N36 helix. This orientation is rotated ~30° to the left relative to the left panel, in order to facilitate visualization of all the side chains.

Figure 7 are a particularly attractive starting point for the design and/or development of new drugs. Not only is this cavity deep and highly conserved, but two of the three key mutations that disrupt membrane fusion, discussed above, map to one wall of this cavity (Figure 7). Because some of the known potent peptide inhibitors (Wild et al., 1994b) extend beyond N36 and C34 and do not involve this cavity region, it is likely that other distinctive surface features exist in the interface between the N and C helices of longer peptides such as N51 and C43 (Lu et al., 1995). The importance of identifying drugs that target the HIV membrane-fusion machinery is emphasized by the success of combination drug regimens for the treatment of AIDS (review, Lipsky, 1996). As yet, these combination therapies do not target the HIV envelope.

Implications for gp41 Function and Viral Membrane Fusion

The structures of the cores of the membrane-fusion subunits from HIV, Mo-MLV, and influenza virus are remarkably similar (Figure 8). It appears that these diverse viruses present fusion peptides to target cells via a common scaffold, in which the fusion peptides are atop a central, three-stranded coiled coil that is supported by additional, carboxy-terminal structures. This scaffold is likely to be a common feature of viral membrane-fusion proteins since many of these proteins contain coiled-coil signature sequences, with 4-3 heptad repeats of hydrophobic amino acids, adjacent to an amino-terminal fusion-peptide region (Gallaher et al., 1989; Chambers et al., 1990; Delwart et al., 1990). Moreover, studies of the fusion proteins of several paramyoviruses have identified regions with similarity to the N- and C-peptide regions of HIV and SIV gp41 (Lambert et al., 1996). These common structural features suggest that the rich body of work investigating the mechanism of membrane fusion for many other viruses, including influenza, is relevant for understanding the mechanism of HIV-mediated membrane fusion.

Given the similarity in structure between the HIV gp41 core and the low-pH-converted conformation of HA_2, it is worth considering whether the structural rearrangements that occur during the transition of HA_2 to the fusogenic state are analogous to those in gp41. In the native, nonfusogenic conformation of influenza HA, part of the N-terminal coiled-coil trimer seen in the fusogenic state (Bullough et al., 1994) is held in a nonhelical, hairpin structure, as a result of extensive interactions with the receptor-binding HA_1 subunit (Wilson et al., 1981). Thus, the receptor-binding HA_1 subunit acts as a "clamp" that binds this N-terminal region of HA_2, holding it in the non-coiled-coil conformation. The receptor-binding domains dissociate in the fusogenic conformation of HA, as in HIV, although in the case of influenza, the HA_1 subunits are still tethered via a disulfide bond to HA_2. Upon release of the HA_1 clamp, a dramatic conformational change in HA_2 occurs, including coiled-coil formation by this N-terminal region (Carr and Kim, 1993; Bullough et al., 1994).

A substantial conformational change in the envelope glycoprotein complex is also thought to be critical during HIV infection, though few details are understood. It remains to be determined whether the HIV envelope complex also utilizes coiled-coil formation as part of a spring-loaded mechanism, or if the gp41 core structure determined here is present in the native as well as the fusogenic state. It is possible that the N36/C34 structure is the core structure of gp41 even when it is bound to gp120, and that release of gp120 simply exposes the

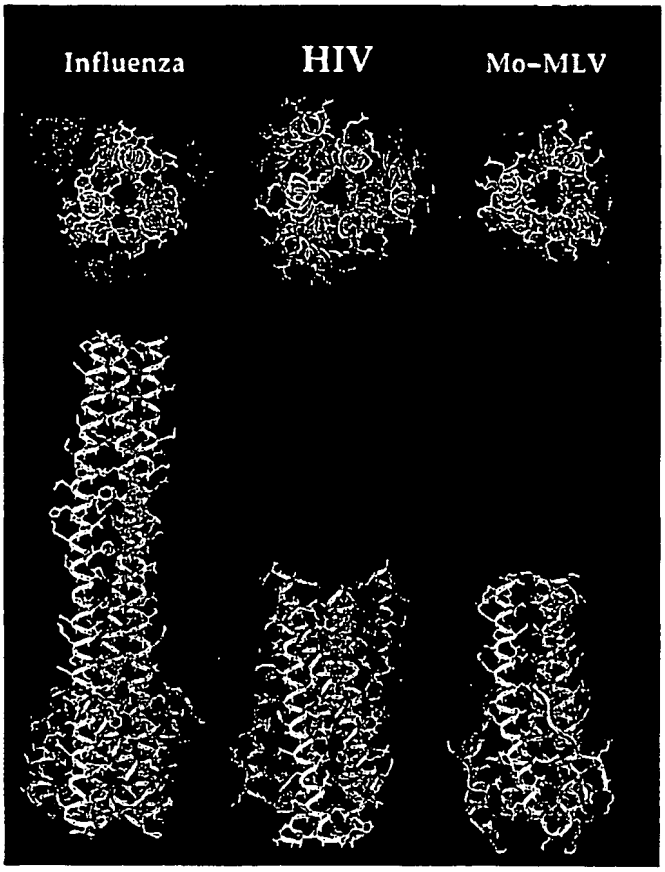

Figure 8. Comparison of Influenza HA_2, HIV gp41, and Mo-MLV TM Structures

The top panel shows an end-on view of the three structures from the top, as in the left panel of Figure 3. The bottom panel shows a side view. The three monomers forming the central coiled coil of each structure are colored yellow, green, and blue. Supporting structures are colored purple. Residues 40–129 of HA_2 (Bullough et al., 1994) and 45–98 of Mo-MLV TM (Fass et al., 1996) are included. The figure was generated using the program Insight (Biosym).

fusion-peptide region of gp41. Alternatively, HIV gp120, like Influenza HA_1, may serve as a clamp that represses formation of the N36/C34 structure presented here, with gp120 shedding allowing its formation. This gp41 core structure serves as the starting point for addressing this and other essential structural questions about the mechanism of HIV entry into cells.

Experimental Procedures

Peptide Purification and Crystallization

Peptides N36 and C34 were synthesized by standard FMOC peptide chemistry and have an acetylated N terminus and a C-terminal amide. N36 corresponds to residues 546–581 of gp160, while C34 corresponds to residues 628–661. After cleavage from the resin, the peptides were desalted on a Sephadex G-25 column (Pharmacia) and lyophilized. Peptides were then purified by reverse-phase high performance liquid chromatography (Waters, Inc.) on a Vydac C18 preparative column. The identity of the peptides was verified by mass spectrometry. Peptide concentration was determined by tyrosine and tryptophan absorbance in 6 M GuHCl (Edelhoch, 1967).

To grow crystals, a 10 mg/ml stock of the N36/C34 complex was diluted 1:1 in a sitting drop with 80 mM NH_4Cl, 20% PEG200, and 50% isopropanol and allowed to equilibrate against a reservoir of 80 mM NH_4Cl, 20% PEG200, and 30% isopropanol. Crystals grew as hexagonal prisms and belonged to the space group P321 ($a = b = 49.5$ Å, $c = 55.3$ Å). For native data sets and heavy atom screens, crystals were flash-frozen in a MSC cryogenic crystal cooler (X-stream), and data was collected on a Rigaku RU-200 rotating-anode X-ray generator with an R-axis IIc detector.

Heavy Atom Screen and Phase Determination

Multiwavelength anomalous diffraction (MAD) data were collected at the Howard Hughes Medical Institute beamline X4A of the National Synchrotron Light Source at Brookhaven National Laboratory. Fluorescence spectra (1.1459–1.1354 Å) were obtained from a single flash-frozen crystal soaked in 0.04% OsO_4 in harvest buffer (80 mM NH_4Cl, 20% PEG200, 30% isopropanol) for 4 hr. Based on the fluorescence profile, individual data sets were collected on Fuji imaging plates at four wavelengths ($\lambda_1 = 1.1398$ Å, $\lambda_2 = 1.1398$ Å, $\lambda_3 = 1.1402$ Å, and $\lambda_4 = 1.1344$ Å). Reflections were integrated and scaled with DENZO and SCALEPACK (Otwinowski, 1993).

Data scaling, phase determination, and map generation were all performed using the CCP4 suite of programs (CCP4, 1994). Anomalous and dispersive difference Patterson maps from MAD data sets all showed a single clear peak corresponding to the osmium binding site. The position of the site was calculated from the single $z = 0$ Harker section and from cross-peaks found at $z = 0.28$ and $z = 0.71$. Phases generated with the program MLPHARE (Otwinowski, 1991) gave an overall figure of merit of 0.89 (Table 1) and produced an interpretable electron density map with a clear solvent boundary. Density modification was subsequently performed using DM (Cowtan, 1994), resulting in maps of high quality in which electron density for the entire main chain and all side chains was evident (Figure 2).

Model Refinement

The polypeptide chain was traced and the side chains readily positioned into a 2.7 Å density-modified map using the program O (Jones

and Kjeldgaard, 1992). The initial model of N36/C34 was refined with the program XPLOR (Brünger, 1992a) against data to 2.0 Å from a native crystal. An anisotropic B-factor was applied to the native structure factors using XPLOR, and a free R set (Brünger, 1992b) was taken from the data prior to refinement (Table 1). The model was refined by iterative cycles of grouped B-factor, positional, and individual B-factor refinement. As the refinement proceeded, 43 waters were added and a bulk solvent correction was applied. At no time during the refinement did the molecule differ enough from the original model so as to require manual rebuilding, though main chain and side chain geometries were optimized in O between cycles of refinement. The quality of the structure was verified by PROCHECK (Laskowski et al., 1993), with all residues but one (Ile-580) occupying most-preferred regions of Ramachandran space. Ile-580 lies in the additionally allowed region of Ramachandran space and is the second residue from the C terminus of the N36 peptide; inspection of the solvent-flattened MAD-phased maps confirmed its position. Refined coordinates will be deposited in the Protein Data Bank (Brookhaven National Laboratory, Upton, NY).

Acknowledgments

We thank the staff, particularly Dr. Craig Ogata, of the Howard Hughes Medical Institute beamline (X4A) at the National Synchrotron Light Source at Brookhaven National Laboratory for invaluable support in collecting MAD data. We are also grateful to Debra Ehrgott and Li Su for help with data collection, Michael Burgess and James Pang for peptide synthesis, and Dr. Steven J. Gamblin for helpful suggestions. D. C. C. is supported by a postdoctoral fellowship from the Jane Coffin Childs Memorial Fund for Medical Research. J. M. B. is a Whitehead Fellow and acknowledges support from the W. M. Keck Foundation. This work was funded by the Howard Hughes Medical Institute and utilized the W. M. Keck Foundation X-ray Crystallography Facility at the Whitehead Institute.

Received April 3, 1997; revised April 7, 1997.

References

Allan, J.S., Allan, J.S., Strauss, J., and Buck, D.W. (1990). Enhancement of SIV infection with soluble receptor molecules. Science *247*, 1084–1088.

Blacklow, S.C., Lu, M., and Kim, P.S. (1995). A trimeric subdomain of the simian immunodeficiency virus envelope glycoprotein. Biochemistry *34*, 14955–14962.

Broder, C.C., and Dimitrov, D.S. (1996). HIV and the 7-transmembrane domain receptors. Pathobiology *64*, 171–179.

Brünger, A.T. (1992a). A system for X-ray crystallography and NMR. X-PLOR Version 3.1. (New Haven, Connecticut: Yale University Press).

Brünger, A.T. (1992b). Free R value: a novel statistical quantity for assessing the accuracy of crystal structures. Nature *355*, 472–475.

Bullough, P.A., Hughson, F.M., Skehel, J.J., and Wiley, D.C. (1994). Structure of influenza haemagglutinin at the pH of membrane fusion. Nature *371*, 37–43.

Cao, J., Bergeron, L., Helseth, E., Thali, M., Repke, H., and Sodroski, J. (1993). Effects of amino acid changes in the extracellular domain of the human immunodeficiency virus type 1 gp41 envelope glycoprotein. J. Virol. *67*, 2747–2755.

Carr, C.M., and Kim, P.S. (1993). A spring-loaded mechanism for the conformational change of influenza hemagglutinin. Cell *73*, 823–832.

CCP4 (1994). Collaborative computational project, Number 4. Acta Cryst. *D50*, 760–763.

Chambers, P., Pringle, C.R., and Easton, A.J. (1990). Heptad repeat regions are located adjacent to hydrophobic regions in several types of virus fusion glycoproteins. J. Gen. Virol. *71*, 3075–3080.

Chen, C.H., Matthews, T.J., McDanal, C.B., Bolognesi, D.P., and Greenberg, M.L. (1995a). A molecular clasp in the human immunodeficiency virus (HIV) type 1 TM protein determines the anti-HIV activity of gp41 derivatives: implication for viral fusion. J. Virol. *69*, 3771–3777.

Chen, J., Wharton, S.A., Weissenhorn, W., Calder, L.J., Hughson, F.M., Skehel, J.J., and Wiley, D.C. (1995b). A soluble domain of the membrane-anchoring chain of influenza virus hemagglutinin (HA_2) folds in Escherichia coli into the low-pH-induced conformation. Proc. Natl. Acad. Sci. USA *92*, 12205–12209.

Chen, S.S. (1994). Functional role of the zipper motif region of human immunodeficiency virus type 1 transmembrane protein gp41. J. Virol. *68*, 2002–2010.

Chen, S.S., Lee, C.N., Lee, W.R., McIntosh, K., and Lee, T.H. (1993). Mutational analysis of the leucine zipper-like motif of the human immunodeficiency virus type 1 envelope transmembrane glycoprotein. J. Virol. *67*, 3615–3619.

Choe, H., Farzan, M., Sun, Y., Sullivan, N., Rollins, B., Ponath, P.D., Wu, L., Mackay, C.R., LaRosa, G., Newman, W., Gerard, N., Gerard, C., and Sodroski, J. (1996). The beta-chemokine receptors CCR3 and CCR5 facilitate infection by primary HIV-1 isolates. Cell *85*, 1135–1148.

Cohen, C., and Parry, D.A. (1990). Alpha-helical coiled coils and bundles: how to design an alpha-helical protein. Proteins *7*, 1–15.

Cohen, J. (1996). Investigators detail HIV's fatal handshake. Science *274*, 502.

Cowtan, K.D. (1994). Joint CCP4 and ESF-EACBM. Newslett. Prot. Crystallogr. *31*, 34–38.

Crick, F.H.C. (1953). The packing of α-helices: simple coiled coils. Acta Cryst. *6*, 689–697.

D'Souza, M.P., and Harden, V.A. (1996). Chemokines and HIV-1 second receptors. Nature Med. *2*, 1293–1300.

Daar, E.S., Li, X.L., Moudgil, T., Ho, D.D. (1990). High concentrations of recombinant soluble CD4 are required to neutralize primary human immunodeficiency virus type 1 isolates. Proc. Natl. Acad. Sci. USA *87*, 6574–6578.

Delwart, E.L., Mosialos, G., and Gilmore, T. (1990). Retroviral envelope glycoproteins contain a leucine zipper-like repeat. AIDS Res. Hum. Retroviruses *6*, 703–706.

Dubay, J.W., Roberts, S.J., Brody, B., and Hunter, E. (1992). Mutations in the leucine zipper of the human immunodeficiency virus type 1 transmembrane glycoprotein affect fusion and infectivity. J. Virol. *66*, 4748–4756.

Edelhoch, H. (1967). Spectroscopic determination of tryptophan and tyrosine in proteins. Biochemistry *6*, 1948–1954.

Fass, D., and Kim, P.S. (1995). Dissection of a retrovirus envelope protein reveals structural similarity to influenza hemagglutinin. Curr. Biol. *5*, 1377–1383.

Fass, D., Harrison, S.C., and Kim, P.S. (1996). Structure of Moloney murine virus envelope domain at 1.7Å resolution. Nature Struct. Biol. *3*, 465–469.

Freed, E.O., and Martin, M.A. (1995). The role of human immunodeficiency virus type 1 envelope glycoproteins in virus infection. J. Biol. Chem. *270*, 23883–23886.

Gallaher, W.R., Ball, J.M., Garry, R.F., Griffin, M.C., and Montelaro, R.C. (1989). A general model for the transmembrane proteins of HIV and other retroviruses. AIDS Res. Hum. Retroviruses *5*, 431–440.

Harbury, P.B., Zhang, T., Kim, P.S., and Alber, T. (1993). A switch between two-, three-, and four-stranded coiled coils in GCN4 leucine zipper mutants. Science *262*, 1401–1407.

Harbury, P., Kim, P.S., and Alber, T. (1994). Crystal structure of an isoleucine-zipper trimer. Nature *371*, 80–83.

Hart, T.K., Kirsch, R., Ellens, H., Sweet, R.W., Lambert, D.M., Petteway, S.R., Jr., Leary, J., and Bugelski, P.J. (1991). Binding of soluble CD4 proteins to human immunodeficiency virus type 1 and infected cells induces release of envelope glycoprotein gp120. Proc. Natl. Acad. Sci. USA *88*, 2189–2193.

Helseth, E., Olshevsky, U., Furman, U., and Sodroski, J. (1991). Human immunodeficiency virus type 1 glycoprotein regions important for association with the gp41 transmembrane glycoprotein. J. Virol. *65*, 2119–2123.

Hendrickson, W.A. (1991). Determination of macromolecular structures from anomalous diffraction of synchrotron radiation. Science *254*, 51–58.

Herskowitz, I. (1987). Functional inactivation of genes by dominant negative mutations. Nature *329*, 219–222.

Hunter, E., and Swanstrom, R. (1990). Retrovirus envelope glycoproteins. Curr. Top. Microbiol. Immunol. *157*, 187–253.

Jiang, S., Lin, K., Strick, N., and Neurath, A.R. (1993). HIV-1 inhibition by a peptide. Nature *365*, 113.

Jones, T.A., and Kjeldgaard, M. (1992). O—The Manual (Uppsala, Sweden: http://kaktus.kemi.aau.dk).

Kalyanaraman, V.S., Rodriguez, V., Veronese, F., Rahman, R., Lusso, P., DeVico, A.L., Copeland, T., Oroszlan, S., Gallo, R.C., and Samgadharan, M.G. (1990). Characterization of the secreted, native gp120 and gp160 of the human immunodeficiency virus type 1. AIDS Res. Hum. Retroviruses *6*, 371–380.

Kraulis, P. (1991). MOLSCRIPT: a program to produce both detailed and schematic plots of protein structures. J. Appl. Crystallogr. *24*, 924–950.

Lambert, D.M., Barney, S., Lambert, A.L., Guthrie, K., Medinas, R., Davis, D.E., Bucy, T., Erickson, J., Merutka, G., and Petteway, S.R., Jr. (1996). Peptides from conserved regions of paramyxovirus fusion (F) proteins are potent inhibitors of viral fusion. Proc. Natl. Acad. Sci. USA *93*, 2186–2191.

Laskowski, R.A., MacArthur, M.W., Moss, D.S., and Thornton, J.M. (1993). PROCHECK: a program to check the stereochemical quality of protein structures. J. Appl. Crystallogr. *26*, 283–291.

Lawless, M., Barney, S., Guthrie, K.I., Bucy, T.B., Petteway, S.R., Jr., and Merutka, G. (1996). HIV-1 membrane fusion mechanism: structural studies of the interactions between biologically-active peptides from gp41. Biochemistry *35*, 13697–13708.

Lipsky, J.J. (1996). Antiretroviral drugs for AIDS. Lancet *348*, 800–803.

Lu, M., Blacklow, S.C., and Kim, P.S. (1995). A trimeric structural domain of the HIV-1 transmembrane glycoprotein. Nature Struct. Biol. *2*, 1075–1082.

Luciw, P.A. (1996). Human immunodeficiency viruses and their replication. In Fields Virology, Third Edition, B.N. Fields, D.M. Knipe, P.M. Howley, R.M. Chanock, J.L. Melnick, T.P. Monath, B. Roizman, and S.E. Straus, eds. (Philadelphia: Lippincott-Raven Publishers), pp. 1881–1952.

Moore, J.P., McKeating, J.A., Weiss, R.A., and Sattentau, Q.J. (1990). Dissociation of gp120 from HIV-1 virions induced by soluble CD4. Science *250*, 1139–1142.

Moore, J.P., Cao, Y., Qing, L., Sattentau, Q.J., Pyati, J., Koduri, R., Robinson, J., Barbas, C.F., III, Burton, D.R., and Ho, D.D. (1995). Primary isolates of human immunodeficiency virus type 1 are relatively resistant to neutralization by monoclonal antibodies to gp120, and their neutralization is not predicted by studies with monomeric gp120. J. Virol. *69*, 101–109.

Nara, P.L., Robey, W.G., Pyle, S.W., Hatch, W.C., Dunlop, N.M., Bess, J.W., Jr., Kelliher, J.C., Arthur, L.O., and Fischinger, P.J. (1988). Purified envelope glycoproteins from human immunodeficiency virus type 1 variants induce individual, type-specific neutralizing antibodies. J. Virol. *62*, 2622–2628.

Nicholls, A., Sharp, K.A., and Honig, B. (1991). Protein folding and association: insights from the interfacial and thermodynamic properties of hydrocarbons. Proteins *11*, 281–296.

Oas, T.G., and Kim, P.S. (1988). A peptide model of a protein folding intermediate. Nature *336*, 42–48.

O'Shea, E.K., Klemm, J.D., Kim, P.S., and Alber, T. (1991). X-ray structure of the GCN4 leucine zipper, a two-stranded, parallel coiled coil. Science *254*, 539–544.

Otwinoski, Z. (1991). Maximum likelihood refinement of heavy atom parameters. In Isomorphous Replacement and Anomalous Scattering. W. Wolf, P.R. Evans, and A.G.W. Leslie, eds. (Warrington, England: SERC, Daresbury Laboratory) pp. 80–86.

Otwinoski, Z. (1993). Oscillation data reduction program. In Data Collection and Processing. L. Sawyer, N. Isaacs, S. Bailey, eds. (Warrington, England: SERC, Daresbury Laboratory) pp. 56–62.

Palker, T.J., Clark, M.E., Langlois, A.J., Matthews, T.J., Weinhold, K.J., Randall, R.R., Bolognesi, D.P., and Haynes, B.F. (1988). Type-specific neutralization of the human immunodeficiency virus with antibodies to env-encoded synthetic peptides. Proc. Natl. Acad. Sci. USA *85*, 1932–1936.

Poumbourios, P., Wilson, K.A., Center, R.J., ElAhmar, W., and Kemp, B.E. (1997). Human immunodeficiency virus type 1 envelope glycoprotein oligomerization requires the gp41 amphipathic alpha-helical/leucine zipper-like sequence. J. Virol. *71*, 2041–2049.

Rabenstein, M.D., and Shin, Y.K. (1996). HIV-1 gp41 tertiary structure studied by EPR spectroscopy. Biochemistry *35*, 13922–13928.

Rabenstein, M., and Shin, Y.K. (1995). A peptide from the heptad repeat of human immunodeficiency virus gp41 shows both membrane binding and coiled-coil formation. Biochemistry *34*, 13390–13397.

Sattentau, Q.J., and Moore, J.P. (1991). Conformational changes induced in the human immunodeficiency virus envelope glycoprotein by soluble CD4 binding. J. Exp. Med. *174*, 407–415.

Sattentau, Q.J., and Moore, J.P. (1993). The role of CD4 in HIV binding and entry. Phil. Trans. Royal Soc. B *342*, 59–66.

Sattentau, Q.J., Moore, J.P., Vignaux, F., Traincard, F., and Poignard, P. (1993). Conformational changes induced in the envelope glycoproteins of the human and simian immunodeficiency viruses by soluble receptor binding. J. Virol. *67*, 7383–7393.

Shugars, D.C., Wild, C.T., Greenwell, T.K., and Matthews, T.J. (1996). Biophysical characterization of recombinant proteins expressing the leucine zipper-like domain of the human immunodeficiency virus type 1 transmembrane protein gp41. J. Virol. *70*, 2982–2991.

Stamatatos, L., and Cheng-Mayer, C. (1995). Structural modulations of the envelope gp120 glycoprotein of human immunodeficiency virus type 1 upon oligomerization and differential V3 loop epitope exposure of isolates displaying distinct tropism upon virion-soluble receptor binding. J. Virol. *69*, 6191–6198.

Stegmann, T., Delfino, J.M., Richards, F.M., and Helenius, A. (1991). The HA_2 subunit of influenza hemagglutinin inserts into the target membrane prior to fusion. J. Biol. Chem. *266*, 18404–18410.

Stegmann, T., and Helenius, A. (1993). Influenza virus fusion: from models toward a mechanism. In Viral Fusion Mechanisms, J. Bentz, ed. (Boca Raton, Florida: CRC Press), pp. 89–111.

Sullivan, N., Sun, Y., Li, J., Hofmann, W., and Sodroski, J. (1995). Replicative function and neutralization sensitivity of envelope glycoproteins from primary and T-cell line-passaged human immunodeficiency virus type 1 isolates. J. Virol. *69*, 4413–4422.

Trkola, A., Dragic, T., Arthos, J., Binley, J.M., Olson, W.C., Allaway, G.P., Cheng-Mayer, C., Robinson, J., Maddon, P.J., and Moore, J.P. (1996). CD4-dependent, antibody-sensitive interactions between HIV-1 and its co-receptor CCR-5. Nature *384*, 184–187.

Tsurudome, M., Glück, R., Graf, R., Falchetto, R., Schaller, U., and Brunner, J. (1992). Lipid interactions of the hemagglutinin HA_2 NH2-terminal segment during influenza virus-induced membrane fusion. J. Biol. Chem. *267*, 20225–20232.

White, J.M. (1992). Membrane fusion. Science *258*, 917–924.

Wild, C.T., Oas, T., McDanal, C.B., Bolognesi, D., and Matthews, T.J. (1992). A synthetic peptide inhibitor of human immunodeficiency virus replication: correlation between solution structure and viral inhibition. Proc. Natl. Acad. Sci. USA *89*, 10537–10541.

Wild, C., Dubay, J.W., Greenwell, T., Baird, T., Jr., Oas, T.G., McDanal, C., Hunter, E., and Matthews, T. (1994a). Propensity for a leucine zipper-like domain of human immunodeficiency virus type 1 gp41 to form oligomers correlates with a role in virus-induced fusion rather than assembly of the glycoprotein complex. Proc. Natl. Acad. Sci. USA *91*, 12676–12680.

Wild, C.T., Shugars, D.C., Greenwell, T.K., McDanal, C.B., and Matthews, T.J. (1994b). Peptides corresponding to a predictive α-helical domain of human immunodeficiency virus type 1 gp41 are potent inhibitors of virus infection. Proc. Natl. Acad. Sci. USA *91*, 9770–9774.

Wild, C., Greenwell, T., Shugars, D., Rimsky-Clarke, L., and Matthews, T. (1995). The inhibitory activity of an HIV type 1 peptide correlates with its ability to interact with a leucine zipper structure. AIDS Res. Hum. Retroviruses *11*, 323–325.

Wiley, D.C., and Skehel, J.J. (1987). The structure and function of the hemagglutinin membrane glycoprotein of influenza virus. Annu. Rev. Biochem. *56*, 365–394.

Wilkinson, D. (1996). HIV-1: cofactors provide the entry keys. Curr. Biol. *6*, 1051–1053.

Wilson, I.A., Skehel, J.J., and Wiley, D.C. (1981). Structure of the haemagglutinin membrane glycoprotein of influenza virus at 3 Å resolution. Nature *289*, 366–373.

Wu, L., Gerard, N.P., Wyatt, R., Choe, H., Parolin, C., Ruffing, N., Borsetti, A., Cardoso, A.A., Desjardin, E., Newman, W., Gerard, C., and Sodroski, J. (1996). CD4-induced interaction of primary HIV-1 gp120 glycoproteins with the chemokine receptor CCR-5. Nature *384*, 179–183.

Structural and Functional Analysis of the HIV gp41 Core Containing an Ile573 to Thr Substitution: Implications for Membrane Fusion[†,‡]

Jie Liu,[§] Wei Shu,[§] Melinda B. Fagan,[∥] Jack H. Nunberg,[∥] and Min Lu*[,§]

Department of Biochemistry, Weill Medical College of Cornell University, New York, New York 10021, and Montana Biotechnology Center, The University of Montana, Missoula, Montana 59812

Received October 25, 2000; Revised Manuscript Received December 22, 2000

ABSTRACT: The envelope glycoprotein of HIV-1 consists of the surface subunit gp120 and the transmembrane subunit gp41. Binding of gp120 to target cell receptors induces a conformational change in gp41, which then mediates the fusion of viral and cellular membranes. A buried isoleucine (Ile573) in a central trimeric coiled coil within the fusion-active gp41 ectodomain core is thought to favor this conformational activation. The role of Ile573 in determining the structure and function of the gp120−gp41 complex was investigated by mutating this residue to threonine, a nonconservative substitution in HIV-1 that occurs naturally in SIV. While the introduction of Thr573 markedly destabilized the gp41 core, the three-dimensional structure of the mutant trimer of hairpins was very similar to that of the wild-type molecule. A new hydrogen-bonding interaction between the buried Thr573 and Thr569 residues appears to allow formation of the trimer-of-hairpins structure at physiological temperature. The mutant envelope glycoprotein expressed in 293T cells and incorporated within pseudotyped virions displayed only a moderate reduction in syncytium-inducing capacity and virus infectivity, respectively. Our results demonstrate that the proper folding of the gp41 core underlies the membrane fusion properties of the gp120−gp41 complex. An understanding of the gp41 activation process may suggest novel strategies for vaccine and antiviral drug development.

Membrane glycoproteins of enveloped viruses control the key process of viral entry by mediating the attachment of the virion to target cells and the fusion of viral and cellular membranes. Envelope glycoproteins on the surface of the virion are thus major targets for the induction of protective immunity and for the development of pharmacologic interventions. The best characterized viral membrane fusion protein is the influenza virus hemagglutinin (HA).[1] In response to the mildly acidic conditions of the mature endosome, influenza fusion is activated in a process requiring complex structural changes in HA from a native (prefusogenic) to a fusogenic (fusion-active) conformation (*1*−*4*). Recent work has led to the hypothesis that the native conformation of HA is metastable; when incubated at the pH of fusion, it is transformed in a "spring-loaded" manner to an energetically more stable fusion-active state (*1*, *2*, *5*, *6*). Inhibition of this type of activation and refolding of the viral envelope protein may be central to strategies for the treatment or prevention of viral infections.

Human and simian immunodeficiency viruses (HIV and SIV) also utilize a membrane fusion event to introduce their infectious genomes into cells. The envelope glycoprotein is synthesized as a gp160 polyprotein and cleaved intracellularly to yield a noncovalent complex of the surface subunit gp120 and the transmembrane subunit gp41 (reviewed in refs *7* and *8*). Considerable evidence now indicates that the primate immunodeficiency virus entry process involves multiple steps. Upon interaction of the viral trimeric gp120−gp41 complex with cellular receptors (CD4 and members of the chemokine receptor family), the envelope glycoprotein undergoes a conformational change that allows the gp41 subunit to form the transient prehairpin intermediate in which the N-terminal fusion peptide and the transmembrane segments are anchored in the cellular and viral membranes, respectively (*9*−*12*). Subsequent helical packing interactions within gp41 resolve the prehairpin intermediate into a fusion-active hairpin structure, leading to close apposition of the two membranes for fusion (*9*, *13*, *14*). The structural consequences of these gp41 conformational changes remain imperfectly understood, in part because the native and prehairpin intermediate structures of gp41 are not known.

The structure of the gp41 ectodomain in its fusion-active state is a trimer of hairpins in which three C-terminal helices pack in an antiparallel orientation into highly conserved

[†] This work was supported by National Institutes of Health Grants AI44669 to J.H.N. and AI42382 to M.L. The work at The University of Montana was furthered by a gift from the James B. Pendleton Charitable Trust.

[‡] The refined coordinates have been deposited in the Protein Data Bank with accession number 1F23.

* To whom correspondence should be addressed: Weill Medical College of Cornell University, 1300 York Ave., New York, NY 10021. Phone: (212) 746-6562. Fax: (212) 746-8875. E-mail: mlu@mail.med.cornell.edu.

[§] Weill Medical College of Cornell University.

[∥] The University of Montana.

[1] Abbreviations: HA, hemagglutinin; HIV-1, human immunodeficiency virus type 1; SIV, simian immunodeficiency virus; mAb, monoclonal antibody; HIVIG, anti-HIV immunoglobulin from infected persons; Env, envelope; $[\theta]_{222}$, molar ellipticity at 222 nm; CD, circular dichroism; HPLC, high-performance liquid chromatography; T_m, transition midpoint temperature.

10.1021/bi0024759 CCC: $20.00
Published on Web 02/10/2001

hydrophobic grooves on the outer surface of the N-terminal trimeric coiled coil (*13*, *15*−*21*). The N-terminal coiled-coil formation appears to play a critical role in initiating the gp41 refolding process leading to membrane fusion (*22*, and references therein). In the simplest model, the N-terminal heptad-repeat region exists in an non-coiled-coil conformation in the native state but forms a coiled-coil trimer in the prehairpin intermediate and fusogenic hairpin conformations (*22*−*28*). Evidence for the functional importance of this structural rearrangement comes from the finding that peptides corresponding to the C-terminal helical region are potent inhibitors of HIV-1 infection in vitro (*29*, *30*); these peptides are thought to pack into hydrophobic grooves of the N-terminal trimeric coiled coil, thereby preventing formation of the fusion-active hairpin structure (*13*, *15*−*17*). One such peptide, T-20, shows efficacy in reducing viral loads in clinical trials (*31*). Furthermore, a prominent hydrophobic cavity on the surface of the gp41 N-terminal coiled-coil core has been shown to serve as a binding pocket for small-molecule fusion inhibitors (*32*, *33*). Thus, understanding the factors that influence the folding and conformation of gp41 is likely to provide insights into the complex biology of HIV-1 entry and its inhibition.

Coiled-coil motifs share a characteristic seven-amino acid (heptad) repeat, $(abcdefg)_n$, with hydrophobic residues at the first (*a*) and fourth (*d*) positions and polar residues generally elsewhere (*34*−*36*). Sequence comparisons between HIV-1 and SIV gp41 show that residues at the *a* and *d* positions of the N-terminal heptad-repeat region are highly conserved (*37*−*39*). There is only one nonconservative substitution (Ile573 in HIV-1 and threonine in the corresponding position in SIV). Interestingly, the hydrophobicity of the side chain at position 573 markedly affects the proper folding of the gp41 core as well as the in vivo phenotypes of the gp120−gp41 complex (*23*, *28*). For example, the Ile573 to serine mutation that impedes formation of the trimer of hairpins also abolishes HIV-1 infectivity (*23*, *28*). Serine and threonine differ by a single methyl group, yet threonine is entirely functional at the corresponding position (573) in SIV gp41. This study directly tests the role of the Thr573 side chain, as opposed to those of serine and isoleucine, in conferring the structural specificity and conformational stability of the gp41 core, as well as in determining the membrane fusion activity of the HIV-1 envelope protein complex. The Ile573 to threonine substitution was found to decrease the thermal stability of the trimer of hairpins by 25 °C, relative to the wild-type molecule. In the 2.3 Å resolution crystal structure of the mutant gp41 core, the O_γ atom of Thr573 is hydrogen bonded to the Thr569 main chain CO group of the same helix, thereby forming a buried polar interaction in an otherwise hydrophobic interface between the helices. This buried polar interaction appears to allow accommodation of the polar atom of Thr573 in the hydrophobic interface of the N-terminal coiled-coil core and thus to maintain the structural integrity of the trimer of hairpins for functional gp41 activation. Indeed, the HIV-1 envelope glycoprotein bearing the Ile573 to threonine mutation exhibits only a moderate reduction in fusion activity and virion infectivity. Our studies validate the notion that the conserved coiled-coil interactions within the N-terminal heptad repeat are important determinants of the gp41 conformational change required for HIV-1 membrane fusion.

MATERIALS AND METHODS

Plasmid Constructions. Plasmids for the expression of the recombinant I573T and I573T/N36(L6)C34 model polypeptides were constructed by oligonucleotide-directed mutagenesis of plasmids pN34/C28(L6) and pN36/L34(L6), respectively (*28*, *40*). Standard protocols for DNA manipulations were followed (*41*). The Ile573 to threonine mutation was introduced into the molecularly cloned *env* gene of the HIV-1 primary isolate ACH168.10 (168P) by using QuikChange mutagenesis (Stratagene, La Jolla, CA) and verified by DNA sequencing (*42*−*44*). The expression of the HIV-1 168P envelope protein was within the context of the eukaryotic expression vector pCR-Uni 3.1 (Invitrogen) (*43*). The DNA sequence of the molecularly cloned 168P *env* (168P23) is referenced by accession number AF035532. Note that the numbering system used to denote the positions of gp41 residues in HIV-1 168P is based on the numbering of residues in HIV-1 HXB2, to facilitate comparison with structural information published for this envelope glycoprotein (*13*, *16*, *17*).

Transfection and Immunoprecipitation. FuGENE-6 reagent (Roche Molecular Biochemicals) was used to transfect human 293T cells (provided by G. Nabel, University of Michigan, Ann Arbor, MI) for transient expression (*45*). Typically, 1 μg of the HIV-1 *env* expression plasmid and 3 μL of FuGENE reagent were used, according to the manufacturer's instructions, to transfect 2×10^5 cells/well in a six-well microculture dish. Transfection efficiencies were determined by immunochemical staining of monoloayers fixed in a cold methanol/acetone mixture (1:1) using anti-HIV immunoglobulin from infected persons (HIVIG) with alkaline phosphate-conjugated goat anti-human IgG antibody (Kirkegaard and Perry Labs, Inc., Gaithersburg, MD) and PhThalo Red chromogen (Kirkegaard and Perry Labs, Inc.). The expression of the 168P *env* within the transfected cell population and on the cell surface was also assessed by Western blot analysis. Surface proteins were labeled with biotin (NHS-LC-biotin; Pierce Chemical Corp., Rockford, IL) as previously described (*45*). Cells were lysed on ice in 50 mM Tris-HCl (pH 7.5), 150 mM NaCl, and 1% Triton X-100 containing aprotinin, leupeptin, and pepstatin (1 μg/mL each), and the envelope glycoprotein was immunoprecipitated using HIVIG and protein A−Sepharose (Sigma). Western blot analysis was performed using either the gp120 V3 loop-directed mAb 50.1 (*46*) or the gp41-directed mAb Chessie 8 (*47*), and horseradish peroxidase-conjugated sheep anti-mouse IgG antibody (Cappel, West Chester, PA). The biotinylated cell surface envelope glycoprotein was detected by using the avidin−horseradish peroxidase conjugate (Biomeda Corp., Foster City, CA). Proteins were visualized by ECL detection (Amersham Pharmacia Biotech). Spontaneous and soluble CD4-induced (10 μg/mL; 1 h at 37 °C) shedding of gp120 into the supernatant of transfected cell cultures was also assessed by Western blot analysis of HIVIG immunoprecipitable protein.

Cell−Cell Membrane Fusion Assay. The ability of wild-type and mutant envelope glycoproteins to mediate cell−cell fusion was determined by coculturing env-expressing cells with U87 cells expressing CD4 and the CXCR4 coreceptor (*43*, *48*, *49*). Transfected envelope glycoprotein-expressing 293T cells and U87-CD4-CXCR4 cells were

resuspended using 0.1 mM EDTA in physiologically buffered saline (PBS), and 1×10^4 cells of each were added to a 96-well microculture dish. Cocultures were fixed and immunochemically stained after 3 and 24 h, and the percentage of envelope protein-expressing cells involved in syncytium formation was determined microscopically.

Generation and Characterization of Pseudotyped Virions. HIV-1 virions containing the wild-type or mutant envelope glycoprotein were constructed by cotransfection of human 293T cells with the env-expressing plasmid and the *env*-defective proviral plasmid pSVNLthyDBgl (*43*, *50*). This latter plasmid contains the HIV NL4-3 provirus with a *BglI*−*BglI* deletion of the *env* gene. Cells were transfected using a 1:1 ratio of the HIV-1 168P *env* plasmid and pSVNLthyDBgl DNAs and FuGENE reagent (total of 1 μg of DNA and 3 μL of FuGENE-6 reagent for 2×10^5 cells per well in a six-well microculture dish). Transfection and harvest conditions were optimized using the wild-type 168P *env* plasmid. Three days post-transfection, cell culture supernatants containing pseudovirions were collected, filtered (0.22 μm), and used without freezing. The relative amount of envelope glycoprotein incorporated within wild-type and mutant pseudovirions was determined by analysis of pelleted particles purified by centrifugation (*51*, *52*). The envelope glycoprotein was quantitated by Western blot analysis using the gp120 V3-directed mAb 50.1 as described above, except that ECL-Plus (Amersham Pharmacia Biotech) was used and specific chemifluoresence was determined using a Fuji FLA-3000G analyzer. The relative amount of p24 was similarly quantified using HIVIG to identify pseudovirion p24 (*45*). The infectivity of pseudovirion-containing supernatant was determined by the enumeration of infected U87-CD4-CXCR4 cells in 96-well microcultures (*43*, *48*). The number of infected foci was determined 2 days after infection by immunochemical staining of cultures fixed in a methanol/acetone mixture using HIVIG, as described above.

Protein Production and Purification. All recombinant polypeptides were expressed in *Escherichia coli* BL21(DE3)/pLysS using the T7 expression system (*53*). Cells, freshly transformed with an appropriate plasmid, were grown to late log phase. Protein expression was induced by addition of 0.5 mM isopropyl thio-β-D-galactoside (IPTG). After an additional 3 h of growth at 30 or 37 °C, the bacteria were harvested by centrifugation, and the cells were lysed with glacial acetic acid as described previously (*54*). Proteins were purified from the soluble fraction to homogeneity by reverse-phase HPLC (Waters) with a Vydac C-18 preparative column using a water/acetonitrile gradient in the presence of 0.1% (v/v) trifluoroacetic acid. The peptide identity was confirmed by matrix-assisted laser-desorption ionization mass spectrometry (PerSeptive Biosystems Voyage Elite). Protein concentrations were determined by measuring the absorbance at 280 nm in 6 M guanidinium hydrochloride (*55*).

Circular Dichroism Spectroscopy. CD spectra were acquired on an AVIV 62DS circular dichroism spectrometer with a thermoelectric sample temperature controller. Samples for wavelength spectra were 10 μM peptide in 50 mM sodium phosphate (pH 7.0) and 150 mM NaCl. The cuvette path length was 0.1 cm. The wavelength dependence of molar ellipticity, $[\theta]$, was monitored at 0 °C as the average of five scans, using a 5 s integration time at 1.0 nm wavelength increments. Spectra were baseline-corrected against the cuvette with buffer alone. The fractional helix content was calculated from the CD signal by dividing the mean residue ellipticity at 222 nm by the value expected for 100% helix formation by helices of comparable size, −33000 deg cm^2 dmol^{-1} (*56*). Thermal stability was determined in the same buffer by measuring $[\theta]_{222}$ as a function of temperature. A 1.0 cm path length cell was used with continuous stirring. Thermal melts were monitored in 2 °C intervals with a 2 min equilibration at the desired temperature, and an integration time of 30 s. Reversibility was checked by repeated scans. The thermal melt of I573T was not reversible, while that of I573T/N36(L6)C34 was reversible with superimposable folding and unfolding curves and >90% of the signal regained upon cooling. The midpoint of the thermal unfolding transition (T_m) was determined from the maximum of the first derivative, with respect to the reciprocal of the temperature, of the $[\theta]_{222}$ values (*57*). The error in the estimation of T_m is ±1 °C.

Sedimentation Equilibrium. Apparent molecular weights were determined by sedimentation equilibrium studies with a Beckman XL-A Optima analytical ultracentrifuge as described previously (*58*). Protein samples were dialyzed overnight against 50 mM sodium phosphate (pH 7.0) and 150 mM NaCl, loaded at initial concentrations of 10, 30, and 100 μM, and analyzed at 20 °C at rotor speeds of 20 000 and 23 000 rpm for I573T, and 17 000 and 20 000 rpm for I573T/N36(L6)C34. Data were acquired at two wavelengths per rotor speed and processed simultaneously with a nonlinear least-squares fitting routine (*59*). Solvent density and protein partial specific volume were calculated according to solvent and protein composition, respectively (*60*). Molecular weights were all within 10% of those calculated for an ideal trimer, with no systematic deviation of the residuals.

Crystallization, Data Collection, and Structure Determination. The I573T/N36(L6)C34 mutant was crystallized by the hanging-drop vapor diffusion method at room temperature. To grow crystals, a 10 mg/mL HPLC-purified protein stock was diluted 1:1 with a reservoir and allowed to equilibrate against the reservoir solution. Initial crystallization conditions were screened by using sparse matrix crystallization kits (Crystal Screen I and II, Hampton Research, Riverside, CA) and then optimized. Crystals of I573T/N36(L6)C34 in space group $P1$ were grown from 0.1 M sodium citrate (pH 4.6), 5% propanol, and 7% polyethylene glycol 4000. For data collection, crystals were transferred to a cryoprotected solution containing 15% (v/v) glycerol in the corresponding mother liquor. Diffraction data were collected at 95 K using an R-axis IV image plate detector mounted on a Rigaku RU200 rotating anode X-ray generator at the X-ray Crystallography Facility at the Weill Medical College of Cornell University. Diffraction intensities were integrated by using DENZO and SCALEPACK software (*61*) and reduced to structural factors with the program TRUNCATE from the CCP4 program suite (*62*).

The structure of I573T/N36(L6)C34 was determined by molecular replacement using the program AMoRe (*63*). The 2.4 Å X-ray structure of the N34(L6)C28 trimer was used as a search model (*17*). The initial model was built by using conventional $(2F_o - F_c)\Phi_{calc}$ and $(F_o - F_c)\Phi_{calc}$ maps at 3.0 Å. Overall anisotropic B-factor and bulk solvent corrections were applied. Many cycles of torsional angle simulated annealing and grouped B-factor refinement (*64*) were fol-

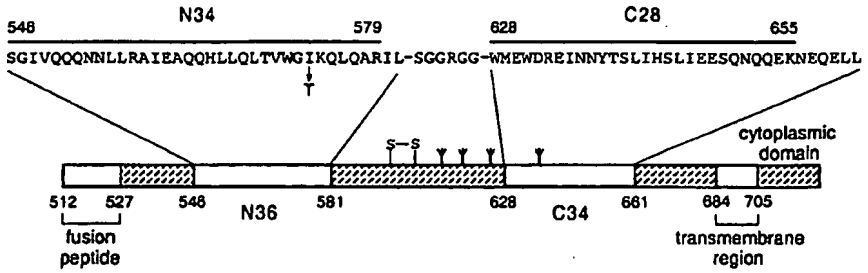

FIGURE 1: Schematic view of the HIV-1 gp41 envelope glycoprotein. The important functional features of the gp41 ectodomain, the peptides identified by protein dissection, and the sequences of N36 and C34 are shown. The N36(L6)C34 model consists of N36 and C34 plus a six-residue linker. The Thr573 to threonine substitution is indicated below the N36 sequence. The disulfide bond and four potential N-glycosylation sites are depicted. The residues are numbered according to their position in gp160 of the HXB2 HIV-1 strain.

lowed by extensive rebuilding. The resulting map revealed traceable electron density for all the amino acid residues except for a few at the helix termini and in the linker region. The final model corresponding to two trimers was built with the program O (*65*). The structure was refined by using positional and *B*-factor refinements (*64*) for all data between 50.0 and 2.3 Å resolution. Crystallographic refinement of the structure was carried out with the program CNS 0.5 (*66*). As the refinement proceeded, 271 waters were added. Model geometry was analyzed by PROCHECK (*67*), with all residues but a few at the helix termini and in the linker region occupying most-preferred regions of the Ramachandran space. Ala578 of monomers A and B, Leu660 of monomer B, Ile580 and Ser1 of monomer D, and Leu581 and Glu659 of monomer E lie in the additionally allowed regions of the Ramachandran plot. The overall temperature factor of the model is 28.5 Å^2. Side chains of Arg579 of monomers A and F, Arg4 of monomers A–C and E, Met629 and Arg633 of monomer B, Glu659 of monomers C and F, Glu654 of monomer E, and Gln577 and Gln658 of monomer F are disordered and were thus modeled as serine. Side chains of Met629 of monomer A, Gln550, Arg579, Ile580, and Lys655 of monomer B, Gln577, Arg579, His643, Asn651, and Gln658 of monomer C, His643, Glu654, and Gln658 of monomer D, Lys655 and Gln658 of monomer E, and Ile580 and Lys655 of monomer F were modeled as alanine, while side chains of Leu581 and Ser1 of monomer A were modeled as glycine. In addition, Ile580 of monomer A, Leu581 of monomers B and C, Ser1, Gly2, and Gly3 of monomers B, C, and F, and Leu661 of monomers A and C–E were left out of the model because of the absence of interpretable electron density for these atoms.

RESULTS

gp41 Ectodomain Core with Buried Thr573 Residues. The Ile573 residue, located at an *a* heptad position in the N-terminal heptad-repeat region of gp41, is completely conserved in 208 of 213 fully sequenced M group HIV-1 strains (*68*). All the remaining five isolates at this position possess a conservative valine substitution. Mutagenesis studies have shown that nonconservative substitutions for Ile573 abolish infectivity and membrane fusion (*23*) and cause a folding defect in the recombinant N34(L6)C26 polypeptide model for the gp41 ectodomain core (*28*). Thus, the high level of sequence conservation of the buried isoleucine residue is thought to result from selective pressure to maintain the trimeric coiled-coil interactions within the fusogenic gp41 conformation needed for initiating HIV-1 membrane fusion. It is therefore puzzling that SIV gp41 contains the polar threonine residue at the corresponding position. To address how this nonconservative mutation affects the folding of HIV-1 gp41, we substituted Ile573 with threonine in N34(L6)C28 (Figure 1). This mutant recombinant polypeptide, named I573T, was produced by bacterial expression and purified by reverse-phase high-performance liquid chromatography.

Sedimentation equilibrium measurements were used to determine the oligomerization state of the I573T mutant. Like the wild-type peptide, I573T sediments as a discrete trimer over a 10-fold range of peptide concentrations (10–100 μM) (Figure 2a and Table 1). On the basis of circular dichroism measurements at a protein concentration of 10 μM in 50 mM sodium phosphate (pH 7.0) and 150 mM NaCl at 0 °C, I573T contains >95% α-helical structure, whereas the same recombinant peptide with the fusion-defective serine mutation (I573S) appears to be ~40% helical (Figure 2b and Table 1). Under these conditions, I573T exhibits a cooperative thermal unfolding transition with an apparent melting temperature (T_m) of 45 °C, as compared to the apparent T_m value of 70 °C for N34(L6)C28 (wild-type) (Figure 2c and Table 1). The I573T trimeric structure is less stable than the wild-type molecule, yet it is considerably more stable than the corresponding I573S mutant (Table 1). This reinforces the observation that buried polar residues in the hydrophobic core of a coiled coil are generally destabilizing (e.g., ref *69*). Nevertheless, it would appear that the I573T mutant can fold into a stable trimer-of-hairpins structure at physiological temperature.

To better understand how the buried threonine side chain influences the folding and stability of the gp41 core, we determined the X-ray crystal structure of the trimeric gp41 core containing the Ile573 to threonine mutation at 2.3 Å resolution. We were unable to obtain crystals of the I573T mutant in the N34(L6)C28 model and so made use of the slightly larger N36(L6)C34 model (*70*) (see Figure 1). Crystals of I573T/N36(L6)C34 have distinct, triclinic symmetry and contain six monomers in the asymmetric unit; each monomer is related by an approximate noncrystallographic 3-fold axis. Using the molecular replacement method, an initial model corresponding to two trimers was built. Iterative rounds of manual rebuilding and refinement increased the quality of the initial electron density map and served to reduce model bias, as guided chiefly by improvement in the free *R*-factor. The structure has been refined to a conventional

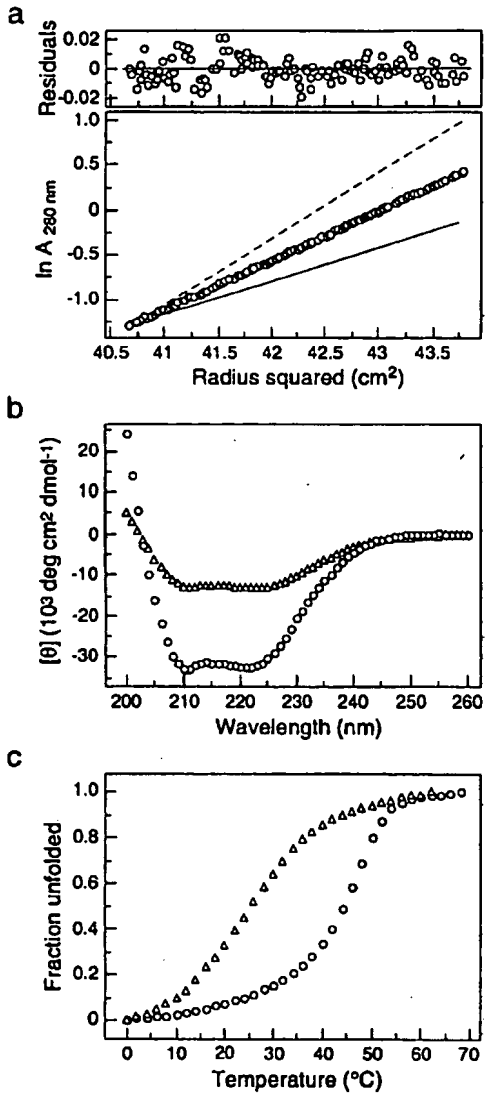

FIGURE 2: Folding of the I573T peptide as an α-helical trimer. (a) Sedimentation equilibrium data (20 000 rpm) of I573T collected at 20 °C in 50 mM sodium phosphate (pH 7.0) and 150 mM NaCl at a protein concentration of ~30 μM. The natural logarithm of the absorbance at 280 nm is plotted against the square of the radial position. The random distributions of the residuals indicate that the data fit well to an ideal single-species model. The slope of the plotted data indicates the I573 peptide is a trimeric species. The calculated data for dimeric and tetrameric models are indicated by solid and dashed lines, respectively. (b) Circular dichroism (CD) spectra of I573T (○) and I573S (△) at 0 °C in 50 mM sodium phosphate (pH 7.0) and 150 mM NaCl at a protein concentration of 10 μM. (c) Thermal melts monitored by CD at 222 nm for I573T (○) and I573S (△). The decrease in the fraction of a folded molecule is shown as a function of temperature.

R-factor of 19.1% and a free *R*-factor of 27.0% for data in the resolution shell from 50.0 to 2.3 Å. The root-mean-square deviations of bond lengths and bond angles from the ideal values are 0.006 Å and 0.9°, respectively. The final $2F_o - F_c$ electron density map is of good quality (Figure 3a) and reveals the positions of all amino acid residues except for a few disordered residues at the helix termini and in the six-residue loop region (see Materials and Methods). The crystallographic statistics are summarized in Table 2.

Table 1: Summary of Circular Dichroism and Sedimentation Equilibrium Data for the HIV-1 gp41 Core Mutants

model	$-[\theta]_{222}$[a] (deg cm² dmol⁻¹)	T_m[a] (°C)	molecular mass (kDa)
N34(L6)C28	31 300	70	24.4
I573S	13 100	25	NA[b]
I573T	32 300	45	24.1

[a] All scans and melts were performed at a protein concentration of 10 μM. [b] NA, not applicable. The I573S peptide forms an insoluble aggregate at concentrations above ~10 μM in 50 mM sodium phosphate (pH 7.0) and 150 mM NaCl.

The overall architecture and helix packing of the I573T/N36(L6)C34 trimer are the same as those of the wild-type gp41 core (*13*, *16*, *17*). Three molecules, each consisting of an N36 helix paired with an antiparallel C34 helix, pack together around the noncrystallographic 3-fold axis to form a trimer of hairpins. Three N36 helices form an interior, parallel coiled-coil trimer with a left-handed superhelical pitch, while three C34 helices wrap in an oblique, antiparallel manner against the surface of the N36 coiled coil (Figure 3b). The root-mean-square (rms) deviation between all C_α atoms of the entire helical regions between I573T/N36(L6)C34 and the wild-type N36/C34 complex (*16*) is 0.54 Å. This correspondence indicates that the Thr573 substitution causes little distortion of the trimer-of-hairpins structure. In addition, comparatively weak electron density and higher-than-average main chain *B*-values suggest that the Ser-Gly-Gly-Arg-Gly-Gly hydrophilic linker of the I573T/N36(L6)C34 mutant may be dynamically disordered. Thus, the linker does not dominate formation of the trimer of hairpins.

In both wild-type and I573T/N36(L6)C34 structures, three N helices are packed together in the classical acute "knobs-into-holes" arrangement characteristic of trimeric coiled coils, in which the $C_\alpha - C_\beta$ bonds in the side chains (knobs) of residues *a* and *d* make an acute angle with respect to the recipient holes formed by spaces between four residues on the neighboring helices (*69*, *71*). The Thr573 side chains, at the *a* position, face each other across the molecular 3-fold symmetry axis and form a network of new hydrogen bonds between the side chain O_γ atom and the backbone carbonyl group of Thr569 in the preceding turn of the same helix (Figure 4). As a consequence, a cavity (22 Å³) is located between the Thr569 and Thr573 layers. No electron density was apparent in this cavity. The Thr573 side chains move closer to each other toward the center of the coiled-coil trimer. The radius of the coiled-coil core at this Thr573 layer, calculated on the basis of the average $C_\alpha - C_\alpha$ distance between the residues at the same heptad layer, is 3.79 Å. In contrast, the radius of the corresponding Ile573 layer in the wild-type N36/C34 structure is 3.94 Å. It would appear that the stabilization energy gained from the favorable hydrogen-bonding and side chain packing interactions allows the polar threonine residues to be accommodated in the interior coiled-coil core without significantly altering the trimer-of-hairpins structure. In addition, the C_γ atoms of the Thr573 side chains are too far from each other to make van der Waals contacts and the buried Thr573 residue therefore contributes little to the interhelical packing interactions.

Membrane Fusion Properties of the I573T Envelope Glycoprotein. Replacement of the buried Ile573 residue by either serine, glycine, or proline completely inhibits the abil-

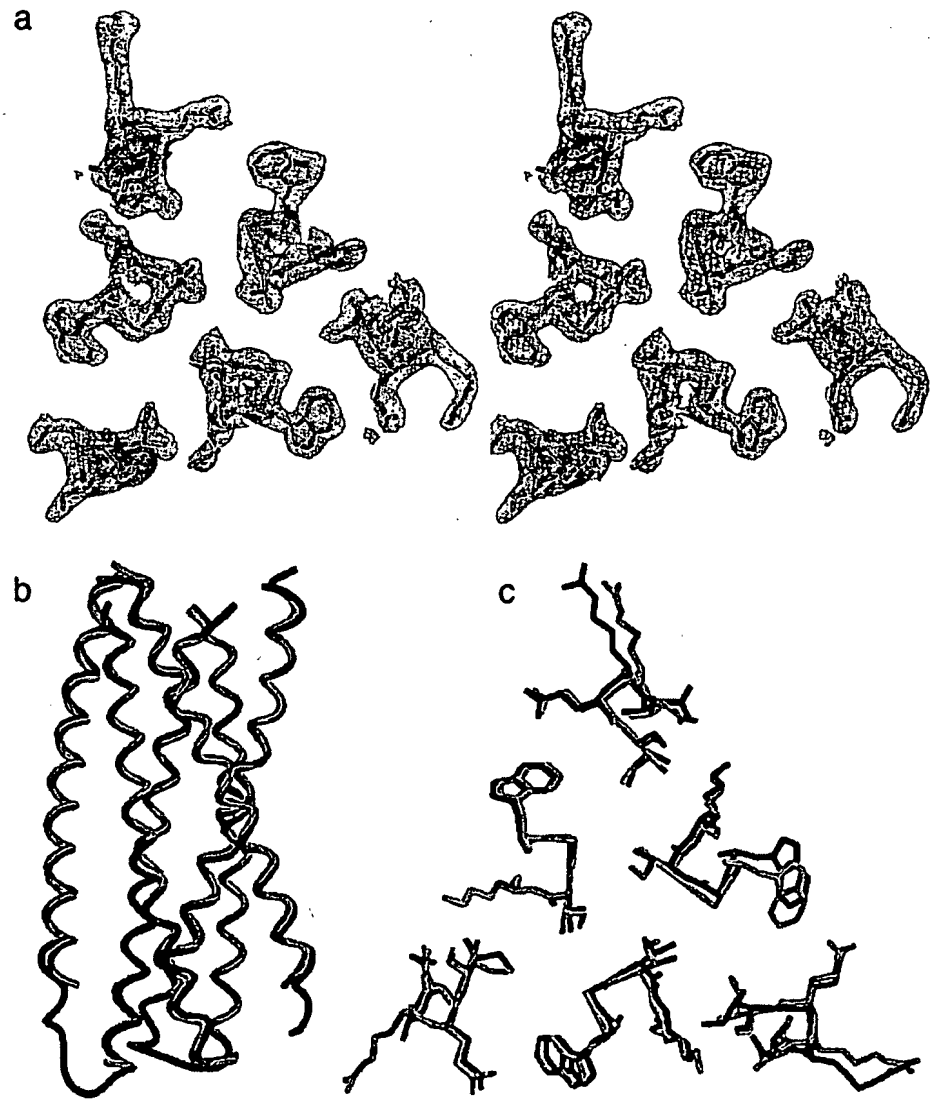

FIGURE 3: Crystal structure of the I573T/N36(L6)C34 trimer. (a) Stereoview of the final electron density map at 2.3 Å resolution, contoured at 1.0 standard deviation above the average density. The acute knobs-into-holes packing of Thr573 in an *a* level is shown. (b) Side view of the C_α traces of the N36 and C34 helices in the N36/C34 complex (green) and I573T/N36(L6)C34 (red) structures which were used for the superposition. The N-terminus of N36 and the C-terminus of C34 are at the top of the figure. (c) A cross section of the helix packing near the Thr573 layer. Structures of N36/C34 (green) and I573T/N36(L6)C34 (red) are overlaid. The figures were generated with the program SETOR (*82*).

ity of the envelope glycoprotein to mediate membrane fusion and also disrupts formation of the trimeric N34(L6)C28 complex (*23*, *28*). The structure and folding of the gp41 core is thus believed to control the key process of HIV-1 membrane fusion (*22*, *28*). Therefore, a mutation that affects the stability of the trimer-of-hairpins structure would be predicted to change the fusion properties of the HIV-1 envelope glycoprotein. Since the I573T mutant clearly maintains the trimer-of-hairpins structure, albeit with less thermal stability, we asked whether the threonine mutation would also affect the membrane fusion activity of the gp120−gp41 complex. To test this, we introduced the Ile573 to Thr mutation into the intact envelope glycoprotein of the HIV-1 primary isolate ACH168.10 (168P). This dual coreceptor-utilizing primary isolate has been well-characterized (*42*, *44*), and the molecularly cloned *env* gene has been used in other studies of envelope glycoprotein biology (*43*, *45*, *72*). The gp41 subunit of the 168P envelope glycoprotein is identical to the wild-type N34(L6)C28 in amino acid sequence throughout the N34 region and at all *a* and *d* positions of the C28 helix.

In keeping with the minimal structural changes induced by the Ile573 to threonine mutation characterized above, we could detect no differences in the biosynthesis of the wild-type 168P and I573T envelope glycoproteins when expressed in human 293T cells. Transient transfection studies yielded comparable frequencies and levels of envelope glycoprotein expression. Furthermore, envelope glycoprotein processing and transport to the cell surface were also comparable, as determined by Western blot analysis of cell surface-expressed gp160 and gp120 (Figure 5a). In both cases, ~30% of the cell surface envelope protein was found as mature, pro-

Table 2: X-ray Data Collection and Refinement Statistics

unit cell dimensions	
a, b, c (Å)	38.92, 41.87, 55.98
α, β, γ (deg)	90.59, 88.93, 96.28
space group	P1
data processing	
resolution (Å)	50.0−2.3
no. of measured reflections	62249
no. of unique reflections	14667
completeness (%)	96.1
R_{merge}[a] (%)	7.6
refinement	
resolution (Å)	50.0−2.3
no. of reflections in the working set	13174
no. of reflections in the test set	1493
no. of protein non-hydrogen atoms	3494
no. of water molecules	271
R_{free}[b] (%)	27.0
R_{cryst}[b] (%)	19.1
average B-factor (Å²)	28.5
rms deviations from ideality	
bond lengths (Å)	0.006
bond angles (deg)	0.9
torsion angles (Å)	15.9

[a] $R_{merge} = \Sigma|I - \langle I\rangle|/\Sigma I$, where I is the intensity of an individual measurement and $\langle I\rangle$ is the average intensity from multiply recorded reflections. [b] $R_{cryst} = \Sigma||F_{obs}| - |F_{calc}||/\Sigma|F_{obs}|$, where F_{obs} and F_{calc} are the observed and calculated structural factors, respectively. No σ cutoff was applied. R_{free} is calculated for a set of reflections that were excluded from refinement.

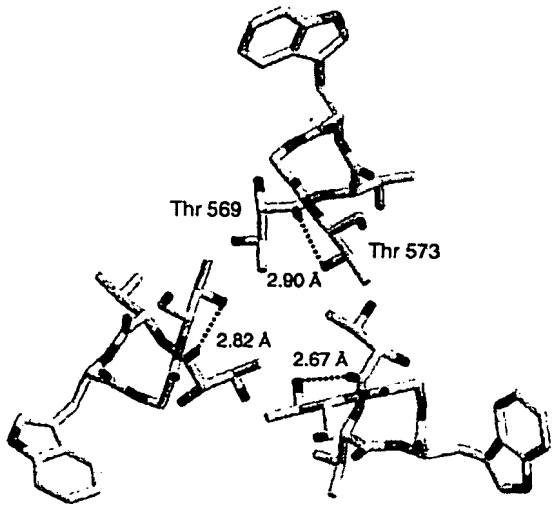

FIGURE 4: Thr573 side chain hydrogen bonding to the Thr569 carbonyl group in the I573T/N36(L6)C34 structure. Oxygen, nitrogen, and carbon atoms are colored red, blue, and yellow, respectively. The hydrogen bond is shown as a purple dotted line. This figure was created with the program SETOR (*82*).

teolytically processed gp120. The accumulation of unprocessed (and fusion-inactive) gp160 presumably reflects saturation of the cellular proteolytic machinery in the context of high levels of envelope protein expression. Examination of the cell culture supernatants from transfected cells also revealed comparable levels of spontaneously shed wild-type 168P and I573T gp120 (Figure 5a). Incubation with soluble CD4 did not significantly increase the amount of gp120 shedding above this level. Thus, the wild-type and I573T envelope glycoproteins were indistinguishable in their biosynthesis transport and processing.

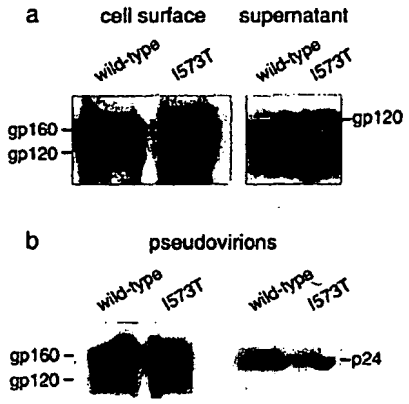

FIGURE 5: Analysis of envelope glycoprotein expression and incorporation into pseudotyped virions. (a) Western blot analysis of wild-type and I573T envelope glycoprotein expression in transfected 293T cells. The cell surface envelope glycoprotein (left) was identified by surface biotinylation as described in Materials and Methods. Shed gp120 was identified in the cell culture supernatant (right) using mAb 50.1. (b) Western blot analysis of centrifugally purified pseudotyped virion particles containing wild-type and I573T envelope glycoprotein. The virion envelope glycoprotein (left) was identified as described using mAb 50.1. The virion p24 core antigen (right) was identified using HIVIG.

The ability of the wild-type and I573T envelope glycoproteins to mediate cell−cell fusion was assessed by coculture of envelope glycoprotein-expressing 293T cells with human U87 glioma cells expressing both CD4 and the CXCR4 coreceptor (U87-CD4-CXCR4) (*43*, *48*, *49*). Envelope glycoprotein-induced cell−cell fusion was assessed microscopically at 3 and 24 h following mixing of the cells. The I573T mutant envelope glycoprotein was entirely competent in inducing multinucleated syncytium formation. In most experiments, however, the I573T mutant yielded a slightly lower percentage of envelope glycoprotein-expressing cells in syncytia and a smaller number of nuclei per syncytia at the 24 h time point (typically 10−20 nuclei/syncytium vs 30−50 nuclei/syncytium in the wild type) (Figure 6). Syncytium formation could be inhibited by incubation with soluble CD4, and both envelope glycoproteins were similarly sensitive to this inhibition, with an IC_{50} (50% inhibitory concentration) of ~100 μg/mL. Thus, and in striking contrast to the previously published I573S mutant envelope glycoprotein (*23*), the I573T protein appears only slightly reduced in its ability to mediate membrane fusion.

Infectivity of HIV-1 Virions Bearing the I573T Envelope Glycoprotein. To test the ability of the I573T mutant envelope glycoprotein to mediate virus−cell fusion and to initiate infection, we generated pseudotyped virion particles bearing the wild-type and I573T envelope glycoproteins. These pseudotyped viruses were produced by cotransfection of 293T cells with a plasmid expressing the respective envelope glycoprotein and a plasmid expressing an otherwise-infectious HIV NL4-3 provirus genome but with a deletion in the *env* gene (*43*, *50*). Particles comprising the NL4-3 core and the respective envelope glycoprotein were harvested from the culture supernatant and contained comparable amounts of virion p24 core antigen (Figure 5b). In addition, both wild-type and I573T envelope glycoproteins were incorporated into virion particles with comparable efficien-

BEST AVAILABLE COPY

FIGURE 6: Syncytium formation by the wild-type and I573T envelope glycoprotein. 293T cells were transfected to transiently express the wild-type or I573T envelope glycoprotein and were cocultured with U87-CD4-CXCR4 target cells for 24 h to assess envelope glycoprotein-mediated cell−cell fusion. The microphotograph demonstrates the functionality of the I573T envelope glycoprotein (b), as well as the slight reduction in the ultimate extent of multinucleated cell (syncytium) formation relative to the wild-type glycoprotein (a). Envelope protein-expressing cells are stained in red.

cies, as determined by the ratio of the envelope glycoprotein to the p24 gag core protein in centrifugally purified particles (Figure 5b). As on the cell surface, mature gp120 comprised only a fraction of the total virion envelope protein. Both wild-type and I573T pseudotyped particles yielded infectious virus. Viral titers were determined by titration of pseudotyped virus stocks onto U87-CD4-CXCR4 cells. In these studies, high concentrations of transfected cell supernatant-containing pseudotyped virus (≤1:10 dilution of supernatant onto target cells) exhibited an unexplained inhibitory effect on infectivity. The nominal titer of infectious wild-type and I573T pseudotyped virions was therefore determined at greater dilutions where the number of foci of infected cells was linearly related to the virus input (Figure 7). This analysis suggests that the infectivity of pseudotyped virions bearing the I573T mutant envelope glycoprotein is not markedly reduced relative to pseudotyped virions bearing the wild-type envelope glycoprotein. It should be noted that the precise interpretation of pseudotyped virion titer is confounded by variability among transfection experiments and by the high level of uncoordinated synthesis and assembly of virion particles in this system. The slight reduction observed in viral infectivity in the I573T virion corresponds with the previously noted reduction in the ability of the I573T envelope glycoprotein to mediate cell−cell fusion, and perhaps with the moderate reduction in the thermal stability of the I573T gp41 core.

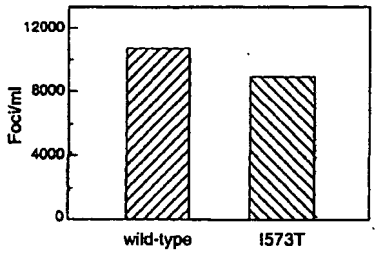

FIGURE 7: Infectivity of pseudotyped virions bearing wild-type or I573T envelope glycoprotein. Pseudotyped virions were prepared as described, and assayed for infectivity using U87-CD4-CXCR4 cells. Infectious titer of pseudovirions per milliliter of transfected cell supernatant. Nominal titers were calculated using data from the 1:16 dilution.

DISCUSSION

Evidence suggests that the HIV-1 envelope glycoprotein can adopt at least three different conformations: the native state, the prehairpin intermediate, and the fusogenic state (reviewed in refs *12* and *73*). This structural polymorphism is the means whereby the gp41 molecule is activated to drive membrane fusion during viral entry. The structural and biophysical properties of a proteolytically resistant ectodomain of HIV-1 gp41 in the putative fusogenic state are well-characterized (*13*, *15*−*17*, *28*, *54*, *74*). Three gp41 molecules form a trimer of hairpins in which an N-terminal three-stranded coiled coil is surrounded by a sheath of three antiparallel C-terminal helices. Earlier genetic studies showed that conservative changes (leucine or valine) in the Ile573 site (an *a* position in the gp41 N-terminal heptad-repeat region) maintain a wild-type fusion phenotype, while non-conservative mutations (serine or proline) result in the envelope glycoproteins that are completely defective in mediating membrane fusion (*23*). Interestingly, a correlation is observed between mutational effects on the thermal stability of the N34(L6)C28 trimer and on the membrane fusion activities of the intact envelope glycoprotein (*28*). It would appear that the free energy made available by the assembly of the fusogenic gp41 core complex is required to bring two lipid bilayers into intimate approximation to initiate fusion (*9*, *12*−*14*). In a similar manner, triggering N-terminal trimeric coiled-coil formation at an early step of the gp41 activation process is postulated to provide a thermodynamic driving force for its initial structural rearrangements toward the prehairpin intermediate, though few details are understood (*22*, *26*, *28*). This conformational change likely facilitates exposure of the hydrophobic, glycine-rich sequence termed the fusion peptide at the N-terminus of gp41, leading to insertion into the bilayer of the target membrane to bridge the two membranes at the fusion site (*1*, *2*, *75*, *76*).

The N-terminal heptad-repeat sequence of gp41 is one of the most highly conserved regions within the HIV-1 envelope glycoprotein, a protein noted for its diversity among even closely related isolates (*37*−*39*). When HIV and SIV gp41 are compared, 10 of 15 residues at the *a* and *d* positions are identical, with a single nonconservative substitution (Ile573 to threonine) present at an *a* position. This high degree of sequence conservation supports the proposal that the hydrophobicity of the substituted residue at position 573 is critical for refolding of gp41 into its fusogenic conformation during membrane fusion. The presence of a polar threonine residue

at this site in SIV gp41 raises questions about this proposal. In this study, we have analyzed the structural role of the Thr573 residue on the folding and stability of the HIV-1 gp41 core. Thermal unfolding experiments indicate that the Ile573 to threonine mutation leads to a destabilization of the trimer-of-hairpins structure by a T_m shift of ~25 °C, with a T_m value of 45 °C for the I573T mutant. By comparison, the fusion-defective Ile573 to serine mutation essentially disrupts the formation of the gp41 core structure (Table 1). The crystal structure of the I573T/N36(L6)C34 mutant at 2.3 Å resolution shows that the buried Thr573 residue is accommodated in the trimer of hairpins, and that the O_γ atom of Thr573 is able to form a new hydrogen bond with the main chain CO group of Thr569 of the same helix. Consequently, the polar atoms of the threonines are inaccessible to solvent, thereby allowing them to pack efficiently in the coiled-coil trimer interface. Indeed, the same buried intrahelical hydrogen bond is formed between Thr569 and the invariant Thr573 residue in the SIV N36/C34 trimer (*19*). Interestingly, in the case of SIV, the replacement of Thr573 with isoleucne further increases the T_m of the trimeric SIV N34(L6)C28 complex from 48 to 69.6 °C, a value close to that of the analogous HIV-1 wild-type molecule (*77*). Therefore, we infer that the buried core residue at position 573 (threonine in SIV vs isoleucine in HIV-1) is responsible for a thermal stability difference between the HIV-1 and SIV gp41 cores. This stability difference may be related to known phenotypic differences between HIV-1 and SIV envelope glycoproteins (*22*, and references therein). For example, it has been reported that the gp120 and gp41 subunits associate more tightly in SIV than in HIV-1 (*78*, *79*). One might envision that this association is strengthened not by stabilization of the native gp120−gp41 complex but rather by the relative destabilization of the fusion-active core of SIV gp41 by the Thr573 side chain.

Our biophysical and structural analyses directly demonstrate that the gp41 ectodomain core with the Ile573 to threonine mutation is stably folded under physiological conditions, even though it is destabilized relative to the wild-type molecule. If the stability of fusion-active gp41 is an important determinant for its fusion potential (*22*, *28*), one might expect the mutant HIV-1 envelope glycoprotein to be functional, albeit perhaps with some impairment in fusion efficiency. Consistent with this prediction, we have shown that the fusion phenotype of the I573T envelope glycoprotein is similar to that of the wild-type envelope protein complex. When assayed for the ability to drive cell−cell fusion, the mutant envelope glycoprotein induces multinucleated syncytia that are only slightly less extensive than those produced by the wild-type glycoprotein. Infectivity studies using pseudotyped virions also show that the mutant virion infects U87 cells with only slightly reduced titer, relative to the wild type. By contrast, the gp120−gp41 complex bearing the highly destabilized Ile573 to serine mutation is defective in mediating membrane fusion (*23*, *28*). Our results provide direct evidence that the stability of the trimer-of-hairpins structure determines the membrane fusion properties of the gp120−gp41 complex. We propose that the receptor-triggered conformational changes of the HIV-1 envelope glycoprotein are thermodynamically controlled, and that the process of membrane apposition and lipid bilayer fusion is driven by the currency of energy released from the formation of the fusion-active gp41 core. We suggest that the conformational state and membrane fusion activity of the gp120−gp41 complex are mechanistically coupled and thermodynamically linked.

A major problem in the development of envelope protein immunogens for HIV-1 vaccines is the lack of information about the antigenic structure of the functioning envelope glycoprotein. Recent studies suggest that the transiently populated intermediate structures within the gp120−gp41 complex are able to elicit broadly neutralizing antibodies (*72*). An understanding of the structural determinants for the native and intermediate conformations of the HIV-1 envelope protein will thus have ramifications beyond general considerations of the biology of viral entry and will be critical in the rational design of potential vaccine immunogens. It is possible, as perhaps in SIV, that introducing mutations to destabilize the HIV-1 N-terminal trimeric coiled-coil interactions within the prehairpin intermediate could block gp41 activation and shift the conformational equilibrium of the envelope protein toward the native state. Efforts to preserve the native envelope glycoprotein structure in vaccine candidates have to date relied on approaches to stabilize the trimeric gp120−gp41 complex (*80*, *81*). Alternatively, mutations such as those at position 573 that destabilize the fusogenic gp41 hairpin structure may result in an increased population of the postulated prehairpin intermediate. The data presented here suggest that the analysis of gp41 ectodomain core mutants may offer a test bed for the definition of the gp41 conformational states and may allow the stabilization of either the native gp120−gp41 complex or intermediate structures. Emerging structural, biophysical, and blological information will provide insights to guide the development of effective HIV vaccines and antiviral agents.

REFERENCES

1. Carr, C. M., and Kim, P. S. (1993) *Cell 73*, 823−832.
2. Bullough, P. A., Hughson, F. M., Skehel, J. J., and Wiley, D. C. (1994) *Nature 371*, 37−43.
3. Huguson, F. M. (1995) *Curr. Biol. 5*, 265−274.
4. Hernandez, L. D., Hoffman, L. R., Wolfsberg, T. G., and White, J. M. (1996) *Annu. Rev. Cell Dev. Biol. 12*, 627−661.
5. Chen, J., Wharton, S. A., Weissenhorn, W., Calder, L. J., Hughson, F. M., Skehel, J. J., and Wiley, D. C. (1995) *Proc. Natl. Acad. Sci. U.S.A. 92*, 12205−12209.
6. Carr, C. M., Chaudhry, C., and Kim, P. S. (1997) *Proc. Natl. Acad. Sci. U.S.A. 94*, 14306−14313.
7. Hunter, E., and Swanstrom, R. (1990) *Curr. Top. Microbiol. Immunol. 157*, 187−253.
8. Luciw, P. A. (1996) in *Fields Virology* (Fields, B. N., Knipe, D. M., Howley, P. M., Chanock, R. M., Melinick, J. L., Monath, T. P., Roizman, B., and Straus, S. E., Eds.) pp 1881−1952, Lippincott-Raven Publishers, Philadelphia.
9. Furuta, R. A., Wild, C. T., Weng, Y., and Weiss, C. D. (1998) *Nat. Struct. Biol. 5*, 276−279.
10. Jones, P. L., Korte, T., and Blumenthal, R. (1998) *J. Biol. Chem. 273*, 404−409.
11. Munoz-Barroso, I., Durell, S., Sakaguchi, K., Appella, E., and Blumenthal, R. (1988) *J. Cell Biol. 140*, 315−323.
12. Chan, D. C., and Kim, P. S. (1998) *Cell 93*, 681−684.
13. Weissenhorn, W., Dessen, A., Harrison, S. C., Skehel, J. J., and Wiley, D. C. (1997) *Nature 387*, 426−430.
14. Hughson, F. M. (1997) *Curr. Biol. 7*, R565−R569.
15. Lu, M., Blacklow, S. C., and Kim, P. S. (1995) *Nat. Struct. Biol. 2*, 1075−1082.
16. Chan, D. C., Fass, D., Berger, J. M., and Kim, P. S. (1997) *Cell 89*, 263−273.

17. Tan, K., Liu, J., Wang, J., Shen, S., and Lu, M. (1997) *Proc. Natl. Acad. Sci. U.S.A. 94*, 12303−12308.
18. Caffrey, M., Cai, M., Kaufman, J., Stahl, S. J., Wingfield, P. T., Covell, D. G., Gronenborn, A. M., and Clore, G. M. (1998) *EMBO J. 17*, 4572−4584.
19. Malaskkevich, V. N., Chan, D. C., Chutkowski, C. T., and Kim, P. S. (1998) *Proc. Natl. Acad. Sci. U.S.A. 95*, 9134−9139.
20. Yang, Z.-N., Mueser, T. C., Kaufman, J., Stahl, S. J., Wingfield, P. T., and Hyde, C. C. (1999) *J. Struct. Biol. 126*, 131−144.
21. Jiang, S., Lin, K., and Lu, M. (1998) *J. Virol. 72*, 10213−10217.
22. Ji, H., Bracken, C., and Lu, M. (2000) *Biochemistry 39*, 676−685.
23. Dubay, J. W., Roberts, S. J., Brody, B., and Hunter, E. (1992) *J. Virol. 66*, 4748−4756.
24. Cao, J., Bergeron, L., Helseth, E., Thali, M., Repke, H., and Sodroski, J. (1993) *J. Virol. 67*, 2747−2755.
25. Chen, S. S., Lee, C. N., Lee, W. R., McIntosh, K., and Lee, T. H. (1993) *J. Virol. 67*, 3615−3619.
26. Wild, C. T., Dubay, J. W., Greenwell, T. K., Baird, T., Oas, T. G., McDanal, C. B., Hunter, E., and Matthews, T. J. (1994) *Proc. Natl. Acad. Sci. U.S.A. 91*, 12676−12680.
27. Weng, Y., and Weiss, D. C. (1998) *J. Virol. 72*, 9676−9682.
28. Lu, M., Ji, H., and Shen, S. (1999) *J. Virol. 73*, 4433−4438.
29. Jiang, S., Lin, K., Strick, N., and Neurath, A. R. (1993) *Nature 365*, 113.
30. Wild, C. T., Shugars, D. C., Greenwell, T. K., McDanal, C. B., and Matthews, T. J. (1994) *Proc. Natl. Acad. Sci. U.S.A. 91*, 9770−9774.
31. Kilby, J. M., Hopkins, S., Venetta, T. M., DiMassimo, B., Cloud, G. A., Lee, J. Y., Alldredge, Y., Hunter, E., Lambert, D., Bolognesi, D., Matthews, T., Johnson, M. R., Nowak, M. A., Shaw, G. M., and Saag, M. S. (1998) *Nat. Med. 4*, 1302−1307.
32. Eckert, D. M., Malashkevich, V. N., Hong, L. H., Carr, P. A., and Kim, P. S. (1999) *Cell 99*, 103−115.
33. Ferrer, M., Kapoor, T. M., Strassmaier, T., Weissenhorn, W., Skehel, J. J., Oprian, D., Schreiber, S., Wiley, D. C., and Harrison, S. C. (1999) *Nat. Struct. Biol. 6*, 953−960.
34. Hodges, R. S., Sodek, J., Smillie, L. B., and Jurasek, L. (1972) *Cold Spring Harbor Symp. Quant. Biol. 37*, 299−310.
35. McLachlan, A. D., and Stewart, M. (1975) *J. Mol. Biol. 98*, 293−304.
36. Conway, J. F., and Parry, D. A. (1990) *Int. J. Biol. Macromol. 12*, 328−334.
37. Delwart, E. J., Mosialos, G., and Gilmore, T. (1990) *AIDS Res. Hum. Retroviruses 6*, 703−706.
38. Chambers, P., Pringle, C. R., and Easton, A. J. (1990) *J. Gen. Virol. 71*, 3075−3080.
39. Gallaher, W. R., Ball, J. M., Garry, R. F., Griffin, M. C., and Montelaro, R. C. (1989) *AIDS Res. Hum. Retroviruses 5*, 431−440.
40. Kunkel, T. A., Roberts, J. D., and Zakour, R. A. (1987) *Methods Enzymol. 154*, 367−382.
41. Sambrook, J., Fritsch, E. F., and Maniatis, T. (1989) *Molecular Cloning: A Laboratory Manual*, Cold Spring Harbor Laboratory Press, Cold Spring Harbor, NY.
42. de Jong, J.-J., Goudsmit, J., Keulen, W., Klaver, B., Krone, W., Tersmette, M., and de Ronde, A. (1992) *J. Virol. 66*, 757−765.
43. LaCasse, R. A., Follis, K. E., Moudgil, T., Trahey, M., Binley, J. M., Planelles, V., Zolla-Pazner, S., and Nunberg, J. H. (1998) *J. Virol. 72*, 2491−2495.
44. Tersmette, M., Gruters, R. A., deWolf, F., deGoede, R. E. Y., Lange, J. M. A., Schellekens, P. T. A., Goudsmit, J., Huisman, H. G., and Miedema, F. (1989) *J. Virol. 63*, 2118−2125.
45. York, J., Follis, K. E., Trahey, M., Nyambi, P. N., Zolla-Pazner, S., and Nunberg, J. H. (2001) *J. Virol.* (in press).
46. White-Scharf, M. E., Potts, B. J., Smith, L. M., Sokolowski, K. A., Rusche, J. R., and Silver, S. (1993) *Virology 192*, 197−206.
47. Abacioglu, Y. H., Fouts, T. R., Laman, J. D., Claassen, E., Pincus, S. H., Moore, J. P., Roby, C. A., Kamin-Lewis, R., and Lewis, G. K. (1994) *AIDS Res. Hum. Retroviruses 10*, 371−381.
48. Follis, K. E., Trahey, M., LaCasse, R. A., and Nunberg, J. H. (1998) *J. Virol. 72*, 7603−7608.
49. Hill, C. M., Deng, H., Unutmaz, D., Kewalramani, V. N., Bastiani, L., Gorny, M. K., Zolla-Pazner, S., and Littman, D. R. (1997) *J. Virol. 71*, 6296−6304.
50. Poon, B., Jowett, J. B. M., Stewart, S. A., Armstrong, R. W., Rishton, G. M., and Chen, I. S. Y. (1997) *J. Virol. 71*, 3961−3971.
51. Starnatatos, L., and Cheng-Mayer, C. (1995) *J. Virol. 69*, 6191−6198.
52. Willey, R. L., Martin, M. A., and Peden, K. W. C. (1994) *J. Virol. 68*, 1029−1039.
53. Studier, F. W., Rosenberg, A. H., Dunn, J. J., and Dubendorff, J. W. (1990) *Methods Enzymol. 185*, 60−89.
54. Ji, H., Shu, W., Burling, F. T., Jiang, S., and Lu, M. (1999) *J. Virol. 73*, 8578−8586.
55. Edelhoch, H. (1967) *Biochemistry 6*, 1948−1954.
56. Chen, Y.-H., Yang, J. T., and Chau, K. H. (1974) *Biochemistry 13*, 3350−3359.
57. Cantor, C., and Schimmel, P. (1980) *Biophysical Chemistry*, Freeman, New York.
58. Shu, W., Ji, H., and Lu, M. (1999) *Biochemistry 38*, 5378−5385.
59. Johnson, M. L., Correia, J. J., Yphantis, D. A., and Halvorson, H. R. (1981) *Biophys. J. 36*, 575−588.
60. Laue, T. M., Shah, B. D., Ridgeway, T. M., and Pelletier, S. L. (1992) in *Analytical Ultracentrifugation in Biochemistry and Polymer Science* (Harding, S. E., Rowe, A. J., and Horton, J. C., Eds.) pp 90−125, Royal Society of Chemistry, Cambridge, U.K.
61. Otwinowski, Z., and Minor, W. (1996) *Methods Enzymol. 276*, 307−326.
62. Collaborative Computational Project No. 4 (1994) *Acta Crystallogr. D50*, 760−763.
63. Navaza, J. (1994) *Acta Crystallogr. A50*, 157−163.
64. Brünger, A. T. (1992) *X-PLOR Version 3.1: A system for X-ray Crystallography and NMR*, Yale University Press, New Haven, CT.
65. Jones, T. A., Zou, J.-Y., and Cowan, S. W. (1991) *Acta Crystallogr. A47*, 110−119.
66. Brünger, A. T., Adams, P. D., Clore, G. M., DeLano, W. L., Gros, P., Grosse-Kunstleve, R. W., Jiang, J.-S., Kuszewski, J., Nilges, M., Pannu, N. S., Read, R. J., Rice, L. M., Simonson, T., and Warren, G. L. (1998) *Acta Crystallogr. D54*, 905−921.
67. Laskowski, R. A., MacArthur, M. V., Moss, D. D., and Thornton, J. M. (1993) *J. Appl. Crystallogr. 26*, 283−291.
68. HIV Sequence Database (1998/1999) Los Alamos National Laboratory, Los Alamos, NM.
69. Harbury, P. B., Zhang, T., Kim, P. S., and Alber, T. (1993) *Science 262*, 1401−1407.
70. Lu, M., and Kim, P. S. (1997) *J. Biomol. Struct. Dyn. 15*, 465−471.
71. Crick, F. H. C. (1953) *Acta Crystallogr. 6*, 689−697.
72. LaCasse, R. A., Follis, E., Trahey, M., Scarborough, J. D., Littman, D. R., and Nunberg, J. H. (1999) *Science 283*, 357−362.
73. Skehel, J. L., and Wiley, D. C. (1998) *Cell 95*, 871−874.
74. Shu, W., Liu, J., Ji, H., Radigen, L., Jiang, S., and Lu, M. (2000) *Biochemistry 39*, 1634−1642.
75. Stegmann, T., Delfino, J. M., Richards, F. M., and Helenius, A. (1991) *J. Biol. Chem. 266*, 18404−18410.
76. Tsurudome, M., Gluck, R., Graf, R., Falchetto, R., Schaller, U., and Brunner, J. (1992) *J. Biol. Chem. 267*, 20225−20232.
77. Jelesarov, I., and Lu, M. (2001) *J. Mol. Biol.* (in press).

78. Sattentau, Q. J., and Moore, J. P. (1993) *Philos. Trans. R. Soc. London, Ser. B 342*, 59−66.
79. Sattentau, Q. J., Moore, J. P., Vignaux, F., Traincard, F., and Poignard, P. (1993) *J. Virol. 67*, 7383−7393.
80. Farzan, M., Choe, H., Desjardins, E., Sun, Y., Kuhn, J., Cao, J., Archambault, D., Kolchinsky, P., Koch, M., Wyatt, R., and Sodroski, J. (1998) *J. Virol. 72*, 7620−7625.
81. Binley, J. M., Sanders, R. W., Clas, B., Schuelke, N., Master, A., Guo, Y., Kajumo, F., Anselma, D. J., Maddon, P. J., Olson, W. C., and Moore, J. P. (2000) *J. Virol. 74*, 627−643.
82. Evans, S. V. (1993) *J. Mol. Graphics 11*, 134−138.

BI0024759

Design of potent inhibitors of HIV-1 entry from the gp41 N-peptide region

Debra M. Eckert* and Peter S. Kim†

Howard Hughes Medical Institute, Whitehead Institute for Biomedical Research, Department of Biology, Massachusetts Institute of Technology, Nine Cambridge Center, Cambridge, MA 02142

Contributed by Peter S. Kim, July 26, 2001

The HIV-1 gp41 envelope glycoprotein promotes fusion of the virus and cell membranes through the formation of a trimer-of-hairpins structure, in which the amino- and carboxyl-terminal regions of the gp41 ectodomain are brought together. Synthetic peptides derived from these two regions (called N and C peptides, respectively) inhibit HIV-1 entry. In contrast to C peptides, which inhibit in the nanomolar range, N peptides are weak inhibitors with IC_{50} values in the micromolar range. To test the hypothesis that the weak inhibition of N peptides results from their tendency to aggregate, we have constructed chimeric variants of the N-peptide region of gp41 in which soluble trimeric coiled coils are fused to portions of the gp41 N peptide. These molecules, which present the N peptide in a trimeric coiled-coil conformation, are remarkably more potent inhibitors than the N peptides themselves and likely target the carboxyl-terminal region of the gp41 ectodomain. The best inhibitors described here inhibit HIV-1 entry at nanomolar concentrations.

To infect a cell, HIV type 1 (HIV-1) must fuse its membrane with the host cell membrane and release its contents into the cell. The fusion process is mediated by the envelope glycoprotein (Env) on the surface of the virus. Env is composed of two subunits: gp120, a surface subunit that binds host cell receptors, and gp41, a transmembrane subunit that ultimately inserts into the host cell membrane and promotes the fusion event. The ectodomain of gp41 contains two helical regions, one near the amino terminus (N helix) and one near the carboxy terminus (C helix). In the fusogenic conformation of gp41, the N and C helices interact with each other in an antiparallel manner, like a hairpin, bringing the amino and carboxy termini of the ectodomain together. This facilitates the juxtaposition of the virus and cell membranes, leading to membrane fusion (1).

The fusogenic structure of gp41 is composed of three gp41 hairpins (i.e., trimer-of-hairpins). The N helices from three gp41 ectodomains form a central three-stranded coiled coil and are surrounded by three antiparallel C helices that bind to conserved grooves on the coiled-coil surface (2–5). Synthetic peptides derived from the N- and C-helix regions of gp41 (called N and C peptides, respectively) inhibit HIV-1 viral infection (3, 6–10). C peptides are potent inhibitors of HIV-1 infectivity with activity at nanomolar concentrations (3, 6, 8, 10, 11), and one, T20, has shown promising results in anti-HIV-1 human clinical trials (12). C peptides likely inhibit formation of the fusogenic six-helix bundle in a dominant-negative manner by binding the N-helix region of gp41 (Fig. 1*A*) (3, 9, 13–16). Recently, efforts to target a hydrophobic pocket on the N helix of gp41 led to the identification of cyclic D peptides that inhibit HIV-1 entry, likely in the same dominant-negative manner (17, 18).

N peptides can also inhibit HIV-1 entry (3, 7). Two possible mechanisms for their inhibitory activity can be envisioned (Fig. 1*B*). First, the N peptides may target an exposed C-helix region of gp41 (3). Alternatively, synthetic N peptides could intercalate with the N helices of gp41, thereby forming a heterotrimeric coiled coil and interfering with the coiled-coil formation of gp41 (7, 19).

N peptides, which aggregate in isolation (3, 20), are far less potent than C peptides. It has been proposed that N peptides are poor inhibitors because their aggregation interferes with their ability to efficiently target gp41 via either mechanism described above (3, 21). However, if an N peptide could be properly sequestered into a nonaggregating trimeric coiled-coil conformation, it should be able to effectively bind and sequester the C helix of gp41 and inhibit HIV-1 entry via the first mechanism described above.

Indeed, recent work has shown that the C-helix region of gp41 is a useful target for inhibiting HIV-1 entry (21). A protein designed to have a very high affinity for C helix is an extremely effective, broad-spectrum antiviral compound, with a low nanomolar IC_{50} value. This molecule, 5-Helix, consists of five of the six helices of the gp41 trimer-of-hairpins joined by short peptide linkers (21). 5-Helix forms the trimer-of-hairpins structure, exposing one C-helix-binding site, and its antiviral activity depends on its ability to bind C helix.

In this study, we designed nonaggregating trimeric coiled-coil N peptides and characterized their inhibitory activity. Each peptide is a chimeric molecule consisting of a designed trimeric coiled coil (22, 23) fused to a portion of the gp41 N helix. One of these peptides, IQN17, was previously shown to form a soluble, stable, trimeric coiled coil (18). These peptides sustain the N helix in a coiled-coil conformation and, strikingly, they have dramatically increased antiviral potency over the corresponding N peptides themselves. The inhibitory activity of the chimeric N peptides is correlated to their stability. The most potent chimeric N peptide described here, IQN23, inhibits HIV-1 entry with an IC_{50} value of 15 nM.

Materials and Methods

Peptide Synthesis and Purification. All peptides were chemically synthesized on a PE Biosystems 431A peptide synthesizer upgraded with feedback monitoring. The standard Fmoc/HBTU [fluoroenylmethyl chloroformate/2-(1H-benzotriazol-1-yl)-1,1,3,3,tetramethyluronium hexafluorophosphate] chemistry (24) was modified with DMSO/NMP resin swelling and acetic anhydride capping after every couple. The peptides were cleaved from the PE Biosystems Pal resin with Reagent K (25). Each peptide has an acetylated amino terminus and a carboxyl-terminal amide.

The sequences of N17, N23, N36, IQN17, IQN23, IQN36, IIN17, $IQ_{22}N17$, $II_{22}N17$, $IQ_{15}N17$, $II_{15}N17$, IZN17, IZN23, and IZN36 are shown in Fig. 2. The first 29 residues of IQN17 are derived from a designed trimeric coiled coil, GCN4-pI_QI' (18), and the final 17 residues are derived from the N-helix region of gp41 from the HXB2 strain of HIV-1. The sequence of GCN4-

Abbreviation: HIV-1, HIV type 1.

*Present address: Merck Research Laboratories, Merck & Co., Inc., P.O. Box 2000, Rahway, NJ 07065-0900.

†To whom reprint requests should be sent at the present address: Merck Research Laboratories, Merck & Co., Inc., 770 Sumneytown Pike, West Point, PA 19486. E-mail: peter_kim@merck.com.

The publication costs of this article were defrayed in part by page charge payment. This article must therefore be hereby marked "*advertisement*" in accordance with 18 U.S.C. §1734 solely to indicate this fact.

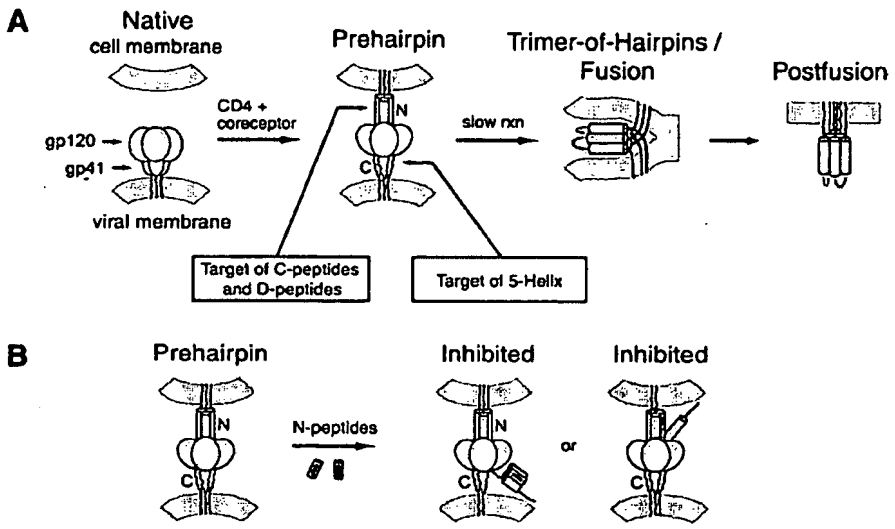

Fig. 1. (*A*) Working model of HIV-1 membrane fusion and its inhibition (for review, see ref. 1). Before exposure to cellular receptors, Env exists in a native state ("Native") on the surface of the virus. After interaction with CD4 and the coreceptor, a conformational change allows gp41 to insert its amino-terminal fusion-peptide domain into the cell membrane, forming a transient prehairpin intermediate ("Prehairpin"). In the prehairpin intermediate, the N-peptide region (gray) and possibly the C-peptide region (yellow) are exposed and vulnerable to inhibitors [e.g., C peptides (3, 6, 7, 9, 10), D peptides (18), and 5-Helix (21)]. Although 5-Helix is depicted as targeting the prehairpin intermediate, it is unknown whether it targets the native state, the prehairpin intermediate, or both (see ref. 1). All of these inhibitors work in a dominant-negative manner by preventing formation of the trimer-of-hairpins (see text). In the absence of inhibitors, the prehairpin intermediate slowly resolves to the trimer-of-hairpins structure that juxtaposes the virus and cell membranes and leads to fusion. (*B*) Representation of two possible mechanisms for N-peptide inhibitory activity. N peptides may target a vulnerable C-helix region of gp41 (yellow). Alternatively, the N peptides (blue) could intercalate with the N helices of gp41 (gray) to form a heterotrimeric coiled coil and interfere with the coiled-coil formation of gp41.

pI_QI' is Ac-RMKQIEDKIEEIESKQKKIENEIARIKKL-IGERY-NH_2. The N17 peptide is 17 aa long and consists of only the gp41 residues of IQN17. IQN17–2Pro contains a Gln→Pro mutation at position 16 of IQN17 and an Ile→Pro mutation at position 37. IQN17 G572D contains a Gly→Asp mutation at position 36 of IQN17. Longer chimeric N peptides were made by inserting additional residues from the HXB2 gp41 N-peptide region, taking care to keep the coiled-coil heptad repeat register

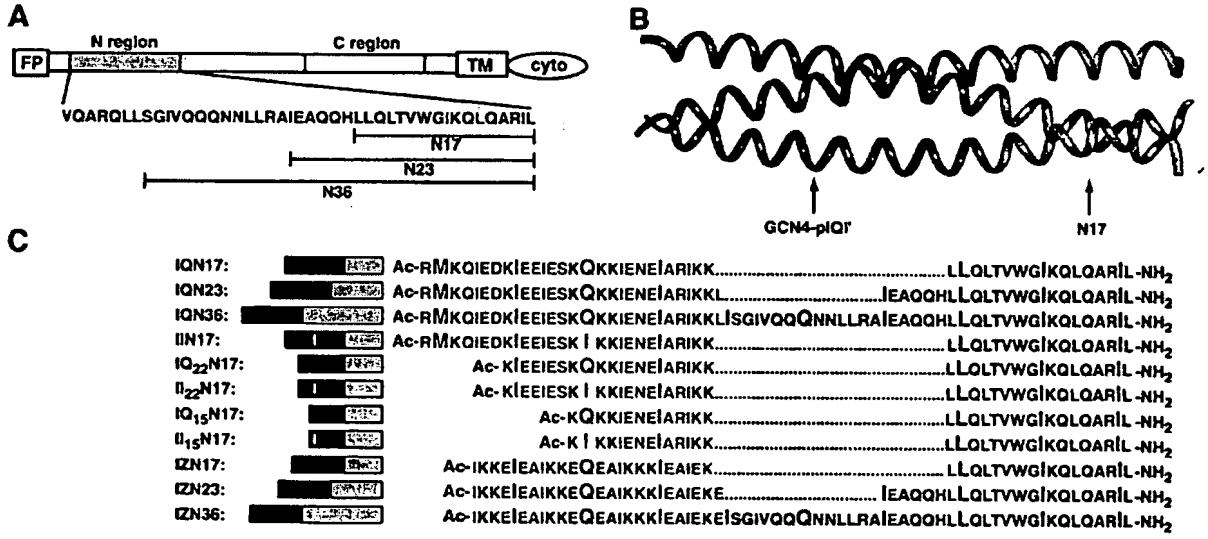

Fig. 2. HIV-1 gp41 structure and chimeric N peptides. (*A*) Schematic of the primary structure of HIV-1 HXB2 gp41, including the sequence of residues 539–581. The N-peptide (gray) and C-peptide regions (yellow) are indicated. The residues corresponding to the N peptides discussed in this study are indicated. (*B*) Model of IQN17, which represents the general structure of the chimeric N peptides discussed in this study. Each chimeric N peptide consists of an amino-terminal designed trimeric coiled coil (purple) fused to a sequence from the N-helix region of gp41 (gray). (*C*) The peptide sequences of the chimeric N peptides. The designed trimeric coiled-coil sequences (purple for GCN4-pI_QI', red for IZ_m) are aligned, as are the gp41 sequences (black). The a positions of the heptad repeats are indicated by a larger font.

intact. These peptides are IQN23 and IQN36. The N23 and N36 peptides contain only the gp41 residues of IQN23 and IQN36, respectively. Sequential heptads were removed from the amino terminus of IQN17 to yield two shorter peptides: $IQ_{22}N17$ and $IQ_{15}N17$. More stable versions of the IQN17, $IQ_{22}N17$, and $IQ_{15}N17$ peptides were made by changing the glutamine residues at position 16 of IQN17, position 9 of $IQ_{22}N17$, and position 2 of $IQ_{15}N17$ to isoleucines. These peptides are called IIN17, $II_{22}N17$, and $II_{15}N17$, respectively. Also, additional chimeric N peptides were made in which a different designed trimeric coiled coil was placed amino-terminal to the gp41-derived residues. The coiled coil, IZ_m, was based on a design described by Suzuki *et al.* (23). Alterations were made at some of the e and g positions of the Suzuki sequence to avoid similarity to GCN4-pI_QI'. Also, one Ile→Gln substitution was made at an a position. These additional chimeric peptides are called IZN17, IZN23, and IZN36. The sequence of IZ_m is Ac-YGGIKKEIEAIKKEQEA-IKKKIEAIEKEIEA-NH_2.

After cleavage from the resin, each peptide was desalted over a Sephadex G-25 column (Amersham Pharmacia) and lyophilized. The peptide was then resuspended in 5% acetic acid and purified over a Vydac C18 (Hesperia, CA) preparative column on a reverse-phase high-performance liquid chromatography apparatus (Waters). The peptide was eluted from the column with a water–acetonitrile gradient in the presence of 0.1% trifluoroacetic acid and lyophilized. The molecular weights of each peptide were confirmed by using matrix-assisted laser desorption ionization-time-of-flight mass spectrometry (PerSeptive Biosystems, Framingham, MA).

For all experiments, peptide stock solutions (typically 200–800 μM) were prepared by resuspending lyophilized peptide in water. The precise concentrations of the peptide stocks were determined by using tyrosine and tryptophan absorbance at 280 nm in 6 M GuHCl (26). The stock solutions were then diluted to the desired concentration in the appropriate buffer for each experiment. After resuspension in water, N17 and N23 solutions were cloudy. The aggregates were pelleted at high speed for 10 min, and the concentration of the supernatant was determined.

CD. All CD measurements were performed on either an Aviv 62 DS or 62A DS (Aviv Associates, Lakewood, NJ) CD spectrometer. Standard scans were performed on 10 μM solutions of peptide in PBS [50 mM sodium phosphate, 150 mM sodium chloride (pH 7.4)] from 200 to 260 nm in a 1-cm pathlength cuvette with a 5-second averaging time. Percent helicity as recorded at 222 nm was calculated according to Chen *et al.* (27). Thermal denaturation scans of 10 μM peptide solutions in PBS were recorded at 222 nm. The peptide was heated at 2-degree intervals starting at 4 or 20°C, with an equilibration time of 1.5 min and an averaging time of 60 seconds. The melting temperatures, or midpoints of the cooperative thermal unfolding transitions (T_m), were estimated from the thermal dependence of the ellipticity at 222 nm. For most of the peptides with a melting temperature of 100°C or higher in PBS, thermal denaturation experiments were performed in PBS in the presence of 2 M guanidine hydrochloride.

Sedimentation Equilibrium. All measurements were recorded on a Beckman XL-A (Beckman Coulter) analytical ultracentrifuge equipped with an An-60 Ti rotor (Beckman Coulter). Peptide stock solutions were diluted to 100–200 μM and dialyzed overnight against PBS. After dialysis, the concentration was redetermined, and the peptides were diluted to 20 μM by using the dialysis buffer. The samples were centrifuged at speeds ranging from 19,000 to 26,000 rpm.

HIV-1 Infectivity Assay. Inhibitory activity of the chimeric N peptides was determined by using an HIV luciferase assay (28). Virus was made by cotransfecting 293T cells with an HIV-1 genome containing a frame-shift mutation in *env* and a luciferase gene replacing *nef* (NL43LucR-E-) along with pCMVHXB2, an expression vector with the HXB2 gp160 gene. Because its genome lacks *env*, the resultant virus is viable only for one round of infection. The cellular debris was removed by low-speed centrifugation. The remaining viral supernatant was used to infect HOS-CD4/fusion cells (N. Landau, National Institutes of Health AIDS Reagent Program) in the presence of 2-fold dilutions of the experimental peptides. Two days postinfection, the cells were lysed, and luciferase activity was monitored on a Wallac AutoLumat LB953 luminometer (Gaithersburg, MD). IC_{50} values (the peptide concentration at which half of the viral infection is inhibited) were calculated by fitting the data to a Langmuir equation [$y = k/(1 + [\text{peptide}]/IC_{50})$], where y = luciferase activity and k is a scaling constant.

Results

Synthetic Peptides from the N-Helix Region of gp41 Weakly Inhibit Viral Infectivity. Previously, a peptide containing 36 amino acids derived from the N-helix region of gp41, called N36, was identified by protein dissection of the ectodomain of gp41 (2, 20). Here, we examined the HIV-1 inhibitory activity of N36 and two shorter N peptides: N17 and N23. N17 comprises the residues that form the hydrophobic pocket of the N-helix trimer that, in the fusogenic gp41 structure, binds to three hydrophobic residues of the C-helix region. N23 and N36 contain the residues of N17 with additional amino-terminal N-helix residues (Fig. 2*A*). N36 aggregates in solution (20), and both N17 and N23 are extremely insoluble (see *Materials and Methods*). These peptides are not very helical in isolation, as determined by CD (Table 1). The inhibitory potencies of N17, N23, and N36 are low, with IC_{50} values of 13, 29, and 2 μM, respectively (Table 1).

The Pocket-Forming Region of the N Peptide Inhibits as a Coiled-Coil Trimer. In the fusogenic trimer-of-hairpins structure, the N peptides form a trimeric coiled coil and bind to three helical C peptides (2–5, 20). If synthetic N peptides could be presented in a trimeric coiled-coil conformation rather than an aggregated state, they might bind the C-helix region of gp41 better than aggregated N peptides. Because the C helix has been shown to be an effective antiviral target (21), coiled-coil N peptides also may have higher inhibitory potency than aggregated N peptides. Previously, such a soluble peptide was designed (18). IQN17 is a chimeric peptide that presents a portion of the N helix comprising a hydrophobic pocket in a trimeric coiled-coil conformation. In IQN17, a designed trimeric coiled coil (GCN4-pI_QI') was fused to the amino terminus of 17 residues of the N helix (N17, as seen above), creating a continuous coiled coil 45 aa in length (Fig. 2 *B* and *C*).

IQN17 is a fully helical and discretely trimeric species at 10–20 μM (ref. 18 and Table 1). IQN17 is extremely stable, with a melting temperature of ≈100°C at 10 μM (Table 1), and guanidine denaturation studies predict it maintains its trimeric state even at low nanomolar concentrations (unpublished results). Additionally, with an IC_{50} value of 190 nM, IQN17 is almost two orders of magnitude more potent than N17 (Table 1). The GCN4-pI_QI' portion of the molecule alone as well as an unfolded IQN17 (containing two proline residues in the hydrophobic core) do not show inhibitory activity (tested up to 25 μM). In addition, a derivative of IQN17 that introduces a charge into the hydrophobic pocket, IQN17 (G572D) has little inhibitory activity, with an IC_{50} value of 15 μM. Therefore, the inhibitory activity of the hydrophobic pocket region of the N peptide is greatly enhanced in a trimeric coiled-coil conformation.

GCN4-pI_QI' was also fused to the amino terminus of N23 and N36 to make IQN23 and IQN36, respectively (Fig. 2*C*). Both of these peptides are extremely helical (Table 1). IQN23 is discretely trimeric, whereas IQN36 is a slightly aggregated trimer

Table 1. Biophysical data and HIV-1 inhibitory activity of chimeric N peptides

Peptide	θ_{222nm} (deg cm²·dmol⁻¹)	% helicity, at 10 μM	M_{obs}/M_{calc}, at 20 μM	IC_{50}, μM, viral infectivity
N17	−10,200	30	ND†	13 ± 4
N23	−10,600	30	ND†	29 ± 10
N36	−24,400	67	ND†	2 ± 0.8
IQN17	−35,800	96	3.1	0.19 ± 0.03
GCN4-pI$_Q$I′	−28,700	80	3.0	>25*
IQN17-2Pro	−7400	20	ND‡	>25*
IQN17 G572D	−39,800	100	3.2	15 ± 5
IQN23	−36,400	97	3.1	0.015 ± 0.007
IQN36	−35,100	92	3.5	0.088 ± 0.035
IZN17	−37,200	100	3.1	0.022 ± 0.011
IZ$_m$	−28,900	81	3.1	>25*
IZN23	−38,800	100	3.1	0.030 ± 0.01
IZN36	−38,600	100	3.4	0.026 ± 0.007

CD scans were performed on 10 μM peptide solutions in PBS. The CD signal at 222 nm (θ_{222nm}) and the percent helicity are reported. Sedimentation equilibrium studies were performed on 20 μM peptide solutions in PBS. The results are reported as a ratio of the experimental molecular weight to the calculated molecular weight for a monomer (M_{obs}/M_{calc}). Inhibition of viral entry was measured in a single-round infectivity assay. The results indicate the mean IC_{50} value (the peptide concentration at which half the viral infection is inhibited) and SEM for no less than two experiments, each performed in duplicate. ND, not determined.
*No activity seen up to 25 μM.
†Aggregated (see *Materials and Methods* and ref. 21).
‡Unfolded, as determined by CD.

(Table 1). Both IQN23 and IQN36 are dramatically better inhibitors than the corresponding N peptides themselves, with IC_{50} values of 15 and 88 nM, respectively (Table 1).

The Inhibitory Potency of IQN17 Is Correlated to Its Stability. If the N-peptide inhibitors must be trimeric to inhibit HIV-1 entry, one might expect the thermodynamic stability of the peptides to be correlated to their inhibitory activity. In particular, a less stable IQN17 derivative that is dissociated at the IC_{50} concentration of IQN17 should be a less potent inhibitor. A series of peptides was made to determine the effect of stability of the trimeric coiled-coil structure on the inhibitory potency of the chimeric N peptides.

The GCN4-pI$_Q$I′ trimeric coiled coil contains one glutamine per monomer (at position 16) that packs into the interior of the coiled coil. This glutamine was shown to decrease stability compared with a coiled coil with an all-isoleucine core (22, 29). The glutamine in the IQN17 core (at position 16) was changed to an isoleucine to make a more stable peptide, IIN17 (Fig. 2*C*). Shorter less stable IQN17 derivatives were made by sequentially removing groups of seven residues from the amino terminus of IQN17. These two IQN17 derivatives contain 22 and 15 aa of the GCN4-pI$_Q$I′ region (IQ_{22}N17 and IQ_{15}N17, respectively) (Fig. 2*C*). The corresponding isoleucine derivatives of these peptides (II_{22}N17 and II_{15}N17) were studied as well.

In each peptide pair (IQN17 and IIN17, IQ_{22}N17 and II_{22}N17, and IQ_{15}N17 and II_{15}N17), the isoleucine derivative is the more stable of the two peptides, as determined by thermal denaturation (Table 2). The isoleucine derivative in both of the two pairs of shorter IQN17 derivatives (IQ_{22}N17 and II_{22}N17 and IQ_{15}N17 and II_{15}N17) has more potent inhibitory activity that is statistically significant (Table 2). However, there is little, if any, difference in the inhibitory activity of the three most stable peptides that have melting temperatures of 100°C or above (IQN17, IIN17, and II_{22}N17). Therefore, the inhibitory activity of the peptides correlates to the stability of the coiled-coil structures, until the point where a highly stable coiled-coil structure is reached.

An Alternate Chimeric N Peptide, IZN17, Is a More Potent Inhibitor. We studied an additional series of chimeric N peptides in which the GCN4-pI$_Q$I′ portion of the molecule was replaced with a different designed trimeric coiled coil. This coiled coil, called "IZ$_m$" for modified isoleucine zipper, is based on a design described by Suzuki *et al.* (23) and is helical and trimeric in solution (Table 1). The resulting chimeric peptides are termed

Table 2. Stability of chimeric N peptides is correlated to inhibition

Peptide	θ_{222nm} (deg cm²·dmol⁻¹)	T_m, °C	T_m, °C, 2 M GuHCl	IC_{50}, μM, viral infectivity
IQN17	−35,800	100	66	0.19 ± 0.03
IIN17	−39,500	ND	~100	0.14 ± 0.05
IQ_{22}N17	−32,400	78	ND	1.4 ± 0.3
II_{22}N17	−39,700	>100	85	0.16 ± 0.01
IQ_{15}N17	−27,600	64	ND	5.5 ± 1.5
II_{15}N17	−30,300	72	ND	2.1 ± 0.8
IZN17	−37,200	>100	74	0.022 ± 0.011

CD scans were performed on 10 μM peptide solutions in PBS. The CD signal at 222 nm (θ_{222nm}) is reported. Thermal denaturation CD scans were performed on 10-μm peptide solutions in PBS and in PBS with 2 M guanidine hydrochloride. The midpoint of thermal denaturation (T_m) was estimated from the thermal dependence of the CD signal at 222 nm. Inhibition of viral entry was measured in a single-round infectivity assay. The results indicate the mean IC_{50} value (the peptide concentration at which half the viral infection is inhibited) and SEM for no less than two experiments, each performed in duplicate. ND, not determined.

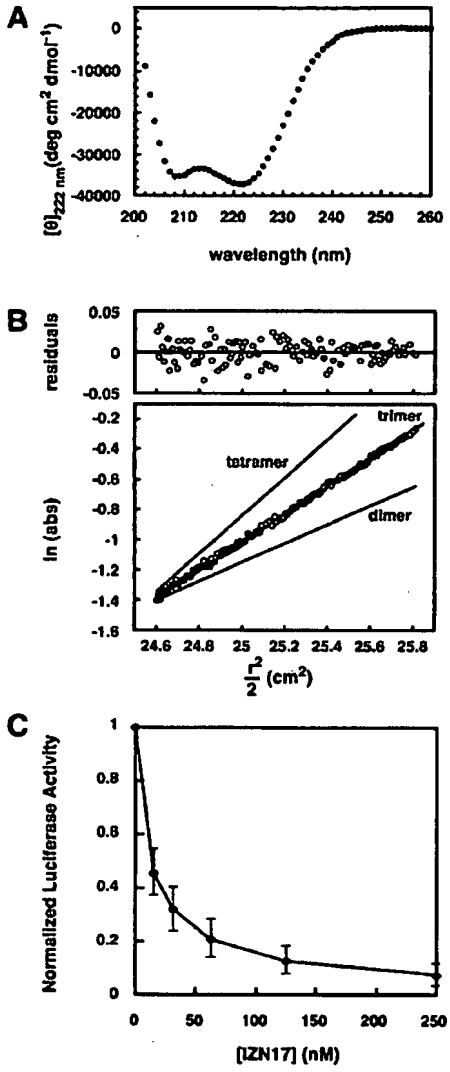

Fig. 3. IZN17: biophysical data and inhibitory activity. (A) The mean of two CD spectra of 10 μM solutions of IZN17 in PBS (pH 7.4), 4°C. IZN17 is fully helical, with an approximate ellipticity of −37,200 deg cm^{2}dmol$^-$ at 222 nm. (*B*) Representative sedimentation equilibrium data of a 20 μM solution of IZN17 in PBS (pH 7.4), 4°C. The slope of the data as plotted is proportional to the molecular mass of the peptide oligomer. Lines indicate the expected slopes for dimeric, trimeric, and tetrameric oligomeric states. The deviation in the data from the line representing the trimeric state is plotted (*Upper*). IZN17 is a discrete trimer under the experimental conditions. (*C*) Inhibition of viral infectivity by IZN17 as determined by an HIV-1 luciferase assay. The data represent the mean +/− SEM of five separate experiments. The approximate IC_{50} value of IZN17 is 22 nM.

IZN17, IZN23, and IZN36 (Fig. 2*C*). Each of the peptides is helical, as determined by CD (Table 1 and Fig. 3*A*). IZN17 (Fig. 3*B*) and IZN23 are discrete trimers, and IZN36 is an aggregated trimer, as determined by sedimentation equilibrium (Table 1). The IC_{50} values of IZN17 (Fig. 3*C*), IZN23, and IZN36 in the HIV-1 infectivity assay are 22, 30, and 26 nM, respectively (Table 1).

Interestingly, IZN17 is close to an order of magnitude more potent than IQN17 in the viral infectivity assay. Although it is not entirely clear why this is the case, there are two potential reasons that may contribute to the increase in potency. First, IZN17 is more stable than IQN17, as determined by thermal denaturation (Table 2). However, this is not likely to contribute significantly to the increased potency of IZN17, because IIN17 is much more stable than IZN17 and yet a less potent inhibitor. Second, IZN17 contains two additional residues from the gp41 N-helix region (residues 20 and 21 of IZN17, corresponding to residues 560 and 561 of HXB2) because of a coincidence in sequence between IZ_m and gp41. The additional gp41 residues could provide an increase in binding affinity to the C-helix region of gp41.

Discussion

Previously studied N peptides are weak inhibitors of HIV-1 entry, with IC_{50} values in the micromolar range (3, 7). Our results demonstrate that N peptides can be potent inhibitors when presented in a trimeric coiled-coil conformation. In the best example, addition of a designed coiled coil to the amino terminus of N23 resulted in a remarkable decrease in the IC_{50} value of three orders of magnitude (Table 1). In addition, the chimeric N peptides likely inhibit HIV-1 entry in a dominant-negative manner by binding to the C-helix region of gp41, as seen in the x-ray structure of fusogenic gp41 (2, 4, 5). Recently, Louis *et al.* described the design of another soluble N-helix trimeric coiled coil, N_{CCG}-gp41, which is stabilized by both fusion to a thermostable subdomain of gp41 and intersubunit disulfide bonds (30). N_{CCG}-gp41 inhibits HIV-1 entry at nanomolar concentrations, in agreement with our results.

The chimeric N peptides studied here inhibit HIV-1 entry with a wide range of IC_{50} values, from 15 nM to 5 μM. Several factors appear to influence their potency. First, increased thermal stability of the coiled coil, within a range, correlates with increased potency. For example, $II_{22}N17$ is much more resistant to thermal denaturation than $IQ_{22}N17$ and is almost an order of magnitude more potent. However, the effects of stability on potency decline once a certain level of stability is obtained. For example, the IC_{50} values of IQN17, IIN17, and $II_{22}N17$ are similar despite large differences in thermal stability. These observations are likely because of the association state of the peptides. As mentioned, guanidine denaturation studies indicate that IQN17 is fully trimeric at low nanomolar concentrations (unpublished results). Because IIN17 and $II_{22}N17$ are more stable than IQN17 according to thermal denaturation studies, they should also be fully trimeric at low nanomolar concentrations. Therefore, at the IC_{50} concentration slightly below 200 nM, IQN17, IIN17, and $II_{22}N17$ are likely completely associated, and the IC_{50} value of IQN17 likely represents a maximum inhibitory potency. The less stable peptides with significantly lower inhibitory potencies ($IQ_{22}N17$, $IQ_{15}N17$, and $II_{15}N17$) are likely at least partially unfolded at 200 nM, leading to a decrease in inhibitory potency.

Second, increasing the length of the gp41 portion can increase the inhibitory activity of the chimeric N peptides (e.g., IQN23 is a much better inhibitor than IQN17). However, adding additional gp41 residues does not always result in a better inhibitor (e.g., IQN36 is less potent than IQN23, possibly because of the increased aggregation of IQN36).

Third, the identity of the designed coiled coil can alter the inhibitory activity of the attached N peptide (e.g., IZN17 is a much better inhibitor than IQN17). It is unclear why the identity of the designed coiled coil affects the inhibitory activity of the chimeric N peptides. In the case of IZN17, it is slightly more stable than IQN17 and also contains two additional residues amino terminal to N17 that are identical to the gp41 N-peptide sequence (residues 20 and 21 of IZN17). These two factors may explain at least some of the increased potency of IZN17. However, it is also possible that because the residues in GCN4-$pI_Q I'$ and IZ_m differ, they differentially affect the binding of the

N-peptide region of the molecule to the C-helix region of gp41. For example, in the context of N17 binding, IZ_m may contribute favorable interactions with gp41 or GCN4-pI_QI' may make unfavorable contacts.

The range of potencies of the panel of chimeric N peptides studied here suggests it may be possible to design additional chimeric N peptides with increased potency. For example, changing the identity or location of the designed coiled coil (such as placing it on the carboxy terminus of the N peptide rather than the amino terminus) and using different regions of the N helix may result in better inhibitors. It is possible that the peptides studied here, or similar ones not yet designed, would provide a useful additional therapy for HIV-1 patients. Indeed, some of these chimeric N peptides are of similar size and potency to synthetic C peptides currently in human clinical trials (12).

Finally, the chimeric N peptides likely present an accurate structure of the N-helix region of gp41 present transiently during the entry process. Indeed, cyclic D peptides that bind to IQN17 have been shown to inhibit HIV-1 entry (18). If an antibody that recognized this structure could be identified, it may have neutralizing activity (see also refs. 18, 31). Therefore, molecules such as the chimeric N peptides may serve as useful components of potential vaccines for raising an anti-HIV-1 neutralizing antibody response.

We thank members of the Kim lab, including Michael Burgess and Ben Sanford for peptide synthesis, Heng Chhay for antiviral assays, Lily Hong for technical assistance, Sam Sia for advice on the design of IZ_m, and Leslie Gaffney for editorial assistance. We also thank members of the Kim laboratory for critically reviewing the manuscript. This research was supported by the National Institutes of Health (GM44162).

1. Eckert, D. M. & Kim, P. S. (2001) *Annu. Rev. Biochem.* 70, 777–810.
2. Chan, D. C., Fass, D., Berger, J. M. & Kim, P. S. (1997) *Cell* 89, 263–273.
3. Lu, M., Blacklow, S. C. & Kim, P. S. (1995) *Nat. Struct. Biol.* 2, 1075–1082.
4. Tan, K., Liu, J., Wang, J.-H., Shen, S. & Lu, M. (1997) *Proc. Natl. Acad. Sci. USA* 94, 12303–12308.
5. Weissenhorn, W., Dessen, A., Harrison, S. C., Skehel, J. J. & Wiley, D. C. (1997) *Nature (London)* 387, 426–430.
6. Jiang, S., Lin, K., Strick, N. & Neurath, A. R. (1993) *Nature (London)* 365, 113.
7. Wild, C., Oas, T., McDanal, C., Bolognesi, D. & Matthews, T. (1992) *Proc. Natl. Acad. Sci. USA* 89, 10537–10541.
8. Wild, C. T., Greenwell, T. & Matthews, T. (1993) *AIDS Res. Hum. Retroviruses* 9, 1051–1053.
9. Wild, C. T., Greenwell, T., Shugars, D., Rimsky-Clarke, L. & Matthews, T. (1995) *AIDS Res. Hum. Retroviruses* 11, 323–325.
10. Wild, C. T., Shugars, D. C., Greenwell, T. K., McDanal, C. B. & Matthews, T. J. (1994) *Proc. Natl. Acad. Sci. USA* 91, 9770–9774.
11. Chan, D. C., Chutkowski, C. T. & Kim, P. S. (1998) *Proc. Natl. Acad. Sci. USA* 95, 15613–15617.
12. Kilby, J. M., Hopkins, S., Venetta, T. M., DiMassimo, B., Cloud, G. A., Lee, J. Y., Alldredge, L., Hunter, E., Lambert, D., Bolognesi, D., *et al.* (1998) *Nat. Med.* 4, 1302–1307.
13. Chan, D. C. & Kim, P. S. (1998) *Cell* 93, 681–684.
14. Chen, C.-H., Matthews, T. J., Mcdanal, C. B., Bolgnesi, D. P. & Greenberg, M. L. (1995) *J. Virol.* 69, 3771–3777.
15. Malashkevich, V. N., Chan, D. C., Chutkowski, C. T. & Kim, P. S. (1998) *Proc. Natl. Acad. Sci. USA* 95, 9134–9139.
16. Rimsky, L. T., Shugars, D. C. & Matthews, T. J. (1998) *J. Virol.* 72, 986–993.
17. Cole, J. L. & Garsky, V. M. (2001) *Biochemistry* 40, 5633–5641.
18. Eckert, D. M., Malashkevich, V. N., Hong, L. H., Carr, P. A. & Kim, P. S. (1999) *Cell* 99, 103–115.
19. Weng, Y. & Weiss, C. D. (1998) *J. Virol.* 72, 9676–9682.
20. Lu, M. & Kim, P. S. (1997) *J. Biomol. Struct. Dyn.* 15, 465–471.
21. Root, M. J., Kay, M. S. & Kim, P. S. (2001) *Science* 291, 884–888.
22. Eckert, D. M., Malashkevich, V. N. & Kim, P. S. (1998) *J. Mol. Biol.* 284, 859–865.
23. Suzuki, K., Hiroaki, H., Kohda, D. & Tanaka, T. (1998) *Protein Eng.* 11, 1051–1055.
24. Fields, C. G., Lloyd, D. H., Macdonald, R. L., Otteson, K. M. & Noble, R. L. (1991) *Peptide Res.* 4, 95–101.
25. King, D. S., Fields, C. G. & Fields, G. B. (1990) *Int. J. Pep. Protein Res.* 36, 255–266.
26. Edelhoch, H. (1967) *Biochemistry* 6, 1948–1954.
27. Chen, Y., Yang, J. T. & Chau, K. H. (1974) *Biochemistry* 13, 3350–3359.
28. Chen, B. K., Saksela, K., Andino, R. & Baltimore, D. (1994) *J. Virol.* 68, 654–660.
29. Harbury, P. B., Zhang, T., Kim, P. S. & Alber, T. (1993) *Science* 262, 1401–1407.
30. Louis, J. M., Bewley, C. A. & Clore, G. M. (2001) *J. Biol. Chem.* 276, 29485–29499.
31. LaCasse, R. A., Follis, K. E., Trahey, M., Scarborough, J. D., Littman, D. R. & Nunberg, J. H. (1999) *Science* 283, 357–362.